The Pennsylvania State University

The Graduate School

Department of Mechanical and Nuclear Engineering

**PIEZOELECTRIC NETWORKING FOR MODE DELOCALIZATION AND**

**VIBRATION SUPPRESSION OF NEARLY PERIODIC STRUCTURES**

A Thesis in

Mechanical Engineering

by

Hongbiao Yu

Submitted in Partial Fulfillment
of the Requirements
for the Degree of

Doctor of Philosophy

August 2007

The thesis of Hongbiao Yu was reviewed and approved* by the following:

Kon-Well Wang
William E. Diefenderfer Chaired Professor in Mechanical Engineering
Thesis Advisor
Chair of Committee

Christopher D. Rahn
Professor of Mechanical Engineering

Panagiotis Michaleris
Associate Professor of Mechanical Engineering

George A. Lesieutre
Professor and Head, Aerospace Engineering

Karen A. Thole
Professor of Mechanical Engineering
Head of the Department of Mechanical and Nuclear Engineering

*Signatures are on file in the Graduate School

# ABSTRACT

This thesis investigates the use of piezoelectric circuitry networking technology for mode delocalization and effective vibration suppression in nearly periodic structures.

Periodic structures, such as bladed-disks in turbo-machinery, are well known to be susceptible to *vibration localization* effect which can be caused by the small differences (also referred to as *mistuning*) in the substructures. As a result of localization, vibration energy is confined to a small number of substructures, and the dynamic behavior of periodic structures can be drastically changed. Consequently, the localization effect could significantly impact the health of such nearly (mistuned) periodic structures.

Extensive studies exist concerning mode localization and forced response of nearly periodic structures. Most investigations have focused on exploring the cause of localization, developing methods to quantify the degree of localization, and predicting the maximum forced response. A few studies have explored means to reduce or eliminate localization effect. Recently, Tang and Wang (2003) proposed a new piezoelectric networking concept for mode delocalization of nearly periodic structures and have shown promising results. This thesis aims to further extend the state of the art of delocalization and vibration control of nearly periodic structures via piezoelectric networking technology.

First, piezoelectric networking for mode delocalization is further investigated analytically and experimentally. An active coupling enhancement approach via negative capacitance is proposed for improving the effectiveness of the network for mode delocalization. The analysis is conducted using the transfer matrix approach and Lyapunov exponent. A localization index is defined from the correlation between Lyapunov exponents and the localized modes of the electromechanically bi-coupled system, and is used in a comprehensive parameter study. Experiments are carried out to validate the delocalization concept on a bladed disk specimen. The effect of negative capacitance on the network's performance is also investigated. Both analysis and experiments verify that the mode localization level of mistuned periodic structures can be effectively reduced by the piezoelectric network, and the performance of the network can

be further improved by the active coupling enhancement approach via negative capacitance.

The investigation on the piezoelectric networking is then extended to vibration suppression of the mistuned bladed disk. Due to the localization effect, mistuned bladed disks in turbo-machinery often suffer from large forced response. This study provides a comprehensive analysis on piezoelectric networking for effective multiple harmonic vibration suppression of mistuned bladed disks. The analysis consists of two parts. In the first part, the bladed disk is modeled as a multi-blade periodic system with disk dynamics neglected. A piezoelectric network is designed and optimized analytically after applying the U-transformation technique. The effectiveness of the optimal network for multiple harmonic vibration suppression is demonstrated and compared to the traditional absorber design. Monte Carlo simulation is performed to further examine the effectiveness of the network for mistuned bladed disk systems. Robustness issues associated with key circuitry elements are also investigated. An approach via negative capacitance to improve the system performance and robustness is explored. The analysis shows that the piezoelectric network is quite effective and robust for multiple harmonic vibration suppression of mistuned bladed disks, and the performance and robustness can be further improved by negative capacitance. Based on the analysis in the first part study, we then extend the investigations to a more complex scenario. A bladed disk model with coupled blade-disk dynamics is developed to better describe the actual system and correspondingly, a new multi-circuit piezoelectric network is proposed and optimized analytically for multiple harmonic vibration suppression. The performance and robustness issues of the network are examined numerically via Monte Carlo simulation. Finally, experiments are carried out to demonstrate the multiple harmonic vibration suppression effect of the newly developed piezoelectric network.

**TABLE OF CONTENTS**

# LIST OF FIGURES

# LIST OF TABLES

# ACKNOWLEDGEMENTS

# Chapter 1

## Introduction

### 1.1 Background

Periodic structures have been widely utilized in a variety of engineering applications. Typical examples include multi-span beams, truss structures, bladed disks in turbo-machinery and satellite antenna. These structures are designed to contain repetitive identical substructures that are connected in some certain manner (often referred to as *coupling*) to form a spatial periodicity. In an ideal situation, the substructures are indeed identical in all aspects, including geometrical and mechanical properties; the structure is called *perfectly periodic* (or *tuned*). Modes of a tuned structure are extended sine/cosine wave type without attenuation. Vibration energy is uniformly distributed among its substructures. This dynamic characteristic has been exploited in the modeling of large complex periodic systems, which significantly reduces the analysis and computation efforts. However, in realistic situations, there are always small variations (hereafter referred to as *mistuning*) among the substructures, such as blade-to-blade differences in geometry and mechanical properties. The structure then becomes *nearly periodic* or *mistuned*. Mistuning is small and random, and can be caused by variations in material properties, manufacturing tolerance, in-service degradation, etc. Mistuning breaks the perfect periodicity and can change the dynamic behavior of periodic structures qualitatively. It is well known that *localization* phenomenon could occur when a periodic

structure is mistuned, especially when the coupling among substructures is weak. In a localized mode, modal energy is confined to a small region of the structure, causing increased local amplitude. Figures 1-1 and 1-2 show examples that illustrate the localization phenomenon in free and forced vibrations. The periodic system is a bladed disk structure with 80 substructures (blades). The mode shown in the figure is the $10^{th}$ mode for the tuned and mistuned cases. In general, tuned modes are extended throughout the substructures, just as the one shown in Figure 1-1(a), and mistuned modes are localized, which, depending on the mistuning level and coupling between substructures, could be as localized as the one shown in Figure 1-1(b). As illustrated in Figure 1-1(b), in the mistuned system, high modal amplitude is only concentrated in a small number of substructures (blades). Due to the localization effects caused by mistuning, the dynamic behavior of the periodic structure is also qualitatively changed under force excitation. Figure 1-2 presents an example of the maximum forced vibration response of the tuned and mistuned bladed disk systems under engine order excitation. As shown in Figure 1-2, not only the amplitude pattern of the mistuned system is drastically changed compared to the tuned system, but also the maximum amplitude is increased. Because of this drastic change in forced response, vibration localization can have significant impact on a structure's health. For instance, when localization occurs to a bladed disk system of modern jet engines, the resulting excessively large forced response can lead to accelerated failure of the engine components via high-cycle-fatigue.
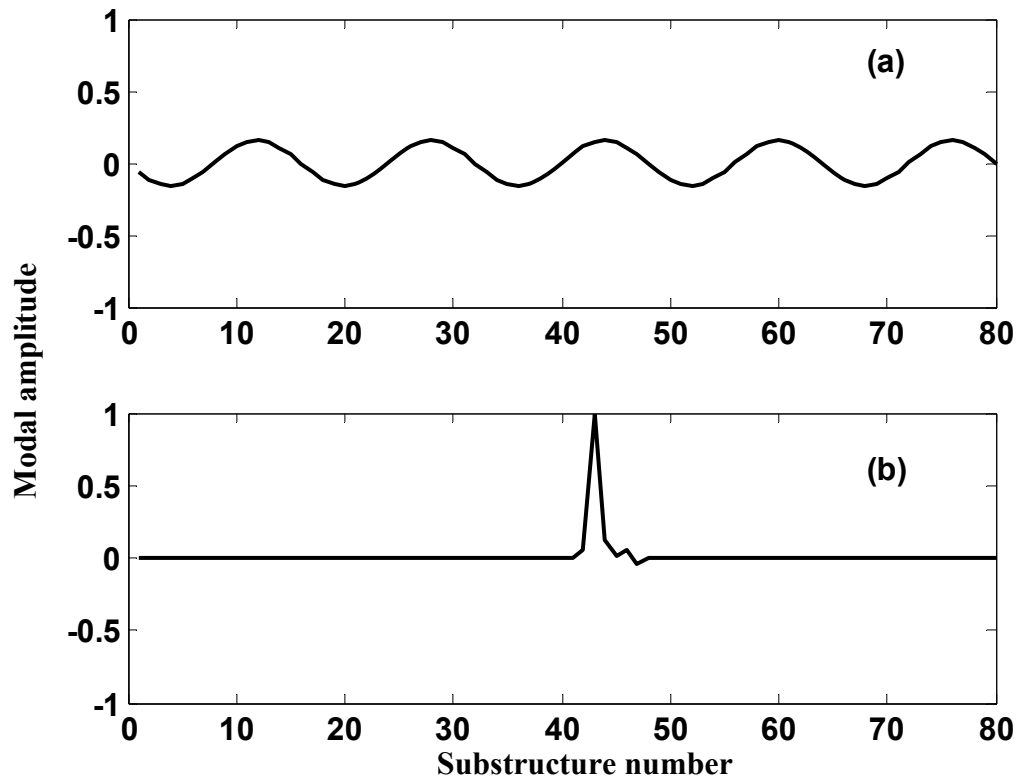
Figure **1-1**: Examples of tuned and mistuned modes (the 10<sup>th</sup> mode) of a periodic system; (a) tuned case; (b) mistuned case.
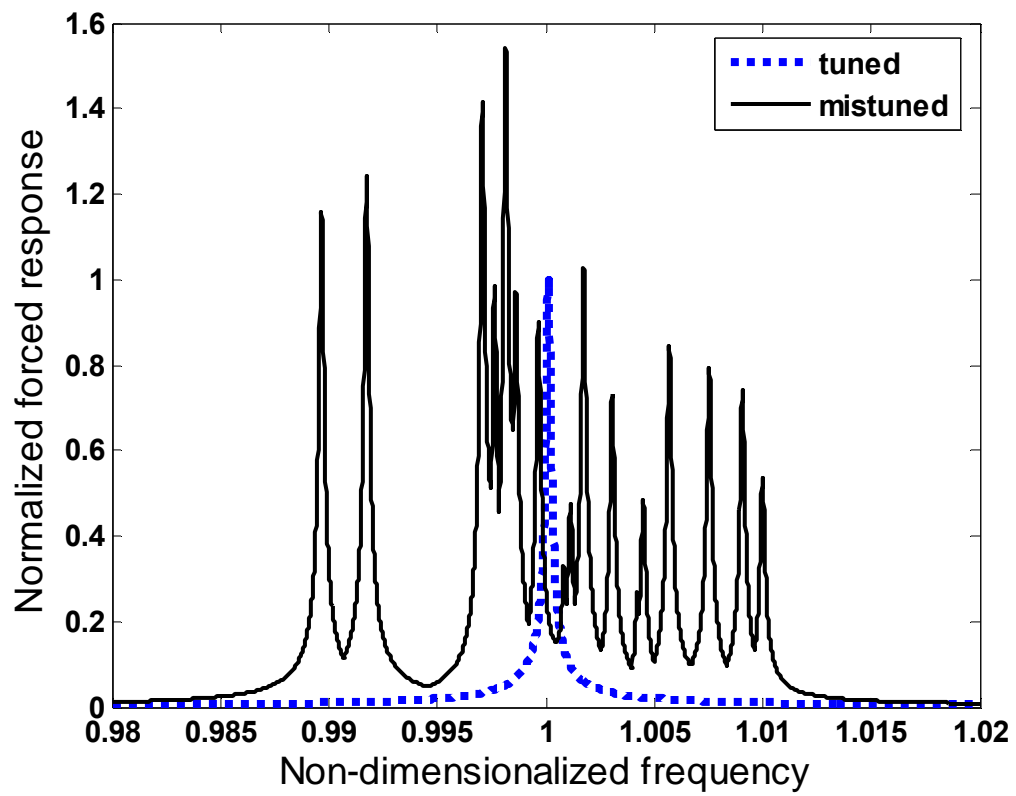
Figure **1-2**:  Examples of forced responses for tuned and mistuned systems.

**1.2 Literature Review**

**1.2.1 Localization in periodic structures**

The localization phenomenon in periodic systems has been extensively studied by researchers and engineers since Anderson's (1958) pioneering work in solid state physics, to name a few, Hodge, 1982; Hodge and Woodhouse, 1983, 1989; Kissel, 1987; Cornwell and Bendikson, 1989; Cai and Lin, 1991; Cha and Pierre, 1991; Bouzit and Pierre, 1992; Lust, et al., 1993; Mester and Benaroya, 1995; Pierre, et al., 1996; Ottarsson and Pierre, 1996; Xie and Ariaratnam, 1996(a,b); Cox and Agnes,1999.

Hodges (1982) was the first to introduce Anderson's localization concept into structural dynamics. Using a set of coupled pendula with randomly varying natural frequencies, Hodge showed that in one dimension all modes are localized for arbitrarily small disorder. Hodge concluded that the degree of localization is dependent on the ratio of disorder strength to the coupling strength. Subsequently, Hodges and Woodhouse (1983) carried out experiments and demonstrated localization phenomenon in a stretched string with masses attached to it. Bendiksen (1987) investigated localization phenomenon in large space structures, and found that weakly coupled structures have high modal densities, and are most likely to have localized modes. Pierre et al. (1987) studied the localization of the modes of disordered multi-span beams both theoretically and experimentally, where they showed small deviation in the span lengths may have drastic effects on the dynamics of the system.

Analysis on localization has been mostly based on the wave propagation theory (Mead, 1975; Cai and Lin, 1991; Pierre et al., 1996). Perfectly periodic structures feature

frequency passband and stopband. Passband is of most interest since most natural frequencies of the tuned periodic system can be found within the passband. Within the passband, wave can propagate throughout the substructures without any attenuation. When mistuning exists, mistuning causes partial reflection of the wave at each bay of the periodic structure, which eventually leads to localization (Pierre et al, 1996). When a wave is localized, wave amplitude is found to decay exponentially for a periodic system with large number of substructures. This decay rate is often referred to as localization factor.

Much research effort has been applied to the calculation of the localization factor. Kissel (1987) used the concept of wave transmission and reflection, and exploited Furstenberg's limit theorem (Furstenberg, 1963) on products of random matrices to state a formula for the frequency dependent localization factor for a generic mono-coupled disordered periodic system. Localization factor in mono-coupled systems has also been calculated using probability theory (Cai and Lin, 1991), stochastic perturbation techniques (Bendiksen, 1987; Pierre et al., 1987; Pierre, 1990), and Monte Carlo numerical simulation (Bouzit and Pierre, 1992). Lyapunov exponent (Kissel, 1991; Castanier and Pierre, 1995; Xie and Ariaratnam, 1996) has been shown to be a good measure of the exponential decay rate of the wave/modal amplitudes, and thus can serve as the localization factor. The Lyapunov exponents of a periodic system (mono-coupled or multi-coupled) can be computed from the global wave transfer matrix that relates the wave amplitude vector at one end of the structure to the wave amplitude vector at the other end. Wolf's algorithm is often used in the calculation of the Lyapunov exponent spectrum (Wolf et al., 1985).

Cyclically periodic structures, such as bladed disk assemblies in turbo-machinery have attracted wide attention in literature (Afolabi, 1985; Wei and Pierre, 1988; Sinha and Chen, 1989; Cornwell and Bendiksen, 1992; Ottarsson and Pierre, 1993; Cha and Pierre, 1997; Kruse and Pierre, 1997; Slater et al., 1999; Bladh et al., 2002; Kenyon and Griffin, 2003; Kenyon et al., 2003). Special interest has been paid to the forced response of mistuned bladed disks which are commonly found in turbo-machinery such as jet engines. The example shown in Figure 1-2 has illustrated that the forced response of mistuned bladed disk can be drastically changed from that of a tuned system due to mistuning. Significant amount of research has focused on the prediction of the maximum forced response (Whitehead, 1966), and on the development of modeling and analysis tools (Sinha and Chen, 1988; Castanier et al., 1997). Few studies have focused on developing methods to reduce the vibration. Since mistuning plays an important role, methods based on intentional mistuning (Castanier and Pierre, 2002) and mistuning pattern optimization (Hou and Cross, 2005) have been proposed. It has been shown that through intentional design of a mistuning pattern, one can reduce the bladed disk's sensitivity to random mistuning, and thereby reduce the forced response.

## 1.2.2 Piezoelectric material based vibration control

Piezoelectric materials, such as lead zirconate titanate (PZT), have been extensively used as sensors and actuators for vibration control because of their numerous merits such as light weight, wide bandwidth, efficient energy conversion, and easy of integration to the controlled structure. These materials can transform mechanical

vibration energy of the structure to which it is bonded or embedded to electrical energy and vise versa. Details about the basic properties and constitutive equations of piezoelectric materials can be found in (IEEE, 1988). Exploiting these materials' energy conversion capability, researchers have developed various schemes for vibration control, such as passive shunts (Forward, 1979; Hagood and von Flotow, 1991; Hollkamp, 1994; Wu, 1999; Behrens et al., 2003), active actuation (Crawley and de Luis, 1987) and active-passive hybrid shunts (Kahn and Wang, 1994; Tsi and Wang, 1996), etc. Comprehensive literature reviews can be found in (Lesieutre, 1998; Tang et al., 2000). For addressing the localization issues, methods using piezoelectric materials have been investigated. Following the principle that higher coupling among substructures will reduce localization, Gordon and Hollkamp (2000) investigated the potential of utilizing piezoelectric strain actuators to increase blade-to-blade coupling of bladed disks, and found that the improvement was marginal. Cox and Agnes (1999), and Agnes (1999) attempted to reduce vibration localization in bladed-disk assemblies by embedding piezoelectric patches to blades with connection in a certain manner. Their studies found that directly shorting the piezoelectric patches had little effect on reducing localization. An inductive element was later added to the shorted piezoelectric patches, where it was observed that this addition could enhance the system coupling. Recently, Tang and Wang (2003) proposed a new approach for vibration delocalization via piezoelectric circuitry networking.

**1.3 Thesis Objectives**

Although promising results for mode delocalization through piezoelectric networking have been shown in (Tang and Wang, 2003), further analytical and experimental investigations through actual circuitry design are needed for thorough understanding of this concept. It is also realized that the performance of the network might be limited by its intrinsic electro-mechanical coupling of piezoelectric transducers. Thus an effective method is needed to increase the electro-mechanical coupling coefficient. Furthermore, vibration suppression using the extended piezoelectric network for mistuned periodic structures has not yet been systematically investigated. Therefore, the goal of this thesis is to advance the state of the art by addressing the following two technical objectives:

(a) To perform investigations on developing piezoelectric networks with enhanced electro-mechanical coupling and utilize them for mode delocalization.

(b) To extend the circuit networking concept for vibration suppression of mistuned periodic structures under spatial harmonic (or engine order) excitations.

Both theoretical analysis and experimental investigation will be performed to provide insight and better understanding related to the piezoelectric networking concept for vibration delocalization and control of nearly periodic structures.

**1.4 Thesis Outline**

The rest of this thesis is organized as follows. In Chapter 2, an analytical study on mode delocalization using the piezoelectric network with enhanced electro-mechanical coupling is presented. The purpose is to examine the piezoelectric networking concept and the idea of negative capacitance for coupling enhancement.

In Chapter 3, experiments are carried out to validate the vibration delocalization concept using the piezoelectric network with enhanced electro-mechanical coupling.

In Chapter 4, the piezoelectric networking concept is extended to address vibration suppression of periodic structures. In this chapter, a simple bladed disk model is adopted. An optimal passive network design is derived analytically. Monte Carlo simulation is used to examine the performance and robustness of the network. An approach using negative capacitance for improvement of the network is investigated.

In Chapter 5, the analysis of piezoelectric networking for vibration suppression of mistuned bladed disk is further extended using a coupled blade-disk model which can better represent the dynamics of an actual system. Based on this model, a new piezoelectric network topology is formulated. The circuitry design is optimized analytically. Monte Carlo simulation is used to examine the performance of this network, and the effect of circuitry parameter variations (mistuning and detuning) on the network. The effect of the negative capacitance on the network's performance and robustness is also examined.

In Chapter 6, experiments are performed to demonstrate the vibration suppression effect of the newly designed piezoelectric network.

Finally, conclusions and recommendations for future work are summarized in Chapter 7.

## Chapter 2

## Mode Delocalization Analysis

### 2.1 Background

It is well known that periodic structures are susceptible to localization effect caused by small mistuning among substructures. The dynamic behavior of a periodic structure can be drastically changed by localization. In a tuned structure, where substructures are identical, modes are extended, vibration energy is uniformly distributed among the substructures. In a mistuned structure, however, modes can become highly localized, especially when the coupling between substructures is weak. Localization could cause severe damage to a structure due to the confinement of vibration energy to a small portion of the whole structure.

While research on the fundamental aspects of localization is extensive, few studies have been performed to develop methods to reduce or control vibration localization in nearly periodic structures. Recently, Tang and Wang (2003) proposed a new approach for vibration delocalization via piezoelectric circuitry networking and showed promising results. An example networking configuration is shown in Figure 2-1. In this case, the original mono-coupled system becomes bi-coupled with an additional electrical coupling. In general, an inductive piezoelectric circuit (*LC* shunt) can absorb vibration energy from the substructure to which it is bonded and store that portion of energy in the electrical form. While in most cases directly increasing the mechanical

coupling between substructures is difficult to achieve due to various design limitations, one can easily introduce strong electrical coupling, such as connecting the *LC* shunts with capacitors ($C_a$) as shown in Figure 2-1(b), to create a new wave channel.  With this coupled piezoelectric circuits design, the otherwise localized vibration energy in a nearly periodic structure can now be transferred into electrical form and propagate in the integrated system through the newly created electro-mechanical wave channel.

## 2.2 Problem Statement and Objective

While the recent investigations (Zhang and Wang, 2002; Tang and Wang, 2003) have illustrated promising delocalization results utilizing piezoelectric networks, the studies are still preliminary.  The concept has not been thoroughly examined via a comprehensive parameter study, and nor has it been realized and validated through actual circuitry design.  Most of all, it was recognized that the effectiveness of the treatment can be limited by the level of the electro-mechanical coupling of the piezoelectric patches. From observing Figure 2-1, one can see that since the electrical coupling established through the external capacitors ($C_a$) can be easily adjusted, the performance bottleneck of the piezoelectric network is the electro-mechanical coupling, i.e., how much mechanical energy can be transferred into electrical energy.  For most of the cases investigated in previous studies, the electro-mechanical coupling coefficient is not high enough to ensure that all the modes are significantly delocalized.  In other words, while the degrees of localization of all the modes were reduced with the treatment, the improvements in some modes were marginal.   This electro-mechanical coupling coefficient is determined by the

piezoelectric material property, the size and the location of patches on the host structures, and the stiffness of the host structures.  Thus it is in general difficult to change with only passive designs.

Based on the above observations, the objectives of this research are (a) to explore the possibility of utilizing an active coupling enhancement approach to increase the system electro-mechanical coupling, such that the effectiveness of the piezoelectric network for delocalization can be further improved; (b) to analyze the integrated system and quantitatively evaluate the delocalization effect; and (c) to implement and validate the proposed concept experimentally.  In this study, the negative capacitance circuit approach (Tang and Wang, 2001) is proposed and investigated for active coupling enhancement.  In this paper, the possibility of increasing the system generalized electro-mechanical coupling coefficient by using negative capacitance is discussed and the relationship between the negative capacitance and the coupling coefficient is presented. An integrated system consisting of a mistuned periodic structure with the piezoelectric network is modeled, and based on this model, the mode shapes of the mistuned system are investigated and the Lyapunov exponents are derived using transfer matrix approach. The correlation between the Lyapunov exponents and the spatial exponential decay of the modal amplitudes is discussed.   A localization index is then defined and used to evaluate the system's delocalization performance in a parameter study.

**2.3 System Model**

To maintain simplicity, the periodic structure considered in this research is assumed to consist of $N$ identical cantilever beams coupled by $N$ springs, as shown in Figure 2-1(a). The lumped springs are used to emulate the coupling effect in a generic periodic structure. Though simple, this model is capable of describing the basic localization phenomenon in periodic structures. The network topology, integrated with the host periodic structure, is shown in Figure 2-1(b).

In this configuration, a piezoelectric patch is embedded in each of the substructures. An inductive shunt circuit (piezoelectric transducer connected in series with an inductor) is applied to each of the substructures in order to absorb the vibration energy and transform it into electric form. Then these individual local circuits are coupled through capacitive elements to form a global network. This network topology creates an additional wave channel, through which the localized vibration energy can be propagated.

**(a)**                                                    **(b)**
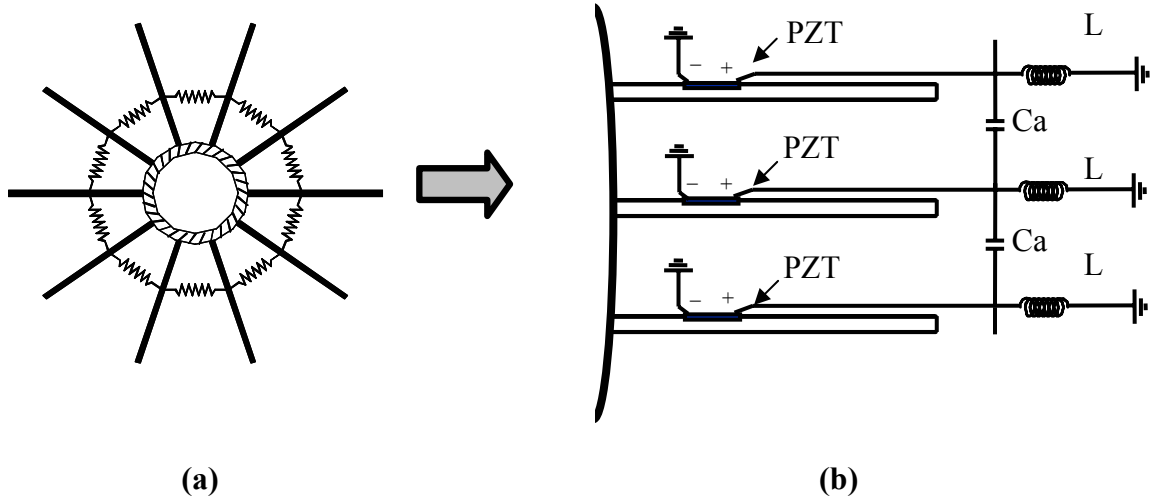
Figure **2-1**: Schematics of (a) mechanical period structure and (b) periodic structure integrated with coupled piezoelectric circuit network.

The system equations of motion can be derived as follows. Let $\phi$ be the first cantilever beam mode of the substructure. The transversal displacement of the $j^{\text{th}}$ beam is approximated as,

$$w_j(x,t) \approx \phi(x)q_j(t) \tag{2.1}$$

The equations of motion for the periodic structure integrated with piezoelectric transducers can be derived using Hamilton's principle (Tang and Wang, 2003), which are,

$$m\ddot{q}_j + c\dot{q}_j + kq_j + k_1 Q_j + k_c(q_j - q_{j-1}) + k_c(q_j - q_{j+1}) = f_j \tag{2.2}$$

$$k_2 Q_j + k_1 q_j = V_j \tag{2.3}$$

where $m$, $c$, $k$, $k_c$, $k_1$ and $k_2$ are, respectively, mass, damping, substructure stiffness, substructure coupling stiffness, cross coupling coefficient related to the electro-

mechanical coupling of the piezoelectric patch, and inverse of the capacitance of piezoelectric patch ($k_2=1/C_{pzt}$), which are given by,

$$m = \int_0^{l_b} \rho_b A_b \phi^2 dx + \int_0^{l_b} \rho_p A_p \phi^2 \Delta H dx \ , \ c = \int_0^{l_b} c_b \phi^2 dx$$

$$k = \int_0^{l_b} E_b I_b \phi''^2 dx + \int_0^{l_b} E_p I_p \phi''^2 \Delta H dx \ , \ k_c = k_s \phi^2 (x_s)$$

$$k_1 = \frac{1}{w_p l_p} \int_0^{l_b} F_p h_{31} \phi'' \Delta H dx \ , \ k_2 = \frac{A_p \beta_{33}}{w_p^2 l_p}$$

Here, $q_j$ and $f_j$ are the generalized mechanical displacement and external force of the $j^{th}$ beam. $Q_j$ and $V_j$ are the charge flowing to and the voltage across the piezoelectric patch attached to the $j^{th}$ beam, respectively. $\Delta H = H(x - x_l) - H(x - x_r)$, where $H(x)$ is the Heaviside step function. $x_l$ and $x_r$ are distances from the piezoelectric patch edges to the root of the cantilever beam, and the length of the patch is thus $l_p = x_r - x_l$. Other relevant notations used here are: $\rho_b$ and $\rho_p$ – density of beam and piezoelectric patch; $A_b$ and $A_p$ – cross sectional area of beam and piezoelectric patch; $E_b$ and $E_p$ – elastic modulus of beam and piezoelectric patch; $I_b$ and $I_p$ – moment of inertial of beam and piezoelectric patch; $l_b$ – length of beam; $w_p$ – width of piezoelectric patch; $F_p$ – moment of area of piezoelectric patch; $c_b$ – beam damping constant; $k_s$ and $x_s$ – stiffness of coupling spring and location of coupling spring; $h_{31}$ – piezoelectric constant; and $\beta_{33}$ – dielectric constant of piezoelectric patch.

Applying circuit network analysis using Kirchhoff's law, the equation for the $j^{th}$ circuit branch can be derived as,

$$V_j = -L\ddot{Q}_j - \frac{L}{k_a} k_2 (2\ddot{Q}_j - \ddot{Q}_{j-1} - \ddot{Q}_{j+1}) - \frac{L}{k_a} k_1 (2\ddot{q}_j - \ddot{q}_{j-1} - \ddot{q}_{j+1}) \qquad (2.4)$$

where $L$ is the circuitry inductance. $k_a = 1/C_a$ denotes the inverse of the coupling capacitance. Substituting Equation (2.4) into Equation (2.3), we can derive the equations of motion of the electro-mechanically integrated system as,

$$m\ddot{q}_j + c\dot{q}_j + kq_j + k_1 Q_j + k_c(q_j - q_{j-1}) + k_c(q_j - q_{j+1}) = f_j \tag{2.5}$$

$$L\ddot{Q}_j + \frac{L}{k_a}k_2(2\ddot{Q}_j - \ddot{Q}_{j-1} - \ddot{Q}_{j+1}) + \frac{L}{k_a}k_1(2\ddot{q}_j - \ddot{q}_{j-1} - \ddot{q}_{j+1}) + k_2 Q_j + k_1 q_j = 0 \tag{2.6}$$

For the original periodic structure without the piezoelectric circuits, the equation of motion is,

$$m\ddot{q}_j + c\dot{q}_j + kq_j + k_c(q_j - q_{j-1}) + k_c(q_j - q_{j+1}) = f_j \tag{2.7}$$

In the above derivation, we assume that the system is perfectly periodic. In reality, however, there will be imperfections. Without loss of generality, in this model we assume that the structural imperfection (mistuning) exists in the stiffness of the substructures, which is the common practice in many localization studies. The stiffness of the $j^{th}$ beam with mistuning is,

$$\tilde{k}_j = k + \Delta k_j \tag{2.8}$$

where $k$ is the nominal stiffness of the perfectly periodic structure, and $\Delta k_j$ is the zero-mean random mistuning in stiffness. In the following we consider harmonic solutions for free vibration, and neglect damping. The equations of motion of the electro-mechanically integrated system can be non-dimensionalized as follows,

$$-\Omega^2 x_j + (1 + \Delta s_j)x_j + R_c^2(x_j - x_{j-1}) + R_c^2(x_j - x_{j+1}) + \delta\xi y_j = 0 \tag{2.9a}$$

$$-\Omega^2[y_j + R_a^2(2y_j - y_{j-1} - y_{j+1}) + \frac{\xi R_a^2}{\delta}(2x_j - x_{j-1} - x_{j+1})] + \delta\xi x_j + \delta^2 y_j = 0 \tag{2.9b}$$

and the equation for the mistuned system without piezoelectric network becomes,

$$-\Omega^2 x_j + (1+\Delta s_j)x_j + R_c^2(x_j - x_{j-1}) + R_c^2(x_j - x_{j+1}) = 0 \qquad (2.10)$$

where the non-dimensionalization parameters are,

$$\omega_m = \sqrt{k/m} \, , \; \omega_e = \sqrt{k_2/L} \, , \; \delta = \omega_e/\omega_m$$

$$\Omega = \omega/\omega_m \, , \; x_j = \sqrt{m}q_j \, , \; y_j = \sqrt{L}Q_j$$

$$\xi = k_1/\sqrt{kk_2} \, , \; R_c = \sqrt{k_c/k} \, , \; R_a = \sqrt{k_2/k_a} \, , \; \Delta s_j = \Delta k_j/k$$

Here $\omega$ and $\Omega$ are the dimensional and non-dimensional harmonic frequencies; $\omega_m$ and $\omega_e$ are the natural frequencies of the uncoupled substructure and circuit, respectively; $\delta$ is the frequency tuning ratio which characterizes the circuitry inductance; $x_j$ and $y_j$ are the non-dimensional generalized mechanical and electrical displacements of the $j^{th}$ substructure and circuit branch respectively; $\xi$ is the generalized electro-mechanical coupling coefficient which reflects the energy transfer capability of the piezoelectric transducer; $R_c$ is the mechanical coupling ratio between the substructures; $R_a$ is the electrical coupling ratio related to the coupling capacitance; and $\Delta s_j$ is the mistuning ratio which is a zero-mean random variable with standard deviation $\sigma$.

## 2.4 Active Coupling Enhancement

The generalized electro-mechanical coupling coefficient ($\xi$) plays an important role in the piezoelectric network delocalization mechanisms, since it characterizes the amount of energy that can be transformed from mechanical into electrical form. Although previous studies have shown promising delocalization results using the

proposed piezoelectric network, it was also recognized that the improvements in some modes were marginal due to the low electro-mechanical coupling coefficient $\xi$. It should be noted that this generalized electro-mechanical coupling coefficient is not the same as the intrinsic coupling factor of the material itself. For piezoelectric materials, the electro-mechanical coupling factor is a non-dimensional number quantifying the energy conversion capability of the materials, the definition of which can be found from (IEEE, 1988). The coupling factor ($k_m$) quantifies the level of coupling at the system level, which can be expressed as (Lesieutre and Davis, 1997): $k_m{}^2 = (c^D - c^E)/c^D$, where $c^D$ is the material stiffness under the open circuit (constant electric displacement) condition and $c^E$ is that under the short circuit (constant electric field) condition. The material coupling factor has different values corresponding to different conditions. For patch application considered in this study (i.e., in the 3-1 direction application where the uniaxial stress is perpendicular to the poling direction), the coupling factor is about 0.35. The largest coupling factor for polycrystalline piezoelectric ceramic materials can be on the order of 0.7, corresponding to energy conversion factor of about 50% (Lesieutre and Davis, 1997). When devices made of piezoelectric materials are integrated to a structure, the generalized electro-mechanical coupling coefficient $\xi$ can be defined at the structural level (Lesieutre and Davis, 1997). The coupling coefficient can be calculated based on the structural open circuit natural frequency ($\omega^D$) and short circuit natural frequency ($\omega^E$):

$\xi = \sqrt{(\omega^D)^2 - (\omega^E)^2}/\omega^D$. This value is in general smaller than the intrinsic electro-mechanical coupling factor of the material itself. The formula of the generalized electro-mechanical coupling coefficient used in this study, $\xi = k_1/\sqrt{kk_2}$, is consistent with the

above definition, which can be easily derived and verified from Equations (2.2) and (2.3)

when the open and short circuit conditions are applied (Tang and Wang, 2001). It is clear

that in a dynamic system, this generalized electro-mechanical coupling coefficient is a

function of the cross coupling term $k_1$, the stiffness of the host structure $k$, and the inverse

of the piezoelectric capacitance $k_2$. To obtain a higher $\xi$, one can either increase $k_1$, or

decrease $k$ and $k_2$. Since $k_1$ is usually fixed once the material type (thus the material

coupling factor), the size and the location of the piezoelectric patch on the host structure

are determined, it is difficult to be increased due to practical limitations. On the other

hand, to increase the generalized electro-mechanical coupling coefficient, one can also

change $k$ and $k_2$. Lesieutre and Davis (Lesieutre and Davis, 1997) proposed a method

using destabilizing mechanical pre-loads to counter the inherent stiffness, thus to reduce

the stiffness $k$ of the host structure, and increase the apparent coupling coefficient.

Although this method is indeed interesting, it might be difficult to implement since it

usually requires pre-conditioning or modification of the host structure. Tang and Wang

(2001) proposed a negative capacitance circuit approach to partially cancel the inherent

capacitance of the piezoelectric patch, which will reduce the electrical stiffness $k_2$ and

increase the coupling coefficient $\xi$. Such an approach can be easily realized utilizing an

electric circuit, which might be much easier to implement than changing $k$ and $k_1$ via

mechanical tailoring. In this study, this negative capacitance approach is adopted to

increase the generalized electro-mechanical coupling coefficient, for the purpose of

enhancing the delocalization performance of the network.

In the formula $\xi = k_1 / \sqrt{kk_2}$, $k_2$ is the inverse of the piezoelectric capacitance $(k_2=1/C_{pzt})$. When a negative capacitance is added in series to the piezoelectric element in the network, the inverse of the total capacitance in each branch of the piezoelectric network becomes,

$$\hat{k}_2 = k_2 - k_n \tag{2.11}$$

where $k_n$ is the inverse of the negative capacitance added $(k_n=1/C_{neg})$. With the negative capacitance, the generalized electro-mechanical coupling coefficient becomes,

$$\xi = k_1 / \sqrt{k\hat{k}_2} \tag{2.12}$$

Since $\hat{k}_2$ is less than $k_2$ (Equation (2.11)), it is obvious that the generalized electro-mechanical coupling coefficient ($\xi$) can be increased by the negative capacitance treatment. However, to ensure stability of the system, there is a limit on the negative capacitance, which is governed by maintaining the positive definiteness of the system generalized stiffness matrix (Equation (2.13)),

$$\begin{bmatrix} k & k_1 \\ k_1 & \hat{k}_2 \end{bmatrix} > 0 \tag{2.13}$$

which means $k\hat{k}_2 > k_1^2$ or $\xi < 1$.

From Equation (2.11), it is clear that $k_n$ must be less than $k_2$, or in other words, the absolute value of the negative capacitance should be larger than the piezoelectric capacitance. The relationship between the generalized electro-mechanical coupling coefficient and the negative capacitance is given in Figure 2-2, where the coupling coefficient for the original system without negative capacitance is assumed to be 0.1, and

the ratio of $k_n/k_2$ is referred to as the *negative capacitance ratio*. It can be seen that the coupling coefficient can increase monotonically and nonlinearly as the negative capacitance ratio ($k_n/k_2$) increases. The closer the negative capacitance value is to the piezoelectric capacitance, i.e., the closer the negative capacitance ratio ($k_n/k_2$) is to 1, the larger the coupling coefficient would be. However, in practice, the circuit will be vulnerable to instability as the ratio gets closer to 1, as indicated by Equation (2.13). The negative capacitance cannot be realized passively and one needs to use an operational amplifier to form a negative impedance converter circuit that requires a power source. Therefore, this approach is referred to as an active coupling enhancement approach.
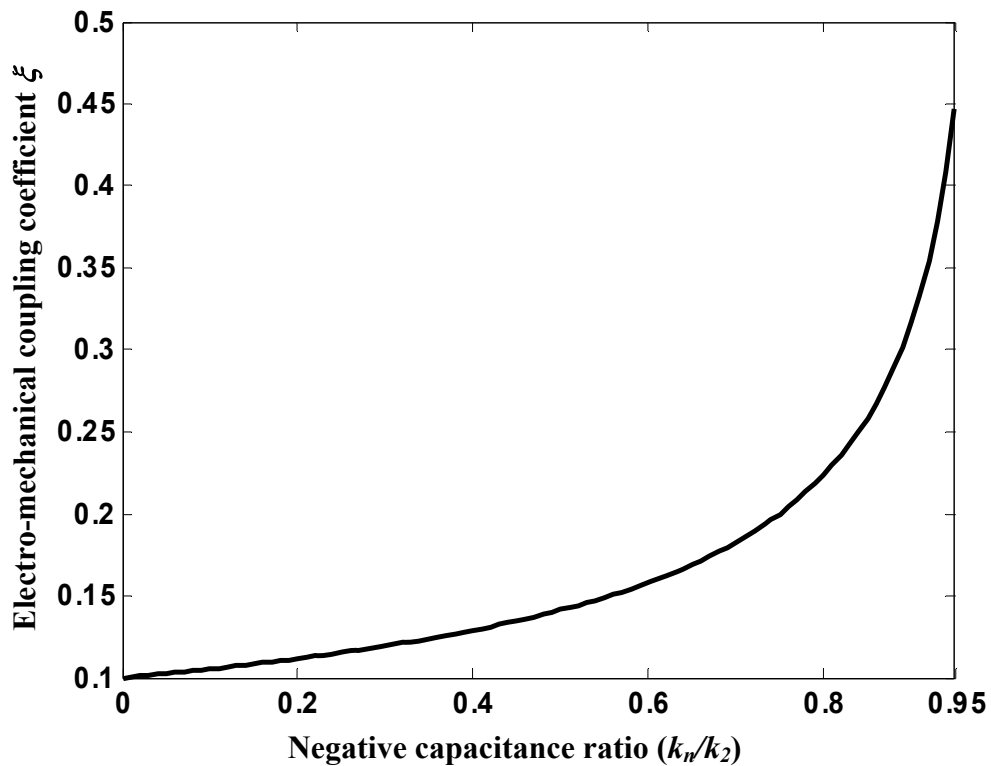
Figure **2-2**: Effect of negative capacitance on the electro-mechanical coupling coefficient.

**2.5 Integrated System Analysis**

As indicated earlier, the localization phenomenon in mistuned periodic structures has been analyzed extensively in the past. The probabilistic nature of the localization phenomenon was recognized and stochastic methods were applied to study the spatial exponential decay rate of the vibration amplitude (Hodges and Woodhouse, 1983; Kissel, 1991; Pierre et al, 1996). Lyapunov exponents calculated from the global stochastic wave transfer matrix have been introduced to approximate the spatial exponential decay rate of the amplitude, and have been demonstrated as a good measure of the localization level (Kissel, 1991; Castanier and Pierre, 1995; Pierre et al., 1996; Xie and Ariaratanam, 1996(a,b)). The wave transfer matrix method and the numerical computation of the Lyapunov exponents for multi-coupled periodic structures have been discussed by Pierre et al. (1996). To formulate the wave transfer matrix expression for the periodic system, a displacement state vector is defined for each bay (a bay consists of two adjacent substructures). Then the transfer matrix that relates the dynamics of two adjacent bays can be derived from the equations of motion. The dimension of the state vector is always twice of the number of inter-bay coupling coordinates $n$, and the dimension of the square transfer matrix is $2n$ by $2n$, which is independent of the number of substructures $N$. The wave transfer matrix for the original system without piezoelectric network can be found in (Tang and Wang, 2003). Below, only the formulation for the system with integrated piezoelectric network is presented. This integrated system is bi-coupled, thus the number of inter-bay coupling is $n=2$, and the dimensions of the displacement state vector and transfer matrix are $4 \times 1$ and $4 \times 4$, respectively. The $4 \times 1$ displacement state vector for

the $j^{\text{th}}$ bay, consisting of both mechanical and electrical generalized displacements from the $j^{\text{th}}$ and the $j+1^{\text{th}}$ substructures, is defined as:

$$\mathbf{u}_j = \begin{bmatrix} x_{j+1} & y_{j+1} & x_j & y_j \end{bmatrix}^{\text{T}} \tag{2.14}$$

The system equations in Equations (2.9(a)) and (2.9(b)) can be rewritten into the transfer matrix expression using the displacement state vector:

$$\mathbf{u}_j = \mathbf{T}_j \mathbf{u}_{j-1} \tag{2.15}$$

where $\mathbf{T}_j$ is the $4 \times 4$ transfer matrix given by Equation (2.16):

$$\mathbf{T}_j = \begin{bmatrix} \dfrac{1+2R_c^2+\Delta s_j-\Omega^2}{R_c^2} & \dfrac{\delta\xi}{R_c^2} & -1 & 0 \\[2ex] -\left(\dfrac{\delta\xi}{\Omega^2 R_a^2}+\dfrac{\xi}{\delta}(\dfrac{1+\Delta s_j-\Omega^2}{R_c^2})\right) & -\left(\dfrac{\delta^2}{\Omega^2 R_a^2}-(2+1/R_a^2)+\dfrac{\xi^2}{R_c^2}\right) & 0 & -1 \\[2ex] 1 & 0 & 0 & 0 \\[1ex] 0 & 1 & 0 & 0 \end{bmatrix} \tag{2.16}$$

Obviously, the transfer matrix is random for mistuned structures because of the random mistuning $\Delta s_j$. For tuned structures, $\Delta s_j=0$, and $\mathbf{T}_j$ is identical for all $j$'s. A Lyapunov exponent is defined as:

$$\gamma(\mathbf{u}_0) = \lim_{N\to\infty} \frac{1}{N}\log\|\mathbf{u}_N\| \tag{2.17}$$

where $\mathbf{u}_0$ is the initial displacement state vector and $\mathbf{u}_N$ is the displacement state vector of the $N^{\text{th}}$ substructure. It can be shown that the Lyapunov exponent can be calculated from the product of the transfer matrices (Tang and Wang, 2003):

$$\gamma_k = \lim_{N\to\infty} \frac{1}{N}\log\left\{\sigma_k(\prod_{j=N}^{1} \mathbf{T}_j)\right\} \tag{2.18}$$

where $\sigma_k(\cdot)$ denotes the singular value operator.

In this study, the Lyapunov exponents of the bi-coupled periodic structure integrated with piezoelectric network are calculated using the Wolf's algorithm (Wolf et al., 1985). The number of Lyapunov exponents equals to twice of the number of coupling coordinates. For this bi-coupled system, there are four Lyapunov exponents in total. In fact, these Lyapunov exponents appear in pairs, with same magnitude but opposite signs, $\pm|\gamma|$. For a periodic structure, both these positive and negative Lyapunov exponents share the same physical meaning. Therefore, calculating the positive Lyapunov exponents is sufficient to identify the entire spectrum. In the following discussion, *Lyapunov exponents* by default refer to the positive ones unless otherwise noted.

For this study, the structural damping and circuitry resistance are neglected so that the vibration localization effect can be clearly identified. The original periodic structure without piezoelectric network is a mono-coupled system, so there is only one Lyapunov exponent and mode localization can be directly evaluated by the Lyapunov exponent, as demonstrated in (Pierre et al., 1996) and (Tang and Wang, 2003). For the periodic structure with the piezoelectric network treatment, the introduction of the strong electrical coupling enabled by the capacitors between the local shunt circuits creates another wave channel. Therefore, the system becomes bi-coupled; and there are two Lyapunov exponents at each frequency. Figures 2-3 to 2-5 show the Lyapunov exponents for the tuned and mistuned ($\sigma = 0.01$) systems with parameters $\xi$=0.1, $R_a$=0.6, $\delta$ =1.2, and $R_c$= 0.005. Here Figure 2-3 is for the tuned case, Figure 2-4 is for the mistuned case and Figure 2-5 provides a zoom-in view around $\Omega$=1 for both the tuned and mistuned cases. The two Lyapunov exponents are referred to as upper and lower branches in Figures 2-3

to 2-5.  For this system, as indicated in Figure 2-3, there are two separate passbands (referred to as passband 1 and passband 2) for the tuned case.  The natural frequencies are found to be inside the passbands.  It is well known that mode shapes of the tuned system are extended without attenuation throughout the substructures, or in other words, having zero decay rates.  This characteristic of tuned system is captured by the zero Lyapunov exponents in the passbands.  When the system has mistuning, there are no longer any passbands; and the lower Lyapunov exponent branch becomes non-zero (see the lower dotted line in Figure 2-5), indicating mode localization caused by mistuning.  When localization occurs, the localized modal amplitudes will have a spatial exponential decay, the rate of which can be approximated by the lower one of the two Lyapunov exponents in the original separate passbands.
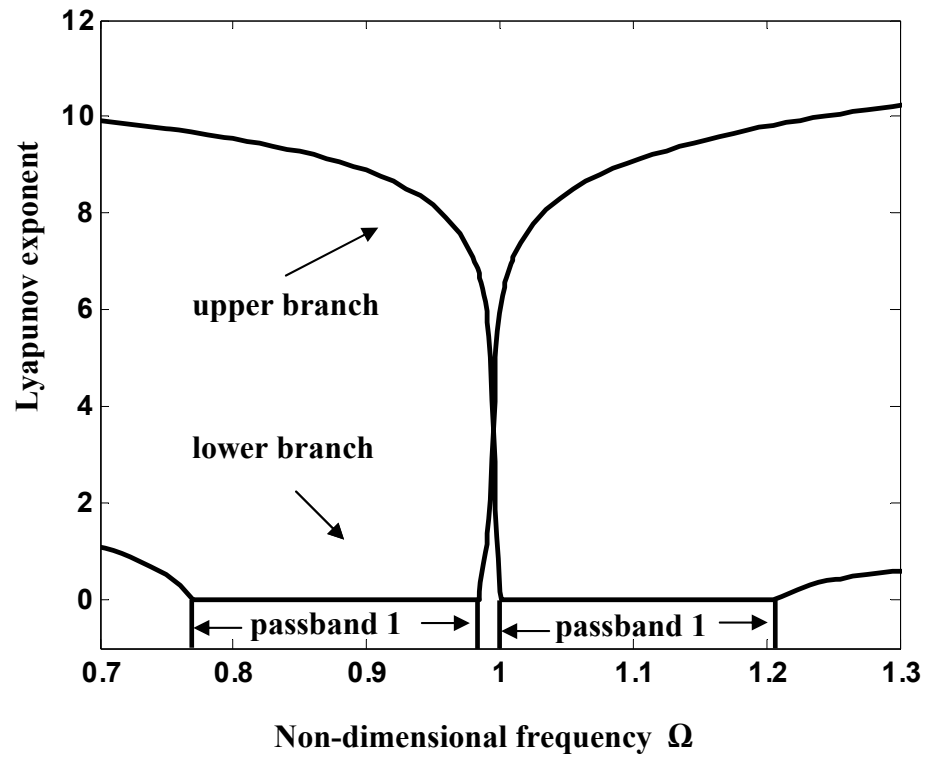
Figure **2-3**: Lyapunov exponents for the tuned system with piezoelectric network.
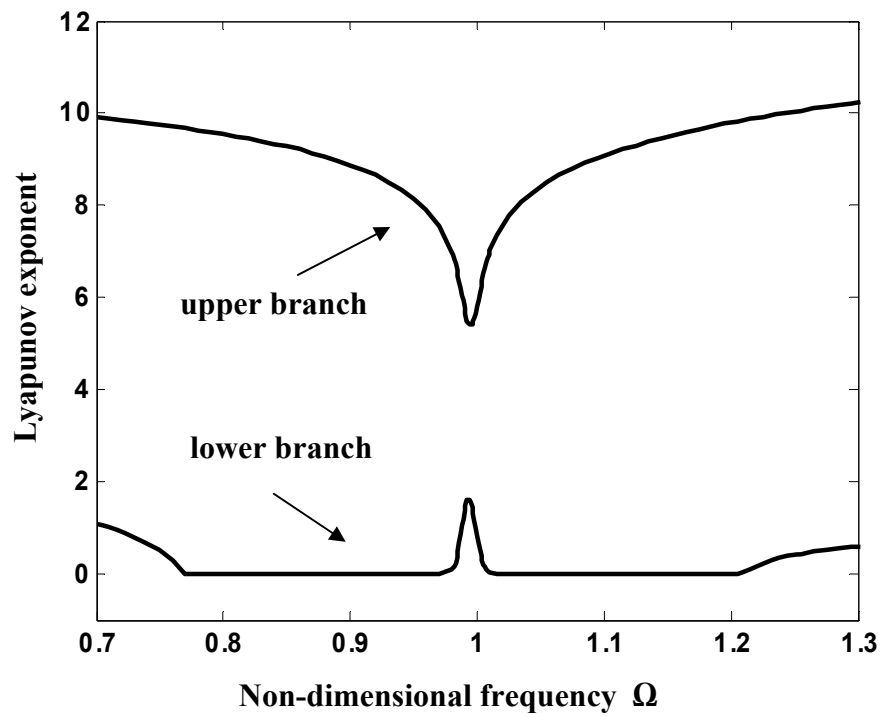
Figure **2-4**: Lyapunov exponents for the mistuned system with piezoelectric network.
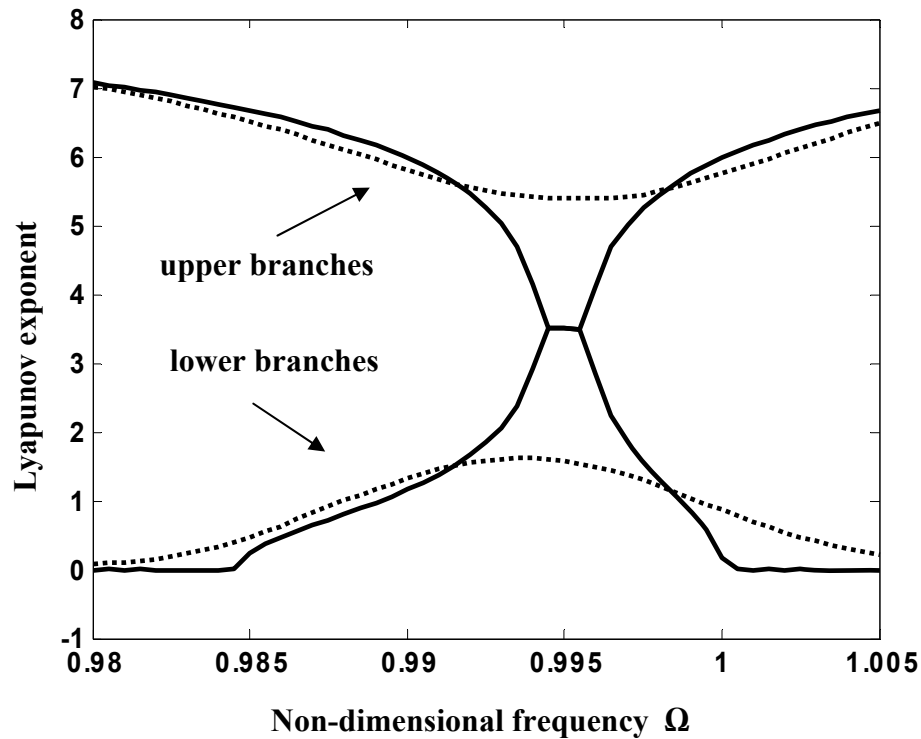
Figure **2-5**: Lyapunov exponents for the tuned and mistuned systems with piezoelectric network.

To support the above argument, the correlation of the modal amplitude exponential decay rates and the lower Lyapunov exponents is studied.  In the following analysis, mode shapes of the mistuned periodic structure with piezoelectric network are obtained by solving the eigenvalue problem of the system, the parameters of which are the same as those used for Figures 2-3 to 2-5.  For modal analysis, the mistuned periodic structure is assumed to have $N$=80 substructures.  To demonstrate the exponential decay of the modal amplitudes, the substructure whichever has the highest amplitude is chosen as the $1^{st}$ substructure.  Two examples are demonstrated in Figure 2-6.  Amplitudes of

two modes are shown, the 70th mode with natural frequency of $\Omega$=0.9832, which lies in the original passband 1 and the 93rd mode with natural frequency of $\Omega$=1.0006, which lies in the original passband 2. The amplitudes of the 70th mode in logarithm scale are plotted with dotted line. It is shown that the modal amplitudes decay exponentially throughout the first half of the substructures. Actually, the exponential growth in the second half of the substructures can be seen as exponential decay at the same rate towards the other direction, due to the cyclic nature of the periodic structure. At its natural frequency $\Omega$=0.9832, the upper and lower Lyapunov exponents are computed to be 6.6969 and 0.2720 respectively. The dash-dotted line is a straight line with a slope of -0.2720, which is directly related to the lower Lyapunov exponent. It can be seen that the exponential decay rate for the 70th mode is well captured by this straight line, which means, the lower Lyapunov exponent can characterize the exponential decay of the modal amplitude. Another example is the 93rd mode, with natural frequency of $\Omega$=1.0006. At this frequency, the upper and lower Lyapunov exponents are calculated to be 5.8572 and 0.7202, respectively. The modal amplitudes in natural logarithm scale are plotted with solid line in Figure 2-6. The dashed straight line has a slope of -0.7202, which is corresponding to the lower Lyapunov exponent at this frequency. Obviously, this straight line can approximate the spatial exponential decay of the mode amplitudes very well. Based on the correlation study, we conclude that it is the lower Lyapunov exponent that can characterize the exponential decay of the mode localization for the mistuned system. Therefore, the lower Lyapunov exponent can be served as a measure to quantify the level of the modal localization.
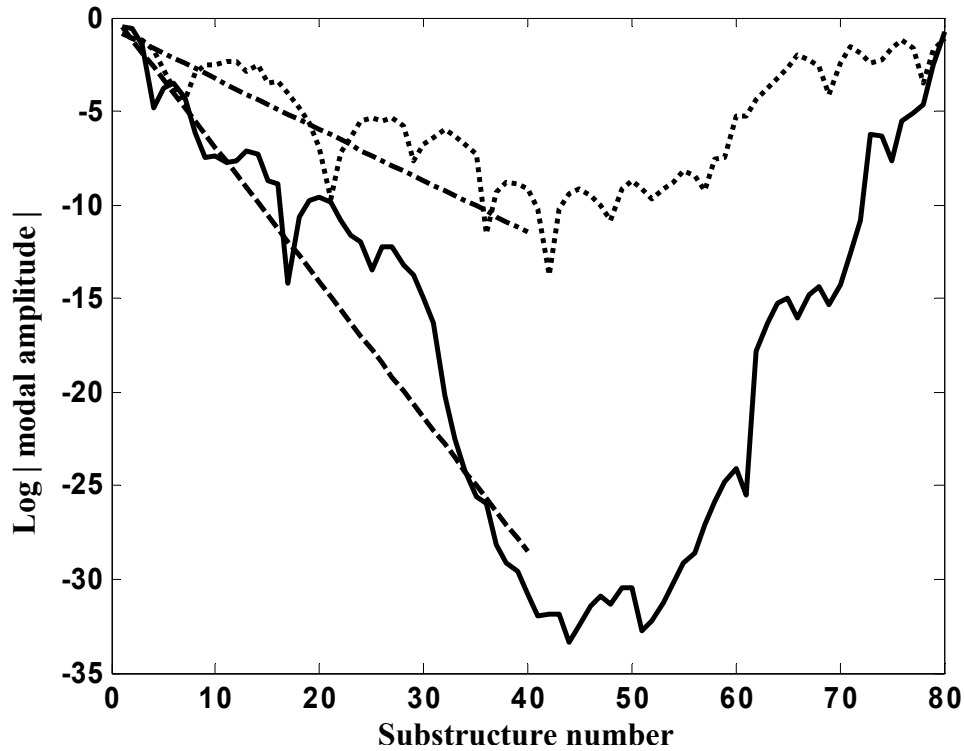
Figure **2-6**: Correlation of modal amplitudes exponential decay rates to the lower Lyapunov exponents. Solid line: modal amplitude of the 93rd mode ($\Omega$=1.0006); Dashed line: straight line with slope (-0.7202) corresponding to the lower Lyapunov exponent at $\Omega$=1.0006. Dotted line: modal amplitude of the 70th mode ($\Omega$=0.9832); Dash-dotted line: straight line with slope (-0.2720) corresponding to the lower Lyapunov exponent at $\Omega$=0.9832.

From the above argument, a mode localization index can be defined as the average of the lower Lyapunov exponents of the mistuned system within the frequency range where the original tuned system exhibits two separate passbands. The effect of negative capacitance on mode delocalization performance of the piezoelectric network

can now be evaluated using the defined index. In the following parametric study, the average of the lower Lyapunov exponents is taken over fifty frequency points in each passband. As discussed earlier, the introduction of negative capacitance into the piezoelectric network can increase the generalized electro-mechanical coupling coefficient $\xi$. To examine the consequence of this coupling enhancement, a single case is first illustrated. In this case study, the system parameters are set to be $R_a$=0.5, $\delta$=0.5, $R_c$=0.005, $\sigma$=0.01. It is shown in Figure 2-7 that the localization index decreases as the electro-mechanical coupling coefficient is increased by adding the negative capacitance. Without negative capacitance ($\xi = 0.1$), the localization index is more than 0.6; with negative capacitance, as the electro-mechanical coupling coefficient $\xi$ is increased, the localization index can be reduced to as low as below 0.1. This reduction in localization index indicates that the level of localization is further reduced by the addition of the negative capacitance.
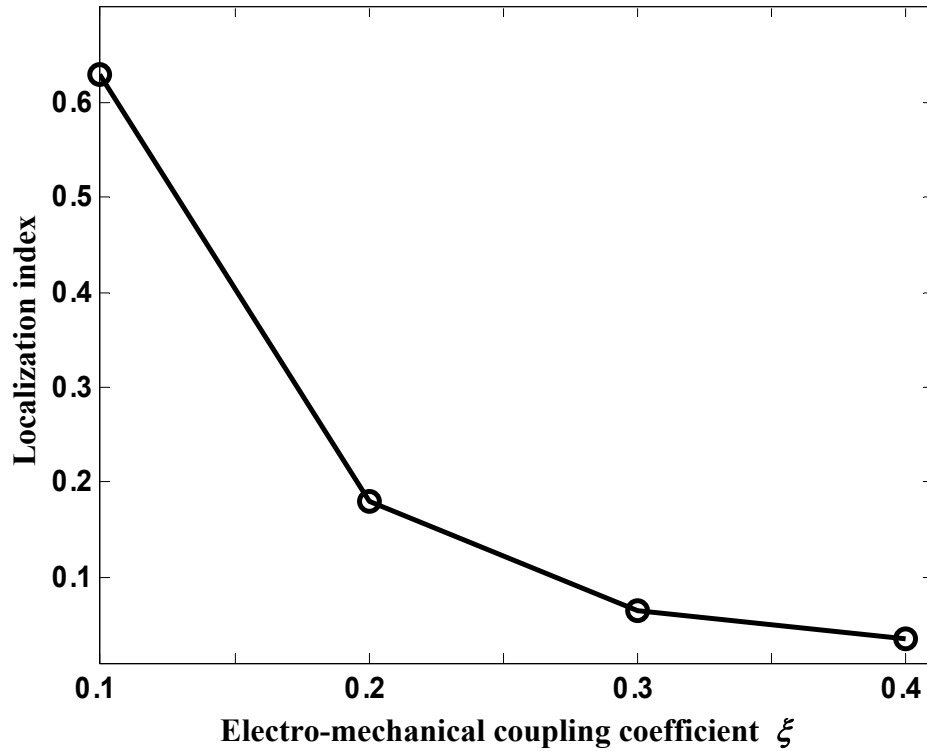
Figure **2-7**:  Localization index versus electro-mechanical coupling coefficient $\xi$ for the mistuned system ($R_a = 0.5$, $\delta = 0.5$, $R_c = 0.005$, $\sigma = 0.01$).

To gain more insight, a more extended parameter study on the effect of negative capacitance on the delocalization performance of the system is carried out using the localization index.   The system parameters $\xi$, $R_a$ and $\delta$   are varied within realistic application ranges, which cover the operation parameter region of the experimental study (see next section).  Figure 2-8 and Figure 2-9 show the contour plots of the localization index versus $\xi$  and $R_a$ (or $\delta$).  In Figure 2-8, $\delta$ is fixed at 0.5, $\xi$ and $R_a$ are varied.  In Figure 2-9, $R_a$ is fixed at 1.2, $\xi$ and $\delta$ are varied.   As shown in both of these two figures,

the localization index tends to decrease as $\xi$ increases. These results indicate that as a consequence of increasing the electro-mechanical coupling coefficient by negative capacitance, the delocalization performance of the piezoelectric network can be improved. Physically, this is because by increasing the system electro-mechanical coupling coefficient one could increase the capability of energy transformation, thereby more localized mechanical energy can be transferred into electrical form and propagate throughout the network.
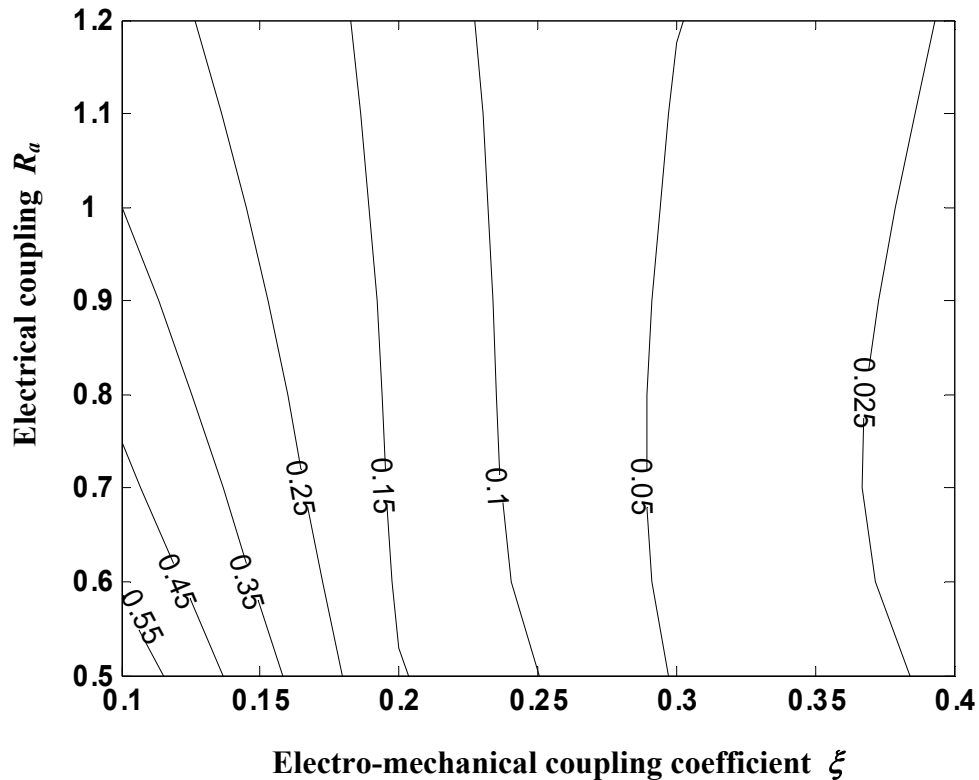


Figure **2-8**: Contour plot of localization index versus $R_a$ and $\xi$ for the mistuned system ($R_c$=0.005, $\delta$ =0.5, $\sigma$ =0.01).
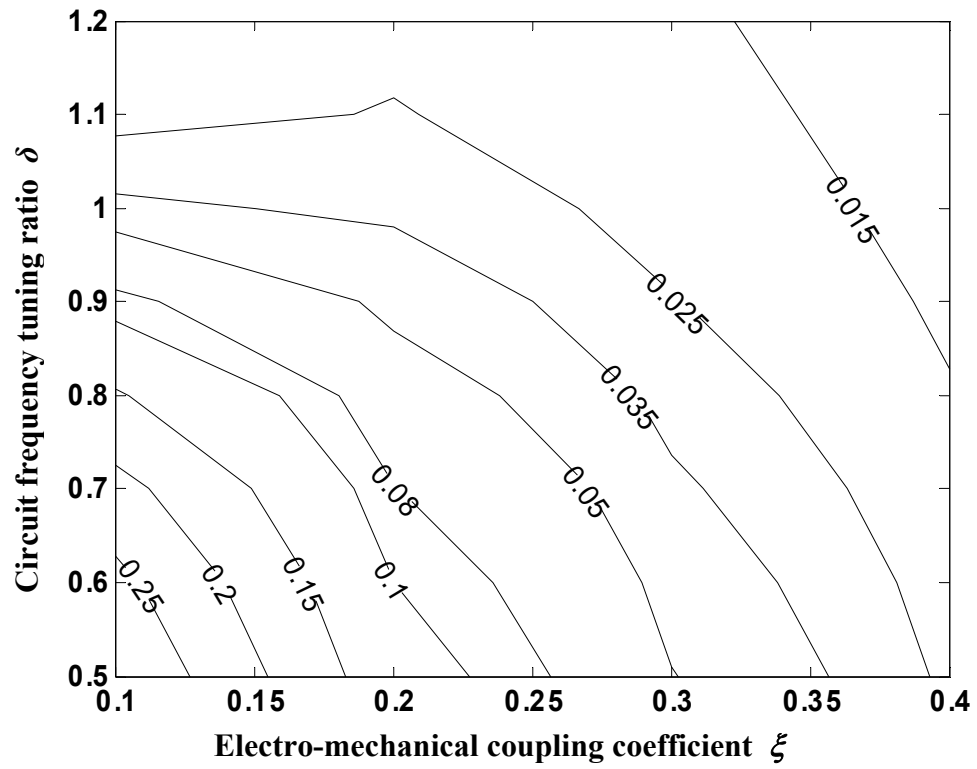
Figure **2-9**: Contour plot of localization index versus $\delta$ and $\xi$ for the mistuned system ($R_c$=0.005, $R_a$ =1.2, $\sigma$ =0.01).

## 2.6 Summary

This research presents vibration delocalization study of nearly-periodic structures using piezoelectric networks with negative capacitance circuitry for active coupling enhancement. The correlation between the Lyapunov exponents and the spatial exponential decay of the modal amplitudes is studied. A localization index is defined for the bi-coupled nearly periodic system and applied to evaluate the effectiveness of the proposed scheme. With this localization index, parametric study is performed where it is found that the negative capacitance circuit approach can greatly enhance the system's ability for vibration delocalization. The negative capacitance can effectively increase the electro-mechanical coupling coefficient, such that more localized mechanical energy can be transferred into electrical form and eventually distributed through the strongly coupled electrical circuits.

## Chapter 3

## Mode Delocalization Experimental Investigation

## 3.1 Objective

In this investigation, experiments are conducted to validate the concept of mode delocalization using piezoelectric network, as studied in Chapter 2. The effect of negative capacitance on the delocalization performance of the network is also examined.

## 3.2 Experimental Setup

The overall experimental setup is shown in Figure 3-1. The mistuned bladed disk is vertically bolted at the hub disk center to a fixture mounted on an isolation table. A shaker is used to provide excitation at the disk hub. Tip displacements of the blades are measured by a laser vibrometer (OFV-303, Polytec Germany), which converts the displacement information into a voltage related output (calibrated in $\mu$m/Volt or $10^{-6}$ meter/Volt). This voltage related output is then recorded by an HP35665A analyzer. The resolution of the vibrometer could be as high as 0.5 $\mu$m/Volt. The laser vibrometer is mounted on two perpendicular stages (X-Y stages as shown in Figure 3-1), which, controlled by LabVIEW programs, can precisely locate the measurement point on each blade tip. The bladed disk specimen with 18 equally spaced blades is fabricated from a single piece of aluminum alloy plate (figure and dimension are listed in Table 3-1), which is mistuned in nature due to manufacturing tolerances. Each blade is bonded with an

identical piezoelectric patch (type 5A, APCI, Ltd., properties shown in Table 3-2) at its
root.

Table **3-1**: Figure and Dimensions of the Bladed Disk Model



| Dimensions ($10^{-2}$m) |
| --- |
| Inner (hole) diameter of the hub disk: 3.81 |
| Outer diameter of the hub disk: 8.89 |
| Length of blade: 10.80 |
| Width of blade: 0.77 |
| Thickness of blade: 0.32 |

Table **3-2**: Geometric Parameters and Material Properties of Piezoelectric Patches

| Geometry ($10^{-2}$m) | | Material Property | |
| --- | --- | --- | --- |
| Length: | 2.54 | Piezoelectric material: | Type 5A |
| | | Relative dielectric constant $K^T$: | 1750 |
| Width: | 0.76 | Electro-mechanical coupling factor $k_{31}$: | 0.36 |
| | | Piezoelectric charge constant: | $175*10^{-12}$ (m/V) |
| Thickness: | 0.10 | Young's modulus: | $6.3*10^{10}$ (N/m$^2$) |
| | | Capacitance ($C_p$): | 3.3 nF |
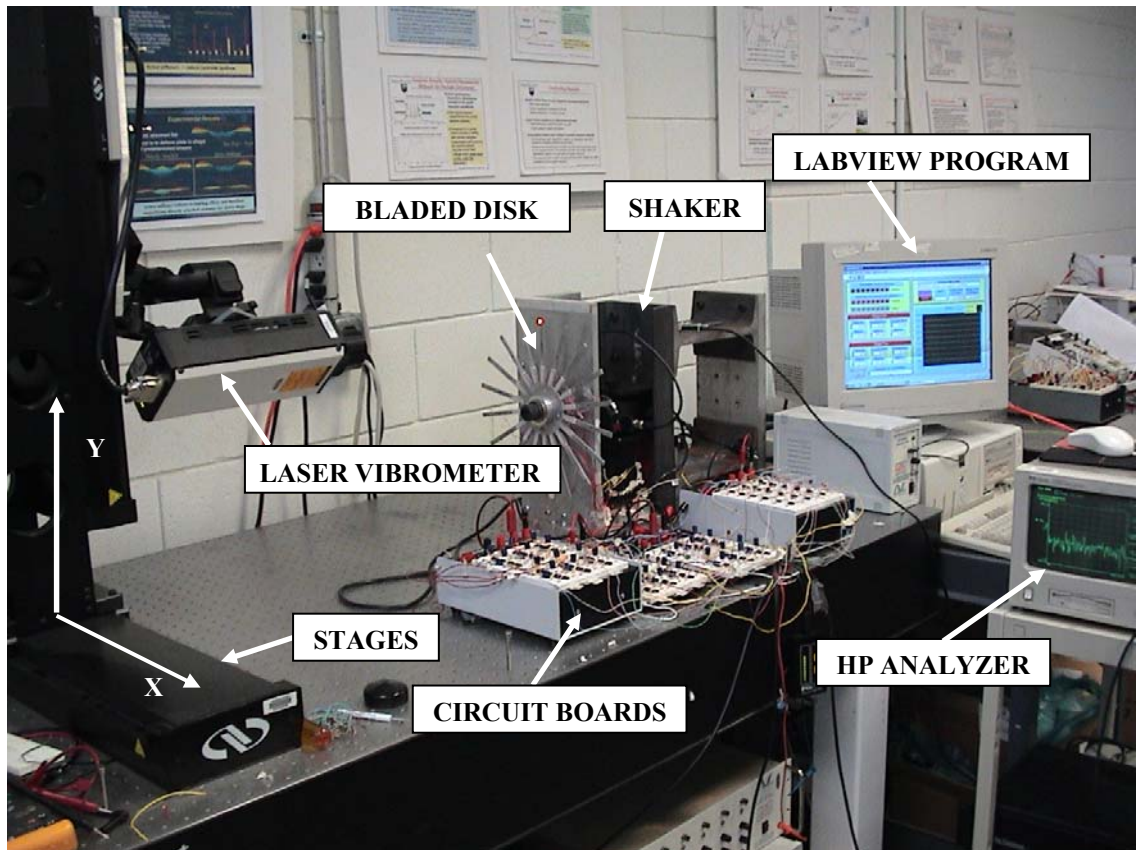
Figure **3-1**: Overall experimental setup.

The bonding process of the piezoelectric patches also contributes to the mistuning of the bladed disk. Therefore, the term *mistuned bladed disk* in the following experiment context refers to the bladed disk with piezoelectric patches attached to it. Each piezoelectric patch has a negative electrode wrap-up design, which improves the bonding effectiveness and provides convenience in wiring. The patches are electrically insulated from the aluminum blades since later on the negative capacitance circuits will be inserted between the piezoelectric patches and the ground. The piezoelectric circuit network is synthesized and integrated with the bladed disk as shown in Figure 2-1(b). Each passive

piezoelectric patch is connected in series with a synthetic inductor to form an *LC* shunt circuit. Then these 18 shunt circuits are coupled through capacitors ($C_a$) each with a value of 2.2 nF (corresponding to non-dimensional $R_a$=1.2, as studied in Figure 2-9).

The circuit diagrams of the synthetic inductor (Chen, 1986) and negative capacitor are shown in Figure 3-2 and Figure 3-3. From Figure 3-2, the equivalent inductance value can be calculated as $L=R_1R_0 C_1$ (Henry). In principle, any desired inductance value can be achieved by adjusting one component in the circuit, i.e., the potentiometer ($R_0$), with the other eight components fixed at appropriate values ($R_1$ and $C_1$). The negative capacitance circuit is essentially a Negative-Impedance Converter (NIC) (Horowitz and Hill, 1989). From Figure 3-3, the equivalent negative capacitance value can be expressed as $C_n = - R_2 C_2 / R_2 = - C_2$. In order to increase the electro-mechanical coupling coefficient, each negative capacitance circuit will be connected in series with each piezoelectric patch. Since the negative capacitance circuit needs to be grounded, it is inserted between the negative electrode of each piezoelectric patch and the ground.
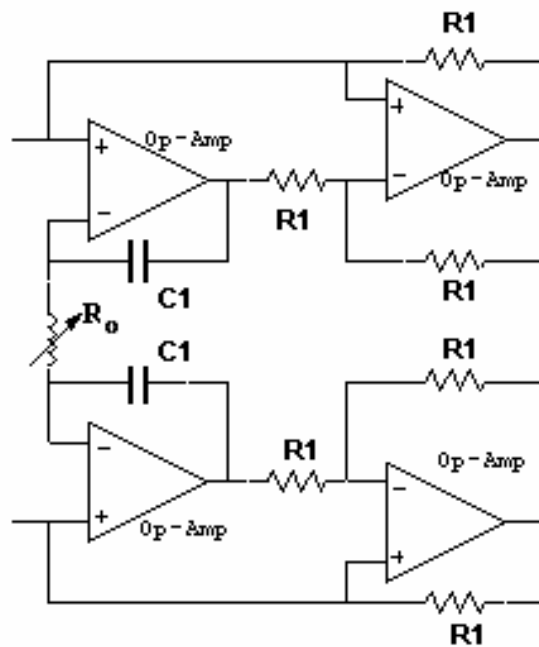
Figure **3-2**: Circuit diagram of the synthetic inductor.
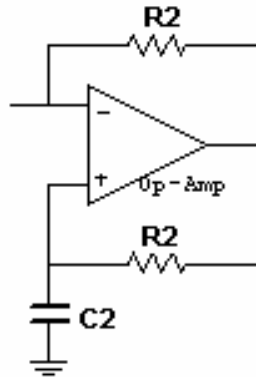
Figure **3-3**:  Circuit diagram of the negative capacitor.

## 3.3 Experimental Results

A sample frequency response function (FRF) of the mistuned bladed disk is shown in Figure 3-4.  The figure shows high modal density within the frequency range from 190 Hz to 250 Hz, which is a characteristic feature of mistuned periodic structures. Due to this feature, it is very difficult to obtain mode shapes using common modal analysis methods.  Therefore, alternatively, the amplitudes of blade tips when the bladed disk is under harmonic excitation at resonant frequencies are chosen as comparison objectives in evaluating the delocalization effect of the piezoelectric circuit network.  To excite the bladed disk at resonance, a series of frequencies within the range of 190 Hz to

250 Hz, most of which are where FRF exhibits a resonant peak, are used for sine wave excitations.
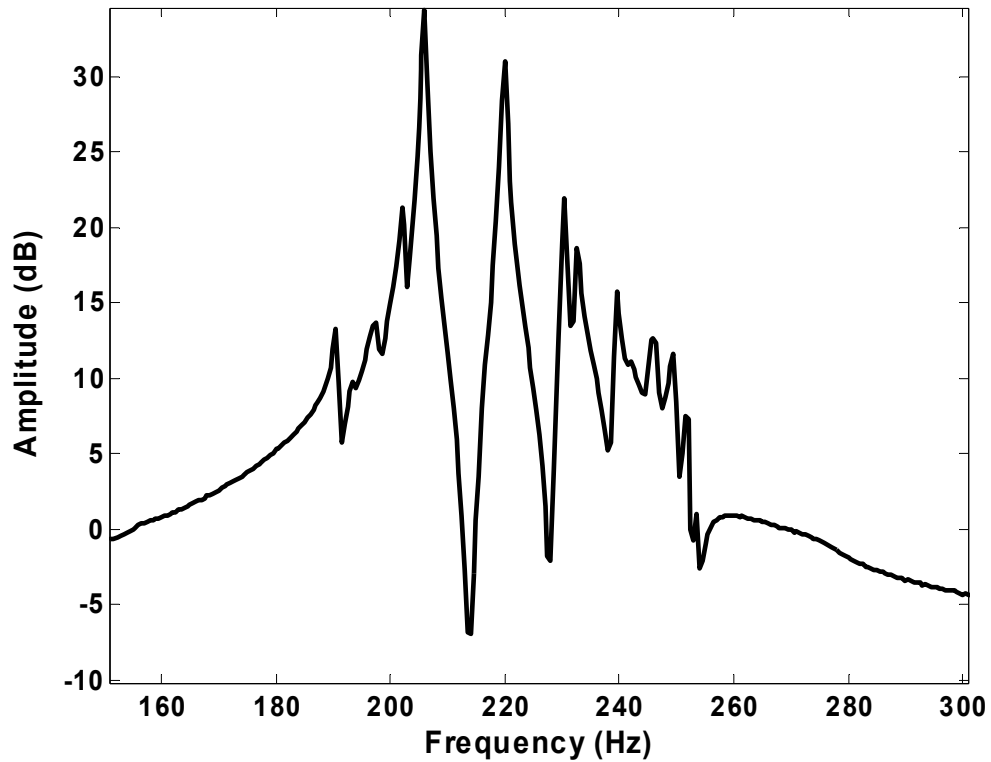


Figure **3-4**: Sample frequency response of the mistuned bladed disk without circuit network.

In the preliminary test, it is found that under excitation frequency of 193.5 Hz and 202.3 Hz, the amplitude distribution shows obvious localization phenomena, illustrated by the dotted lines in Figure 3-5 and Figure 3-7.  In this investigation, we will thus focus our attention around these two resonant frequencies, and compare the amplitude distribution of the mistuned bladed disk with and without piezoelectric circuit network.

**3.3.1 Results of network without negative capacitance**

First, the mistuned bladed disk without circuit network is excited at 193.5 Hz. The tip displacements of all the 18 blades are measured with the laser vibrometer. Then the circuit network is connected to the piezoelectric patches on the bladed disk. The network has 18 synthetic inductors tuned to the same value. The circuit frequency, defined as $f_e = 1/\sqrt{LC_p}/2\pi$ (Hz), where $C_p$ is the piezoelectric capacitance, can be tuned to different values by adjusting the synthetic inductance ($L$). Six different circuit frequency tunings are investigated, ranging from 193.5 Hz to 234 Hz (corresponding to the non-dimensional parameter $\delta$ of range 0.88 ~ 1.06, which is covered in Figure 2-9), as shown in Figure 3-5. At each circuit frequency, the resonant response amplitudes of the blade tips are measured. These amplitudes are plotted in Figure 3-5 for the mistuned bladed disk with and without circuit network. The amplitude data shown in this figure reflect the "*relative amplitude*" (the relative amplitude of each blade is defined to be the difference between its absolute amplitude and the lowest amplitude among all the 18 blades), which also applies to all other figures showing amplitude hereafter. It should be noted that when the piezoelectric circuit network is connected to the mistuned bladed disk, the resonant frequencies are slightly changed. In order to maintain the resonant excitation, for each particular circuit frequency tuning ($f_e$), the new resonance of the system is identified and the structure is excited at the new resonant frequency. This also applies to the case when negative capacitance circuits are introduced into the network.
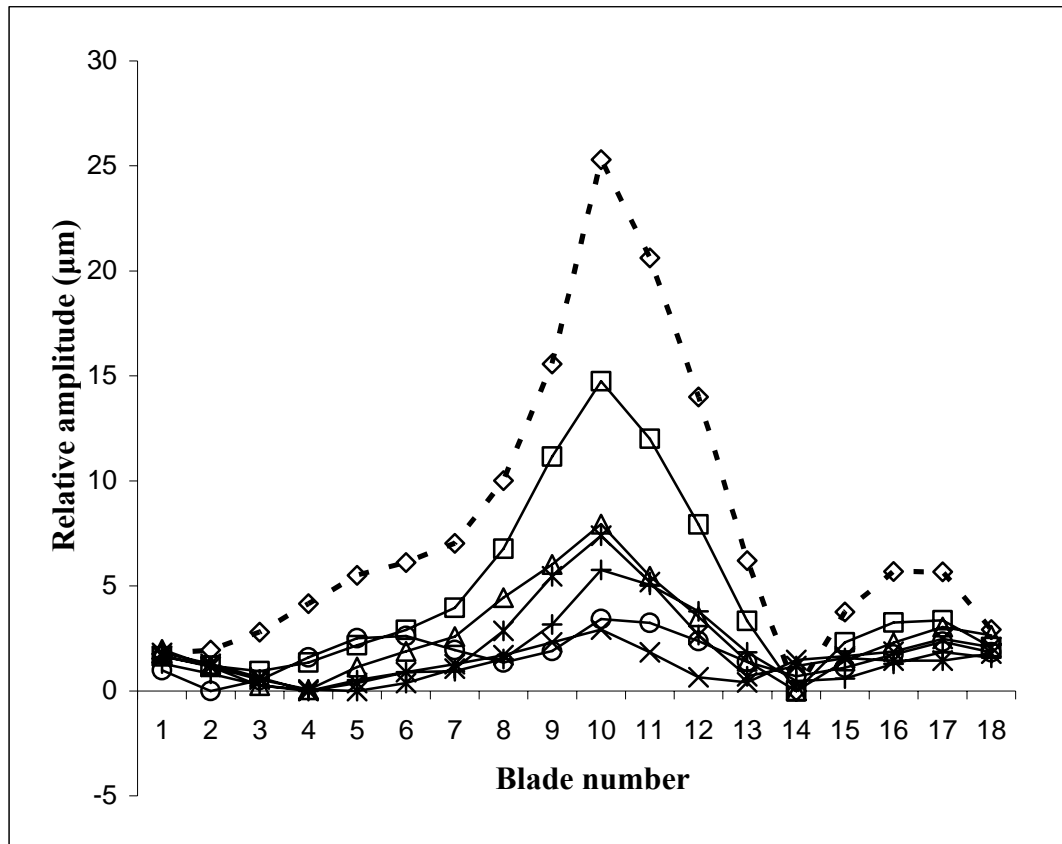
Figure **3-5**:  Relative amplitudes of 18 blades for mistuned bladed disk without network and with network at various circuit frequency tunings ($f_e$) from 193.5 Hz to 234 Hz. Legends: dotted line: (◇) without network;  solid lines: (□) $f_e$ = 193.5 Hz; (Δ) $f_e$ = 201 Hz; (×) $f_e$ = 206 Hz; (*) $f_e$ = 212 Hz; (○) $f_e$ = 222 Hz; (+) $f_e$ = 234 Hz.

The dotted data line in Figure 3-5 shows that the relative vibration amplitudes are high over a small region (only 4-5 blades) around blade number 10.  Outside this region, amplitudes are relatively small.  This indicates that vibration is highly localized in the mistuned bladed disk.  With the treatment, the solid lines corresponding to various circuit tunings show a more even distribution of the amplitudes over the 18 blades.  This more even amplitude distribution indicates a reduction of the level of localization.
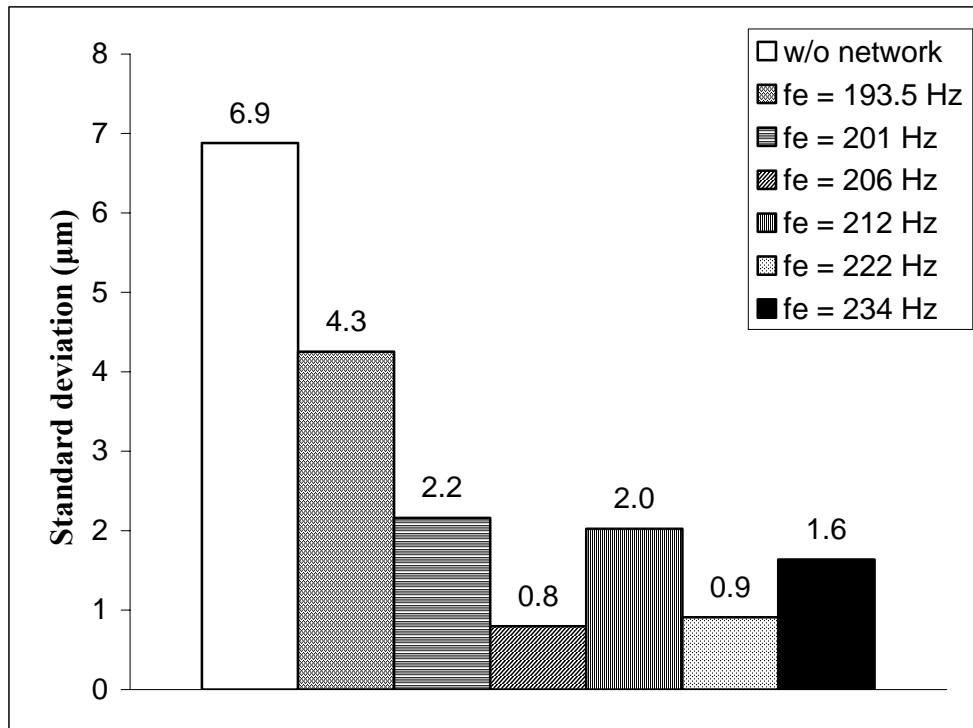
Figure **3-6**: Standard deviations of blade relative amplitudes for the system without network (1$^{st}$ column) and with network at various circuit frequency tunings ($f_e$) (all other columns).

As a tool to quantify how the amplitude data is distributed spatially, standard deviations are plotted in Figure 3-6. However, it should be noted that the standard deviation is not used as an exact index for quantifying localization, but only as a measurement of the scatterness of the amplitude data distribution. As Figure 3-6 shows, the standard deviations for the mistuned bladed disk with treatment are much smaller than that without treatment.

Moreover, delocalization effect of the piezoelectric circuit network is also demonstrated when the mistuned bladed disk is excited under the resonant frequency of (and around) 202.3 Hz. Resonant response amplitudes for the mistuned bladed disk with and without piezoelectric network are plotted in Figure 3-7. Without network, blade

amplitudes are confined only in small regions around blade number 2, 3 and 7. With the

piezoelectric circuit network (at three circuit frequency tunings: $f_e$= 201 Hz, 206 Hz, and

222 Hz), the blade amplitudes again become more evenly distributed over the 18 blades,

which means the level of localization is reduced.
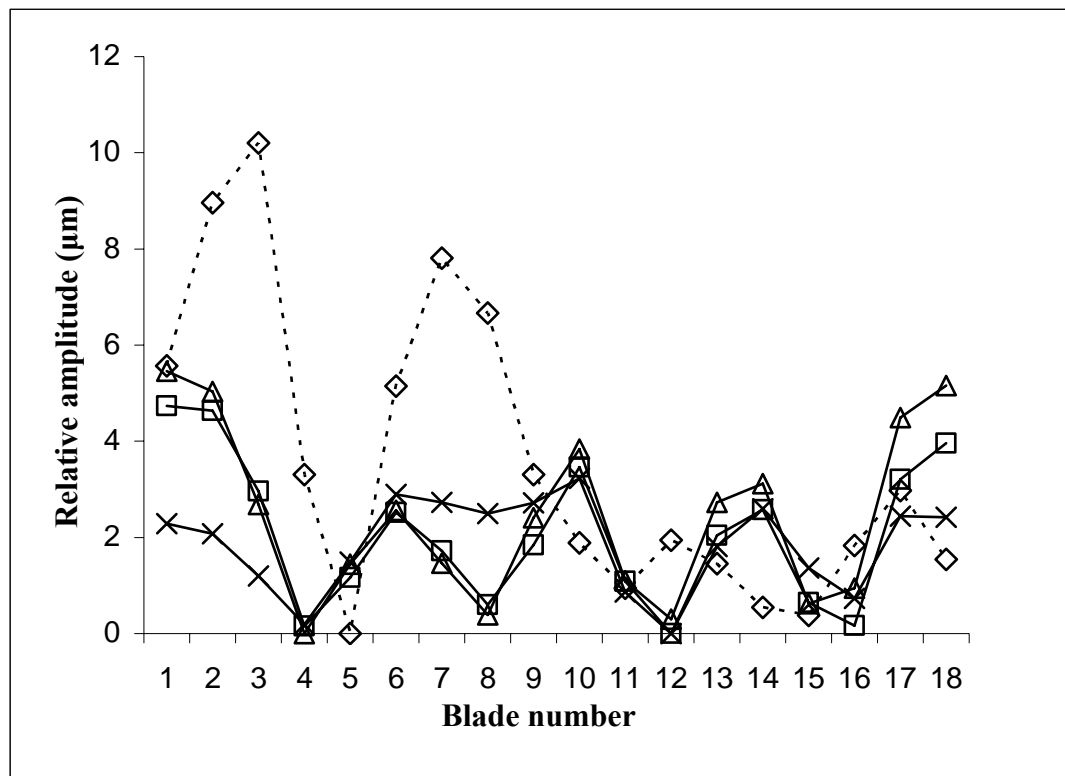


Figure **3-7**: Blade relative amplitudes distribution for the system without network (dotted
line) and with network (solid lines) at resonances around 202.3 Hz. Legends: (◊) without
network; (□) $f_e$ = 201 Hz; (Δ) $f_e$ = 206 Hz; (×) $f_e$ = 222 Hz .

**3.3.2 Results with negative capacitance**

Next, negative capacitance circuits are incorporated into the piezoelectric network, and their effects on the delocalization performance are examined. The analytical results suggest that the electro-mechanical coupling coefficient ($\xi$) of the piezoelectric patch can be increased by the negative capacitance. As a result of this coupling enhancement, the overall delocalization effect of the piezoelectric circuit network can be further improved. To validate this prediction, negative capacitance circuits are built and connected in series with piezoelectric patches to the negative electrodes. The same experimental approach used in (Tang and Wang, 2001) is adopted here to measure the electro-mechanical coupling coefficient. The value of $\xi$ is calculated according to $\xi = \sqrt{((\omega^D)^2 - (\omega^E)^2)/(\omega^D)^2}$, which is based on the resonant frequencies of the substructure under open circuit condition ($\omega^D$) and short circuit condition ($\omega^E$) (Lesieutre and Davis, 1997) Note that this formula is exactly the definition of the electro-mechanical coupling coefficient at the structural level. The original electro-mechanical coupling coefficient of the piezoelectric patch is measured to be $\xi = 0.1224$. With a negative capacitance of $C_n = -4.7$ nF, the coupling coefficient is measured to be $\xi = 0.1930$, which is a 57.7% increase. This range of $\xi$ is covered in the analytical study shown in Figure 2-9.

Eighteen negative capacitance circuits with the same value ($C_n = -4.7$ nF) are then built and integrated into the piezoelectric network. The network with negative capacitance is also referred to as the *augmented network*. Tip displacements of the 18 blades are re-measured for bladed disk with this augmented network. Resonant response

amplitudes are compared to previous results shown in Figure 3-5 and Figure 3-7 in order to evaluate the delocalization performance improvement. First, the responses at the resonance around 193.5 Hz are examined and amplitudes are plotted in Figure 3-8 (a)-(f), with each corresponding to a circuit frequency tuning ($f_e$). It can be seen that for all of these six circuit frequency tunings, the vibration amplitude distributions with the augmented piezoelectric network become more uniform. This is predicted because with negative capacitance, the network has a larger electro-mechanical coupling ($\xi$). Therefore, the network is capable of transforming more mechanical energy into electrical form, which is then propagated throughout the network by the coupling capacitors.
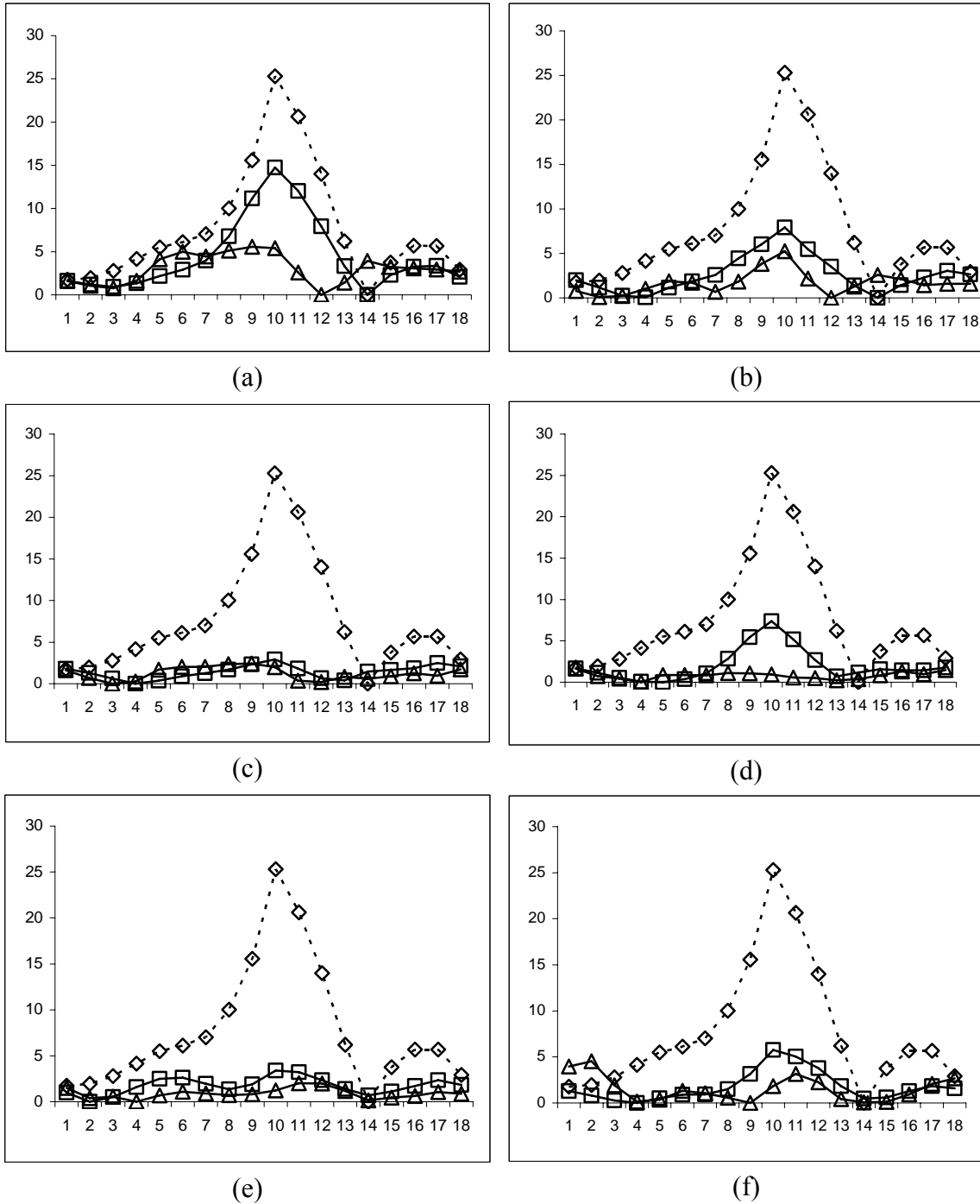
Figure **3-8**: Blade relative amplitudes of system without network (◊ in dotted line); with network (□ in solid line); and with network augmented by negative capacitance (Δ in solid line); (a) $f_e$ = 193.5 Hz; (b) $f_e$ = 201 Hz; (c) $f_e$ = 206 Hz; (d) $f_e$ = 212 Hz; (e) $f_e$ = 222 Hz; (f) $f_e$ = 234 Hz; Horizontal axis: blade number; Vertical axis: relative amplitude (unit: μm).

Again, the standard deviations of the amplitudes are calculated and shown in Figure 3-9 for the mistuned bladed disk without any treatment, with network but no negative capacitance, and with the augmented network, marked as Case 1, Case 2 and Case 3, respectively. The decreasing trend of the standard deviations from Case 1 to Case 3 indicates that vibration amplitudes become more and more evenly distributed. These results show that the delocalization ability of the piezoelectric network is improved by the integrated negative capacitance circuits. Amplitudes of the mistuned bladed disk under resonant excitation frequencies of (and around) 202.3 Hz are also compared for Cases 1, 2 and 3, as shown in Figure 3-10 and Figure 3-11, with $f_e$ = 201 Hz and 206 Hz, respectively. Both figures show that amplitude localization is further reduced and the distribution is more even for Case 3, as compared to that of Case 2. The results again illustrate improvements in the delocalization performance when negative capacitance circuits are added.
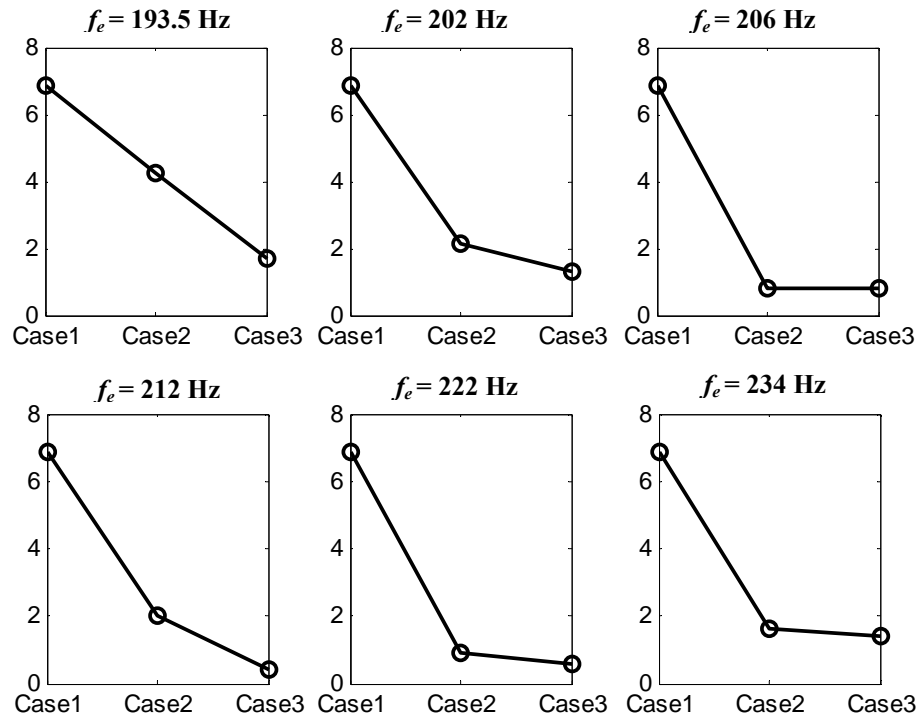
Figure **3-9**: Standard deviations of blade relative amplitudes for Case 1 (mistuned bladed disk without network), Case 2 (with network) and Case 3 (with network augmented by negative capacitance). Vertical axis: standard deviation (unit: μm).
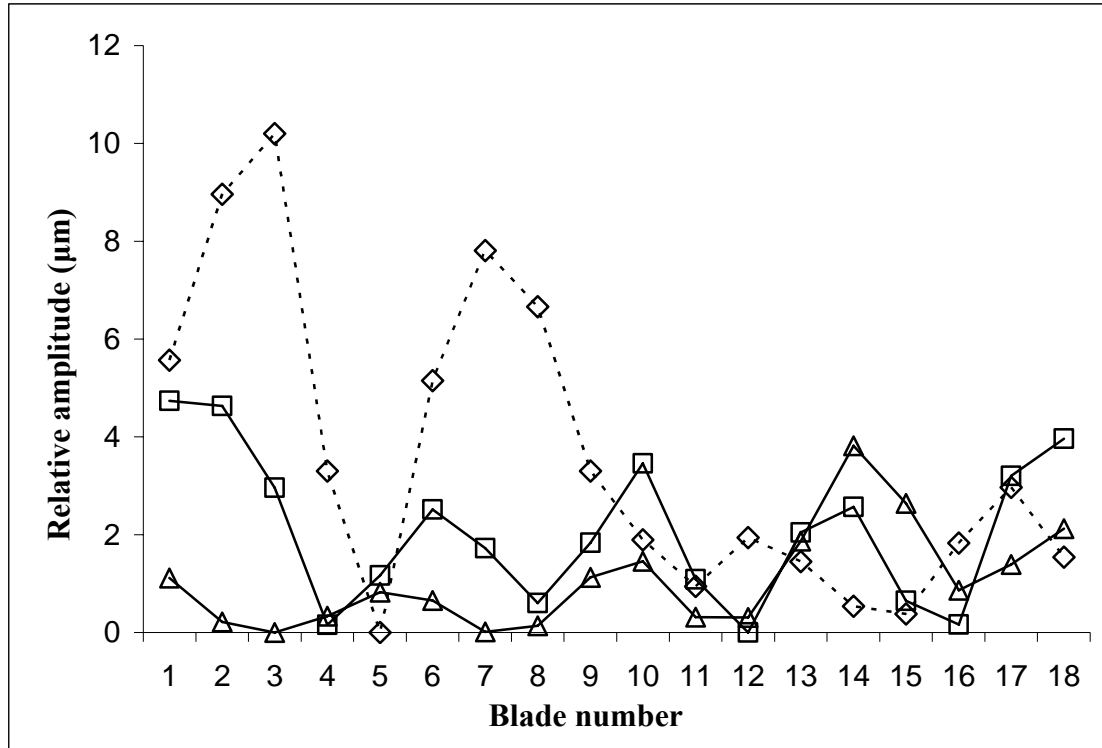
Figure **3-10**:  Relative amplitudes distribution for the system without network (◊ in dotted line), with network (□ in solid line) and with network augmented by negative capacitance (Δ in solid line) at frequency $f_e$ = 201 Hz;
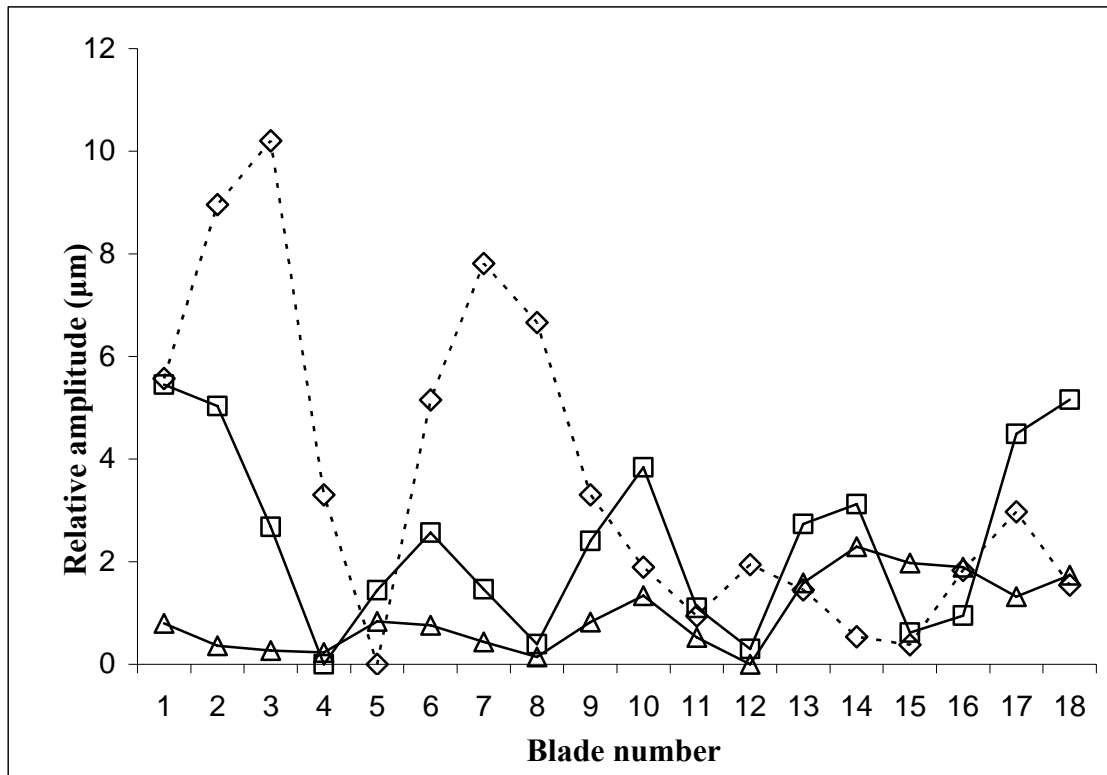
Figure **3-11**: Relative amplitudes distribution for the system without network (◊ in dotted line), with network (□ in solid line) and with network augmented by negative capacitance (Δ in solid line) at frequency $f_e = 206$ Hz;

## 3.4 Summary

Experiments are carried out to validate the vibration delocalization concept using piezoelectric network. A network is implemented and integrated with a mistuned bladed disk. The experimental results showed that the level of localization can be reduced by using the piezoelectric network over a range of circuit frequency tunings and that the electro-mechanical coupling coefficient of the system can be increased by the negative capacitance, thereby the delocalization effect can be further enhanced.

**Chapter 4**

**Vibration Suppression Analysis: Simple Bladed Disk Model and Network**

**4.1 Background**

As studied in Chapters 2 and 3, mode localization can occur to a periodic structure when mistuning is present in the substructures with weak mechanical coupling. Modern bladed disk systems in turbo-machinery are especially sensitive to mistuning, and thus are very susceptible to localization. The effect of mode localization can result in large forced vibration amplitude when the rotating bladed disks are under harmonic aerodynamic loading (known as engine order excitation). The large forced response caused by mistuning can lead to accelerated fatigue and failure of engine components.

Vibration localization study in mistuned bladed disk systems has attracted a lot of attention in recent decades. Mistuning has been known as the primary factor that causes excessively large forced response compared to the ideally tuned system. Many of the researches have focused on the analysis and experimental investigation of this phenomenon and on developing tools for predicting the maximum forced response (Whitehead, 1966; Griffin and Hoosac, 1984; Afolabi, 1985; Sinha and Chen, 1989; Cha and Pierre, 1997; Kruse and Pierre, 1997; Castanier et al., 1997; Slater et al., 1999; Keynon et al., 2003). Only a few of them have focused on exploring means of eliminating the effect of localization. One school of thought is to develop methods via mechanical tailoring, where intentional mistuning (Catanier and Pierre, 2002; Choi et al.,

2003; Kenyon and Griffin, 2003; Hou and Cross, 2005) was introduced to reduce the sensitivity of the structural response to mistuning.

## 4.2 Problem Statement and Research Objective

In previous studies (Zhang and Wang, 2002; Tang and Wang, 2003; Yu et al., 2006), the piezoelectric networking concept has been realized and shown to be effective for vibration mode delocalization. However, in bladed disks with mistuning, the more pressing issue is on vibration suppression under forcing inputs (e.g., engine order excitations). A variety of piezoelectric material based circuits have been studied for suppressing mechanical vibration in the past (Hollkamp, 1994; Wu, 1999; Behrens et al., 2003). Hagood and von Flotow (1991) first systematically studied piezoelectric passive shunt circuits for vibration suppression. They derived the analytical solution to the optimal resistance-inductance tuning of a piezoelectric damped absorber for single degree of freedom mechanical systems. A significant amount of studies in this field have been carried out since then. Comprehensive reviews of this subject can be found in (Lesieutre, 1998; Tang et al., 2000). Recently, Tang and Wang (1999) have explored the feasibility of utilizing piezoelectric absorber circuits for vibration control of periodic structures, where they derived an active compensation law to achieve multi-harmonic excitation suppression. While the results are interesting, their investigations did not address the mistuning or uncertainty issues.

Building upon the findings in (Tang and Wang, 1999), the objective of this research is to advance the state of the art of vibration suppression of the mistuned bladed disks with piezoelectric damper-absorber circuitry. It is aimed to provide an effective means to reduce the forced response in bladed disks, addressing the mistuning and uncertainty issues. The new advancements are summarized as follows:

(a) Unlike the treatment in (Tang and Wang, 1999), where active compensation is required to obtain optimal absorber tuning, this system utilizes simple passive coupling capacitors to create a networked architecture and achieve the optimal design goal.

(b) In this investigation, a coupling enhancement concept via negative capacitance is explored for performance improvement.

(c) In this study, the network's vibration suppression ability for the mistuned bladed disk system is systematically investigated through Monte Carlo simulation. Both the effectiveness and the robustness issues of this approach are discussed.

## 4.3 Modeling and Network Design

To analyze the proposed piezoelectric network for vibration suppression, we begin with the model derivation of the bladed disk with an integrated piezoelectric network, followed by the optimal network design.

**4.3.1 Modeling**

As a typical example of periodic structures, a bladed disk is considered as the baseline system in this study. For simplicity, the model of the bladed disk is assumed to be composed of $N$ blades evenly spaced along the circumference of a center disk, as shown in Figure 4-1. Each blade is modeled as a cantilever beam. Coupling through the disk is modeled by the spring connecting adjacent blades. Mistuning is assumed to be present only in blade stiffness. Identical piezoelectric patches are attached to each blade. The piezoelectric network is constructed as follows: first an inductor ($L$) and a resistor ($R$) are connected to each piezoelectric patch (with electric capacitance $C$) in order to form a resonant $LRC$ circuit. For reasons to be clear later, these shunts are then networked through passive capacitors ($C_a$).



(a)                                         (b)
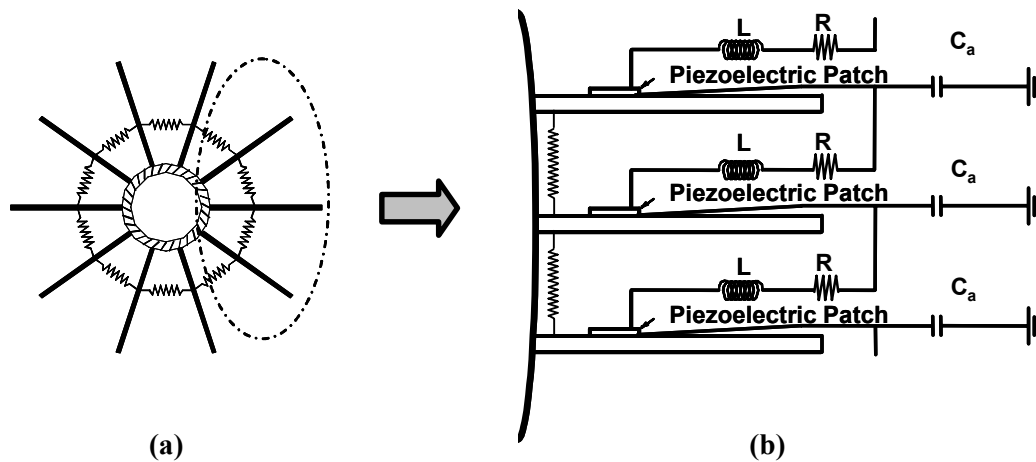
Figure **4-1**: System schematics of (a) bladed disk; and (b) bladed disk integrated with piezoelectric network.

Detailed derivation of the model can be found in (Tang and Wang, 2003). Here we will give a brief description. For each cantilever beam, we only consider the transverse motion $w(x,t)$. We expand the transverse motion of the beam using only its first beam mode, $\phi(x)$. Then $w(x,t) \approx \phi(x)q(t)$. After formulating the energy expressions and using Hamilton's principle, the equations of motion for the mechanical periodic system with and without piezoelectric circuits can be derived. The equation of motion for the $j^{th}$ blade without the piezoelectric circuits is shown in Equation (4.1).

$$m\ddot{q}_j + c\dot{q}_j + (k + \Delta k_j)q_j + k_c(2q_j - q_{j-1} - q_{j+1}) = f_j \tag{4.1}$$

And the equations of motion for the $j^{th}$ blade integrated with the $j^{th}$ circuit branch are shown in Equation (4.2),

$$m\ddot{q}_j + c\dot{q}_j + (k + \Delta k_j)q_j + k_c(2q_j - q_{j-1} - q_{j+1}) + k_1 Q_j = f_j \tag{4.2a}$$

$$L\ddot{Q}_j + R\dot{Q}_j + k_2 Q_j + k_a(2Q_j - Q_{j-1} - Q_{j+1}) + k_1 q_j = 0 \tag{4.2b}$$

where $m$, $c$, $k$, $k_c$, are respectively, mass, damping, stiffness of substructure (blade), and substructure coupling stiffness. $L$, $R$, $k_2$ are circuitry elements: inductance, resistance, inverse of piezoelectric capacitance $C_{pzt}$ ($k_2 = 1/C_{pzt}$) respectively. $\Delta k_j$ is the assumed mistuning in blade stiffness. $k_1$ is the piezoelectric coupling coefficient. $k_a$ is related to the coupling capacitance ($C_a$) of the network ($k_a = 1/C_a$). $q_j$ and $Q_j$ are the generalized mechanical displacement and electrical charge in the circuit respectively.

$f_j$ is the external force applied to the $j^{th}$ blade. In this case, we assume engine order excitation force. As the engine rotates through the air flow field, bladed disk assemblies experience periodic disturbances such as wakes caused by the fixed upstream stator vanes. The frequencies of the periodic disturbances are integer multiples (i.e.,

engine order) of the engine rotating frequency. Resonant forced vibration condition can be established when the engine order frequency coincides with the natural frequency of the bladed disk system, and will cause large vibration amplitude (Duffield and Agnes, 2001). The engine order excitation can be expressed as $f_j = F_0 e^{i(\omega t + \phi_j)}$. Here $F_0$ is the magnitude of the force. $i = \sqrt{-1}$. $\omega$ is the frequency of the excitation force. $\phi_j$ is the phase of the force at the $j^{th}$ blade, and $\phi_j = \dfrac{2\pi(E-1)(j-1)}{N}$, where $E$ is the engine order number. As it shows in these expressions, on each blade, the force has same magnitude with different phases. The phase difference between adjacent blades is determined by engine order $E$, which is $(E-1)\theta$, where $\theta$ is determined by the total number of blades, $\theta = 2\pi / N$.

One can also perform the analysis from a non-dimensional perspective. Starting from Equations (4.1) and (4.2), by assuming harmonic motion, one can derive the non-dimensional equation of motion for the original bladed disk system as follows,

$$-\Omega^2 \bar{q}_j + (1 + \Delta s_j)\bar{q}_j + i2\Omega\zeta_c\bar{q}_j + R_c^2(2\bar{q}_j - \bar{q}_{j-1} - \bar{q}_{j+1}) = \bar{f}_j \tag{4.3}$$

And for the bladed disk system integrated with piezoelectric network,

$$-\Omega^2 \bar{q}_j + (1 + \Delta s_j)\bar{q}_j + i2\Omega\zeta_c\bar{q}_j + R_c^2(2\bar{q}_j - \bar{q}_{j-1} - \bar{q}_{j+1}) + \delta\xi\bar{Q}_j = \bar{f}_j \tag{4.4a}$$

$$-\Omega^2 \bar{Q}_j + \delta^2\bar{Q}_j + i2\Omega\delta\zeta_r\bar{Q}_j + \delta^2 R_a^2(2\bar{Q}_j - \bar{Q}_{j-1} - \bar{Q}_{j+1}) + \delta\xi\bar{q}_j = 0 \tag{4.4b}$$

The parameters for non-dimensionalization are defined as:

$$\omega_e = \sqrt{k_2 / L} , \ \omega_m = \sqrt{k / m} , \ \Omega = \omega / \omega_m , \ R_c = \sqrt{k_c / k} ,$$

$$\delta = \omega_e / \omega_m , \ R_a = \sqrt{k_a / k_2} , \ \xi = k_1 / \sqrt{k k_2} , \ \zeta_r = R / 2 m \omega_e \qquad (4.5)$$

$$\zeta_c = c / 2 m \omega_m , \ \bar{q}_j = \sqrt{m} q_j , \ \bar{Q}_j = \sqrt{L} Q_j , \ \Delta s_j = \Delta k_j / k , \ \bar{f}_j = f_j \sqrt{m} / k$$

where $\omega_e$ and $\omega_m$ are the natural frequencies of the local electrical circuit and local

blade. $\Omega$ is the non-dimensional frequency. $\delta$ is the circuit frequency tuning ratio,

which is related to the inductance. $R_a$ is related to the coupling capacitance. $\xi$ is the

generalized electro-mechanical coupling coefficient of piezoelectric patch. $\zeta_r$ is the

modal damping ratio in the electrical circuit, related to resistance. $R_c$ is the non-

dimensional coupling between blade. $\zeta_c$ is the modal damping of the substructure

(blade). $\bar{q}_j$ and $\bar{Q}_j$ are the non-dimensional generalized mechanical and electrical

displacement. $\Delta s_j$ is the non-dimensional mistuning. $\bar{f}_j$ is the non-dimensional force.

**4.3.2 Optimal absorber design through networking**

To design the absorber circuitry, first consider the *tuned* mechanical systems in

Equations (4.1) and (4.2), i.e., $\Delta k_j = 0$. Equations (4.1) and (4.2) can be written into

matrix forms by grouping equations from $j = 1$ to $N$ for a system with $N$ subsystems (with

or without circuits),

$$[M]\ddot{\underline{q}} + [C]\dot{\underline{q}} + [K]\underline{q} = \underline{f} \qquad (4.6)$$

where $[M]$, $[C]$, $[K]$ are all circulant matrices (Davis, 1979).

$$[M] = circ(a_m, 0, ..., 0) = \begin{bmatrix} a_m & & \\ & \ddots & \\ & & a_m \end{bmatrix} \tag{4.7}$$

$$[C] = circ(a_c, 0, ..., 0) = \begin{bmatrix} a_c & & \\ & \ddots & \\ & & a_c \end{bmatrix} \tag{4.8}$$

$$[K] = circ(a_k, b_k, 0, ..., 0, b_k) = \begin{bmatrix} a_k & b_k & 0 & ... & 0 & b_k \\ b_k & a_k & b_k & 0 & ... & 0 \\ & \ddots & \ddots & \ddots & & \\ & & \ddots & \ddots & \ddots & \\ 0 & ... & 0 & b_k & a_k & b_k \\ b_k & 0 & ... & 0 & b_k & a_k \end{bmatrix} \tag{4.9}$$

For the original mechanical system without piezoelectric networks, i.e., for Equation (4.1), the displacement vector is of size $1 \times N$, $\underline{q} = [q_1, q_2, ..., q_N]^T$. The elements in those circulant matrices $[M]$, $[C]$, $[K]$ are scalars listed below:

$$a_m = m, \ a_c = c, \ a_k = k + 2k_c, \ b_k = -k_c. \tag{4.10}$$

For the mechanical system integrated with piezoelectric networks, i.e., for Equation (4.2), the displacement vector is of size $1 \times 2N$, $\underline{q} = [q_1, Q_1, q_2, Q_2, ..., q_N, Q_N]^T$. Parameters in these circulant matrices are $2 \times 2$ matrices in Equation (4.11), thus $[M]$, $[C]$, $[K]$ are also called *block-circulant* matrices.

$$a_m = \begin{bmatrix} m & \\ & L \end{bmatrix}, \ a_c = \begin{bmatrix} c & \\ & R \end{bmatrix},$$

$$a_k = \begin{bmatrix} k + 2k_c & k_1 \\ k_1 & k_2 + 2k_a \end{bmatrix}, \ b_k = \begin{bmatrix} -k_c & 0 \\ 0 & -k_a \end{bmatrix}. \tag{4.11}$$

The forcing vector for mechanical system is:

$$\underline{f} = F_0 e^{i\omega t}[e^0, e^{i\phi_2}, ..., e^{i\phi_j}, ..., e^{i\phi_N}]^T \qquad (4.12)$$

For the mechanical system with integrated piezoelectric networks, since we assume no external voltage source is applied, the forcing vector is:

$$\underline{f} = F_0 e^{i\omega t}[e^0, 0, e^{i\phi_2}, 0, ..., e^{i\phi_j}, 0, ..., e^{i\phi_N}, 0]^T \qquad (4.13)$$

U-transformation (Tang and Wang, 1999) can be applied to diagonalize (or block-diagonalize) the circulant matrices (or block-circulant matrices) in Equation (4.6). For mechanical system alone, the U-transformation matrix is an $N \times N$ matrix, denoted as $[U_m]$, whose $(p,q)^{\text{th}}$ element is defined as:

$$[U_m]_{pq} = \frac{1}{\sqrt{N}} e^{i\theta(p-1)(q-1)} \qquad (4.14)$$

For mechanical system with network, the U-transformation matrix is a $2N \times 2N$ matrix, denoted as $[U_{me}]$, which is an expansion of $[U_m]$, i.e., $[U_{me}] = [U_m] \otimes I_2$, where $\otimes$ is the Kronecker tensor product.

If we let

$$\underline{q} = [U]\underline{x}, \qquad (4.15a)$$

and substitute (4.15a) into the matrix form of Equation (4.6), and pre-multiply by $[U]^*$,

$$[U]^*[M][U]\underline{\ddot{x}} + [U]^*[C][U]\underline{\dot{x}} + [U]^*[K][U]\underline{x} = [U]^*\underline{f} \qquad (4.15b)$$

where $[U]^*$ is the complex conjugate transpose of $[U]$, the system equations in Equation (4.6) are transformed into the spatial harmonic space, where the originally coupled stiffness matrix $[K]$ can be decoupled so that the stiffness matrix becomes diagonal (for

mechanical system without circuit) or block-diagonal (for mechanical system with circuit).

To design the absorber circuitry, let us take Equation (4.2) with $\Delta k_j = 0$, and neglect structural damping $c$ since bladed disk systems usually have very light damping. After U-transformation Equation (4.2) becomes:

$$m\ddot{x}_j + [k + 2k_c(1 - \cos((j-1)\theta))]x_j + k_1 y_j = h_j \tag{4.16a}$$

$$L\ddot{y}_j + R\dot{y}_j + [k_2 + 2k_a(1 - \cos((j-1)\theta))]y_j + k_1 x_j = 0 \tag{4.16b}$$

where $h_j = \sqrt{N}F_0 e^{i\omega t}$. Note that in Equation (4.16), $j$ denotes the $j^{th}$ spatial harmonic. The non-zero $h_j$ exists only when the spatial harmonic equals to the engine order number, i.e., $j=E$, otherwise, it will be zero. In this case, the state vectors are $\underline{q} = [q_1, Q_1, q_2, Q_2, ..., q_N, Q_N]^T$ and $\underline{x} = [x_1, y_1, ..., x_N, y_N]^T$.

Assuming harmonic motion, the frequency response function between the blade motion and the force can be obtained from Equation (4.16):

$$x_j / h_j = \frac{1}{\alpha - \dfrac{k_1^2}{\beta}} \tag{4.17}$$

where

$$\alpha = -\omega^2 m + k + 2k_c(1 - \cos((j-1)\theta)) \tag{4.18a}$$

$$\beta = -\omega^2 L + i\omega R + k_2 + 2k_a(1 - \cos((j-1)\theta)) \tag{4.18b}$$

First let us examine the traditional absorber design without the network capacitance, i.e., $k_a=0$. By following the procedure in (Tang and Wang, 1999) or (Den Hartog, 1934) for vibration absorber design, one can find the optimal inductance $L$ to be,

$$L_{opt} = \frac{mk_2}{k + 2k_c(1 - \cos((j-1)\theta))} \tag{4.19}$$

In this case, it is obvious that the optimal tuning is dependent on the spatial harmonic number $j$. In other words, the non-networked traditional absorber can only be optimally designed to suppress a specific spatial harmonic excitation.

By applying the coupling capacitance and forming the network, one can derive the optimal inductance:

$$L_{opt} = \frac{m[k_2 + 2k_a(1 - \cos((j-1)\theta))]}{k + 2k_c(1 - \cos((j-1)\theta))} \tag{4.20}$$

While the expression in Equation (4.20) is still $j$-dependent, by properly tuning the coupling capacitance $k_a$, one can design an $L_{opt}$ that is independent of the spatial harmonic number $j$. This can be accomplished by letting

$$k_a = \frac{k_2 k_c}{k} \tag{4.21}$$

in Equation (4.20). Then the optimal $L$ will become,

$$L^* = \frac{mk_2}{k} \tag{4.22a}$$

It is thus obvious that this expression is no longer $j$-dependent, meaning that it will be effective for all spatial harmonic excitations.

For resistance tuning, previous study (Zhang and Wang, 2002) has found that the system performance is not very sensitive to small perturbation in the resistance, thus a single resistance value is used for all spatial harmonics by taking $j=1$. Thus,

$$R^* = \frac{k_1}{k}\sqrt{2mk_2} \tag{4.22b}$$

The corresponding non-dimensional optimal parameters to Equations (4.21)-(4.22) are:

$$R_a = R_c, \ \delta^* = 1, \ \zeta_r^* = \xi / \sqrt{2} \tag{4.23}$$

## 4.4 Analysis of Network Performance

It should be noted that the optimal absorber design in Equation (4.22) is derived in the context of perfectly tuned periodic structure system (i.e., tuned bladed-disk in this case). However, in reality, periodic structures such as bladed disks in turbo-engines are often mistuned due to factors such as manufacturing tolerance and in-service wear. Mistuning in bladed disk can drastically change the system dynamic characteristics and increase the maximum forced response compared to the ideally tuned case. Therefore, mistuned bladed disk system is considered next to examine the performance of the optimal network.

### 4.4.1 Comparison with traditional absorber

First, we examine the above described optimal network using single random mistuning. In Figure 4-2, we compare the multiple-harmonic vibration suppression effects of the traditional absorber and the optimal network for bladed disk under summation of engine order excitations. Shown in this figure are the maximum blade responses versus frequency. Here, the mistuned system is realized by generating a random mistuning set for the mechanical stiffness matrix. In this case, the non-

dimensionalized system equations are used. The mechanical parameters used in the simulation are: $R_c$=0.5, $N$=10. The random mistuning follows normal distribution, with a standard deviation of $\sigma = 0.05$. The optimal network is designed according to Equation (4.23) with a default electro-mechanical coupling coefficient $\xi$=0.1. The non-dimensional equivalence to the traditional absorber design in Equation (4.19) is

$\delta_{opt} = \sqrt{1 + 2R_c^2(1 - \cos(j-1)\theta)}$. For the traditional absorber, harmonic number $j$ is arbitrarily picked to be $j$=2 in the above equation. In Figure 4-2, the maximum blade response of the baseline system without control is plotted in grey solid line, that with traditional absorber in black dotted line, and that with optimal piezoelectric network in black solid line. As one can see that the traditional absorber can only effectively suppress a few frequency-response peaks, and loses its effectiveness on others. Nevertheless, the optimal network can effectively suppress the vibration at all peaks. This is because the traditional absorber can only be optimally tuned to a specific harmonic, while the optimal network, through networking, can be tuned to suppress all spatial harmonics (i.e., harmonic independent).
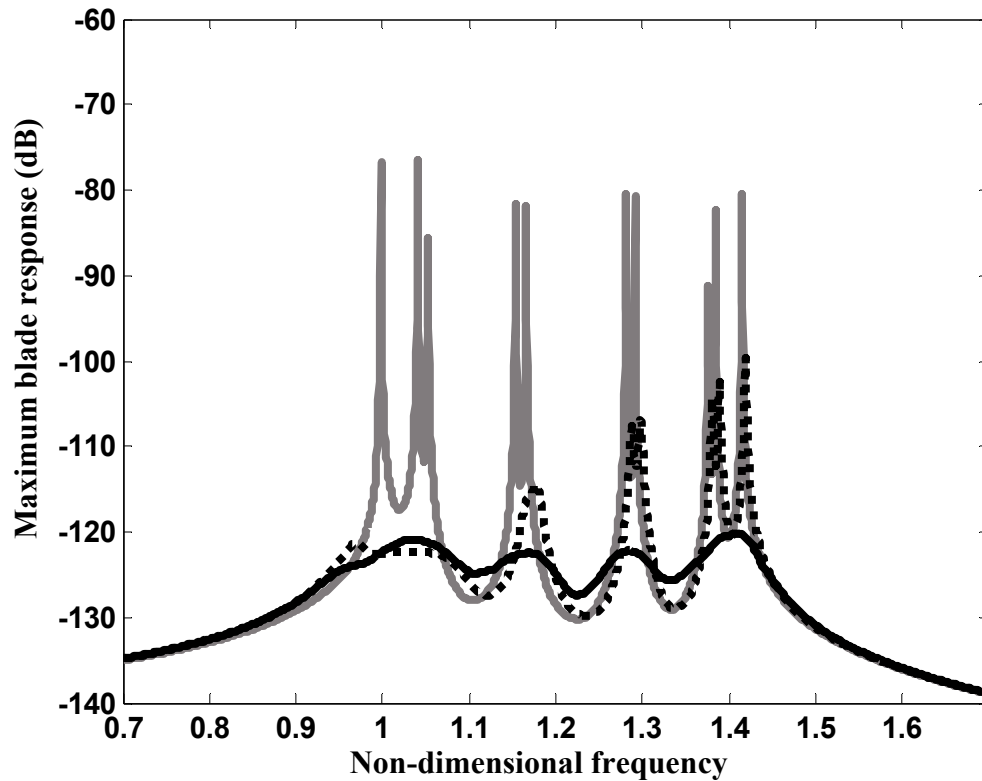
Figure **4-2**: Comparison of suppression effectiveness between traditional absorber and optimal network. Gray solid line: without control; Black solid line: with optimal network; Black dotted line: with traditional absorber.

### 4.4.2 Monte Carlo simulation

In this section, we examine the optimal network's vibration suppression performance systematically from a statistical point of view, from which we can establish a more rigorous conclusion.

In this study, Monte Carlo simulation is used to analyze the network's vibration suppression performance. Due to the random nature of mistuning, for a given standard deviation $\sigma$, there are virtually infinite number of sets of mistuning realizations that

follow the same random distribution pattern. Each realization of mistuned system may yield different maximum forced response. Hence, one has to simulate a large number of the mistuning realizations in order to draw a solid conclusion. Monte Carlo simulation is thus well-suited for this study.

For a given standard deviation $\sigma$ of the random mistuning, a large number (say, $P$=500 sets) of mistuning realizations will be generated according to the distribution pattern, in this case, normal distribution. Correspondingly, there will be $P$ mistuned bladed disk assemblies. For each mistuned assembly, its maximum blade amplitude will be calculated using frequency sweep under all possible engine order excitations ($E$=1~$N$). One engine order is considered for each calculation. The maximum blade response for this specific realization of mistuned system is obtained from all blades, at all frequencies and under all engine orders. The same process is applied to the mistuned bladed disk incorporated with the networks and the maximum blade response is obtained in the same way. A ratio $r$ is then defined based on Equation (4.24).

$$r = \frac{\max(A_{me})}{\max(A_m)} \tag{4.24}$$

where,

$\max(A_{me})$ = maximum forced response of the mistuned system with networks;

$\max(A_m)$ = maximum forced response of the mistuned system without networks.

For all $P$ mistuned bladed disk realizations, one will get $P$ ratios. Since the ratio $r$ is between the maximum forced response of mistuned system with and without network, smaller $r$ means better suppression performance. Then, the vibration suppression *performance index* of the network is defined as the 95$^{th}$ percentile value of the $P$ ratios

generated by the Monte Carlo simulation. The 95th percentile is the statistical value from a set of data that only 5 percent of the data lies above.

### 4.4.3 Results of systems with random mistuning

In this section, the effectiveness of the network against mistuning level is studied using Monte Carlos simulation and the performance index defined above. As mentioned earlier, the networked absorber design in Equation (4.22) is derived from tuned bladed disk system where mistuning is not considered. In reality, the bladed-disk is often mistuned. Here, we perform the study within a reasonable range of the standard deviation σ, 0~0.08, where σ =0 corresponds to the tuned system. The random mistuning is assumed to be normally distributed and only exists in stiffness (mass mistuning can be tackled in the same way). For Monte Carlo simulation, the non-dimensionalized equations of motion in Equation (4.4) are used. The parameters used in Figure 4-3 are: $R_c$=0.05, $N$=20, $P$=500, damping in the structure is assumed to be very small, with damping ratio $\zeta_c = 0.001$. Network is optimally tuned according to Equation (4.23). Here for the original piezoelectric patches that are used on the bladed disk, we assume the electro-mechanical coupling coefficient to be $\xi$=0.1, which will be the default value without negative capacitance. As we discussed in section 2.4 of Chapter 2, this coefficient is physically determined by the property of the material and the host structure and is difficult to alter by passive means. However, one can use a negative capacitance treatment to increase this coefficient, the effect of which will be discussed later.
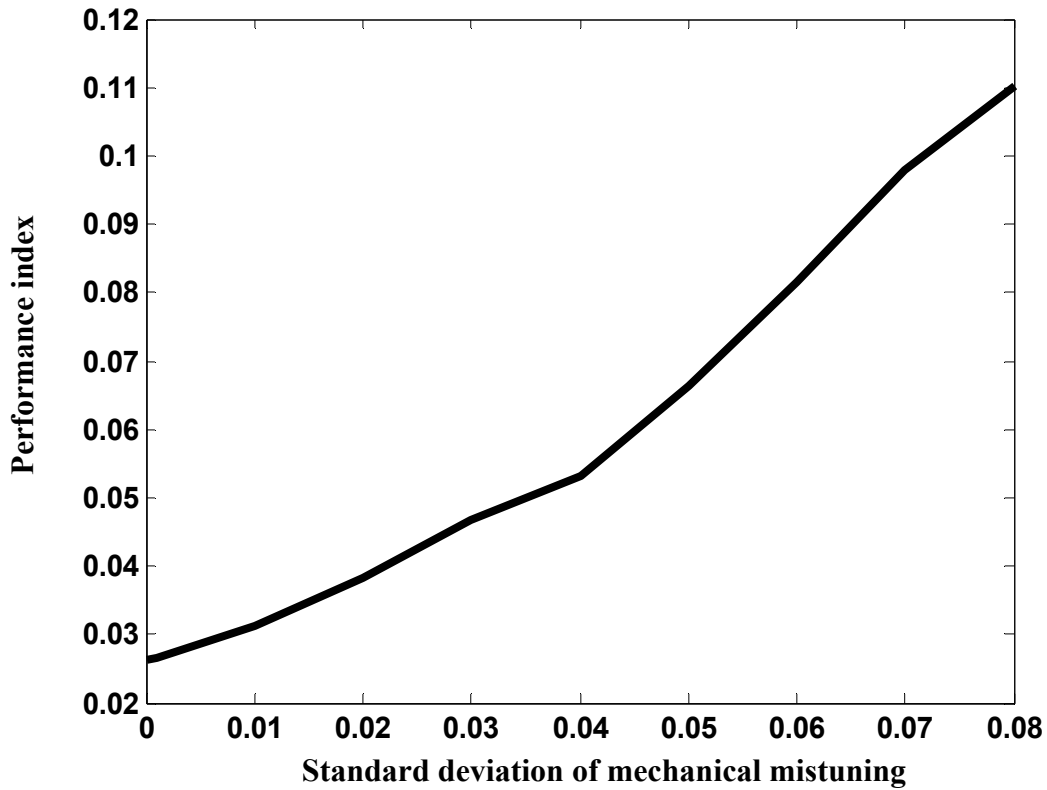
Figure **4-3**: Performance index versus standard deviation of mechanical mistuning.

Observing Figure 4-3, when σ =0, i.e., when the bladed disk system is tuned, the performance index is $r$=0.025, which means that with the network, the maximum blade response is reduced by 97.5%. As the mistuning level increases, the performance degrades, as seen in the increasing trend of the performance index. However, even with σ =0.08, which is considered as a quite large mistuning level, the performance index is still smaller than 0.12. This means the maximum blade amplitude is still reduced by approximately 88%. Such a result shows that our piezoelectric system, although designed based on tuned system, performs very well for mistuned system.

The same approach is carried out to analyze the system with random mistuning in electrical elements and similar results can be concluded. That is, the system's performance is quite robust against moderate differences among the electrical circuitry parameters as well as that among the mechanical structural parameters.

### 4.4.4 Results of systems with circuitry detuning

In this section, the performance robustness of the network in terms of circuitry detuning is investigated. Detuning means that the nominal values of a circuitry parameter in all local circuits are uniformly off-tuned by the same amount. Such detuning could be results of modeling or design errors, where the relative errors could be larger than those caused by random mistuning. In a case study, the detuning effect on $\delta$ is examined and the results are shown in Figure 4-4 with parameters $R_c$=0.05, $N$=20, $\zeta_c$=0.001, and engine order $E$=11. Here, one random set of mistuning is used instead of using the Monte Carlo simulation. The frequency response with maximum blade amplitude is illustrated for comparison. The circuit frequency tuning ratio $\delta$ is detuned from its optimal value 1.0 to 0.95 (-5% detuning) and 0.9 (-10% detuning). Figure 4-4 shows the maximum blade response in dB. With -5% detuning and -10% detuning in the optimal circuitry, the circuit becomes non-optimal and the maximum blade response is increased by 7dB and 11dB. However, the overall amplitude reduction is still significant (over 40dB reduction) compared to the maximum response of the original mechanical system without network. Case studies involving same detuning in other circuitry parameters show similar results: the maximum blade response is slightly increased when compared

with the perfectly tuned case but is still significantly lower than that of the original mechanical system. In other words, the network is quite robust against small to moderate detuning in the circuitry parameters. However, as can be seen, the vibration suppression performance degrades when the detuning increases. Therefore, if worse detuning happens, the performance might no longer satisfy the performance requirement. In this case, the negative capacitance can be included to further improve the robustness of the network, as will be discussed later.
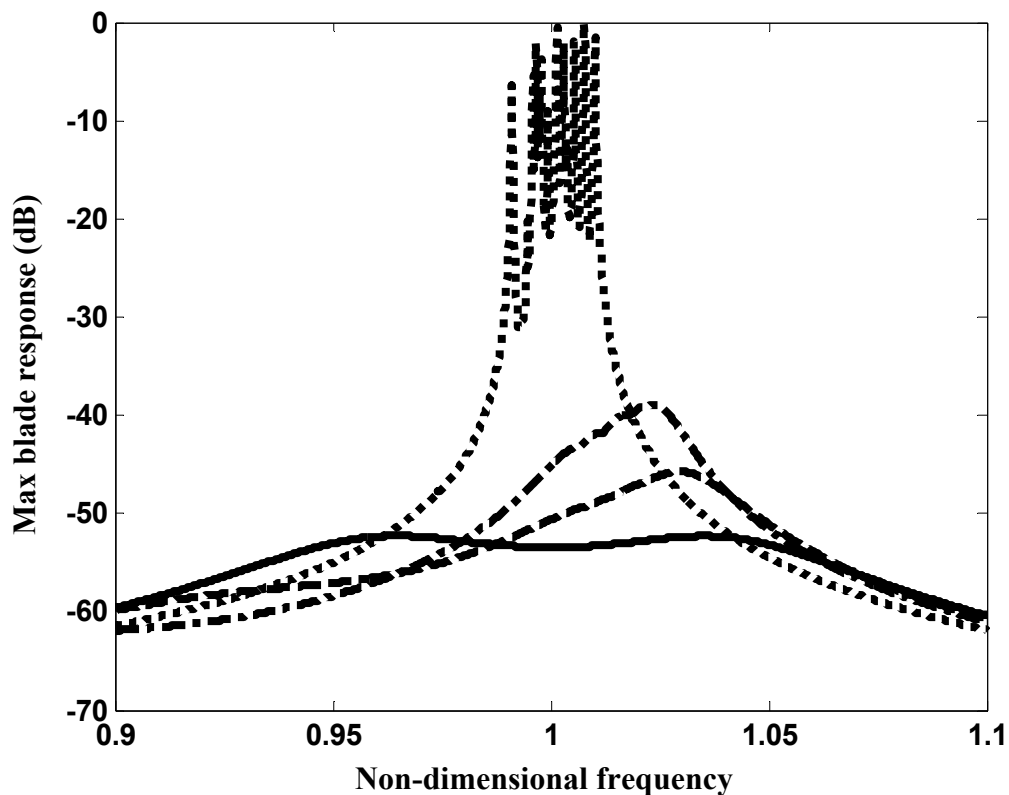


Figure **4-4**: Maximum blade response versus frequency. Dotted line: original mechanical system without network; solid line: system with optimal tuning ($\delta$ =1.0); dashed line: system with -5% detuning ($\delta$ =0.95); dash-dotted line: system with -10% detuning ($\delta$ =0.9).

A more comprehensive study is conducted via Monte Carlo simulation using the performance index. Figure 4-5 shows the effect of detuning in the circuit frequency tuning ratio on the performance of the network. Parameters used in generating Figure 4-5 are: $R_c$=0.05, $N$=20, $P$=500, with all engine orders ($E$=1~N) and optimal circuit tuning as in Equation (4.23). The optimal tuning is $\delta$=1.0, corresponding to the lowest point on the curve. Then $\delta$ is detuned from 0.5 (-50% detuning) to 1.5 (+50% detuning). In either direction departing from the optimal tuning, the performance index increases, indicating performance degradation. This range of detuning is quite large, emulating possible worst cases. However, even with this large range, the performance index is still less than 0.45, which means that 55% reduction is guaranteed in the maximum blade response. This may or may not meet the suppression requirement in practice, depending on how the suppression reduction threshold is set. With smaller detuning range, say, 20% detuning, the performance index is smaller than 0.1, indicating that 90% of reduction is guaranteed with 20% detuning in $\delta$. Therefore, it can be concluded that the network performs quite robustly with moderate detuning.
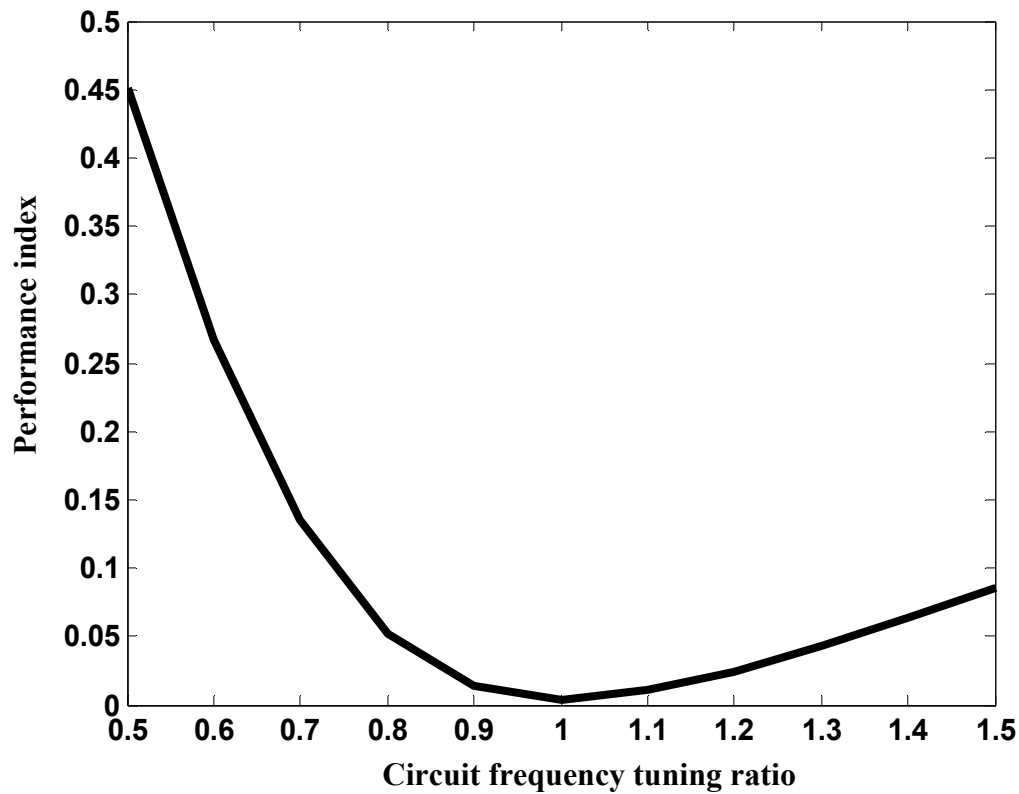
Figure **4-5**: Effect of detuning in circuit frequency tuning ratio $\delta$ on the network performance for $\xi = 0.1$.

The effects of detuning of the other two circuit parameters, circuit resistive modal damping ratio $\zeta_r$ and coupling capacitance $R_a$, are shown in Figure 4-6 and Figure 4-7 respectively. Parameters used in Figure 4-6 are the same as those used in Figure 4-5 except that $\delta$ is kept at optimum and only $\zeta_r$ is detuned. It can be seen from Figure 4-6 that the network performance is not very sensitive to detuning in $\zeta_r$. In Figure 4-6, $\zeta_r$ is detuned from the optimal value 0.0707 to 0.02 (-72% detuning) and 0.15 (+112% detuning), the maximum performance index is still below 0.06, meaning a 94% reduction in maximum blade response is guaranteed. Secondly, it is seen that detuning toward

lower damping ratio degrades the performance faster than detuning toward larger damping ratio. In practice, it is more likely to have detuning toward larger damping ratio, because there is always unknown resistance in the circuit that is not taken into account. In Figure 4-7, to better illustrate the detuning effect, $R_c$=0.5 is used, other parameters are the same as that in Figure 4-5 except $R_a$ (the only detuned parameter). The optimal $R_a$=0.5 is detuned within a range from 0.3 (-40% detuning) to 0.7 (+40% detuning). One can see that if the detuning is within roughly 20% range, the performance index can be kept below 0.1. As the detuning level becomes larger, the performance index can go up to as high as 0.6.

In summary, the network performance is robust for moderate range of detuning in the circuitry parameters. To compensate for the more serious degradation in performance when large detuning occurs, a network enhancement concept is proposed and presented in the next section.
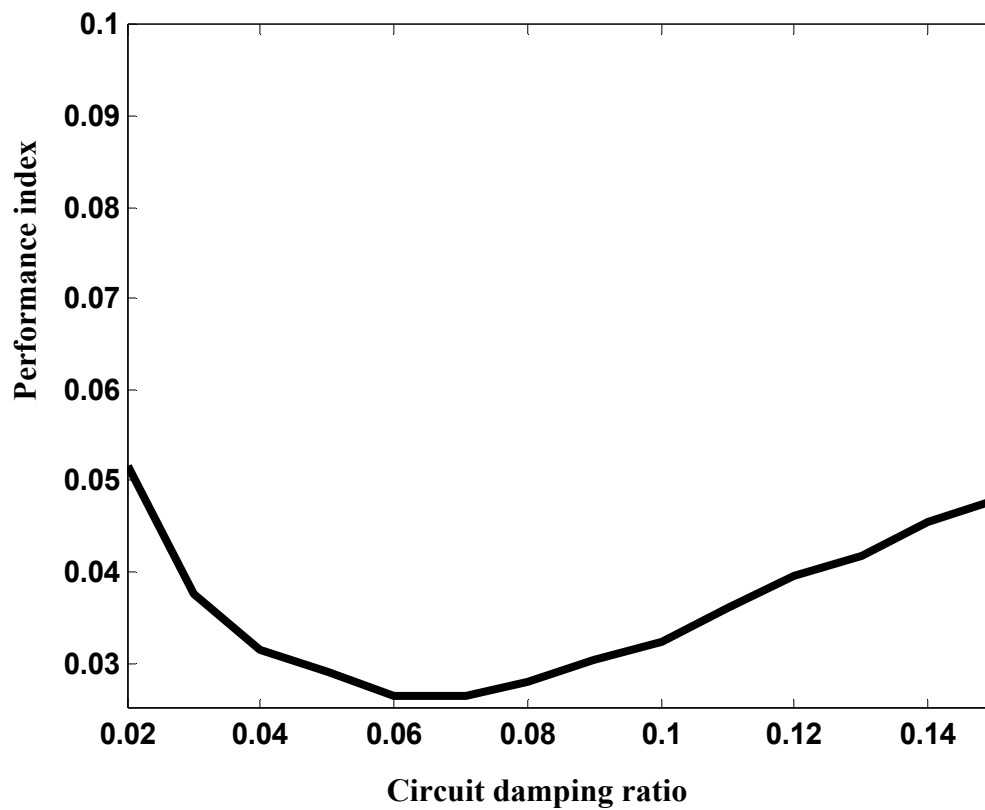
Figure **4-6**:  Effects of detuning in circuit damping ratio on network performance for $\zeta_r=0.1$ (optimal $\zeta_r=0.0707$).
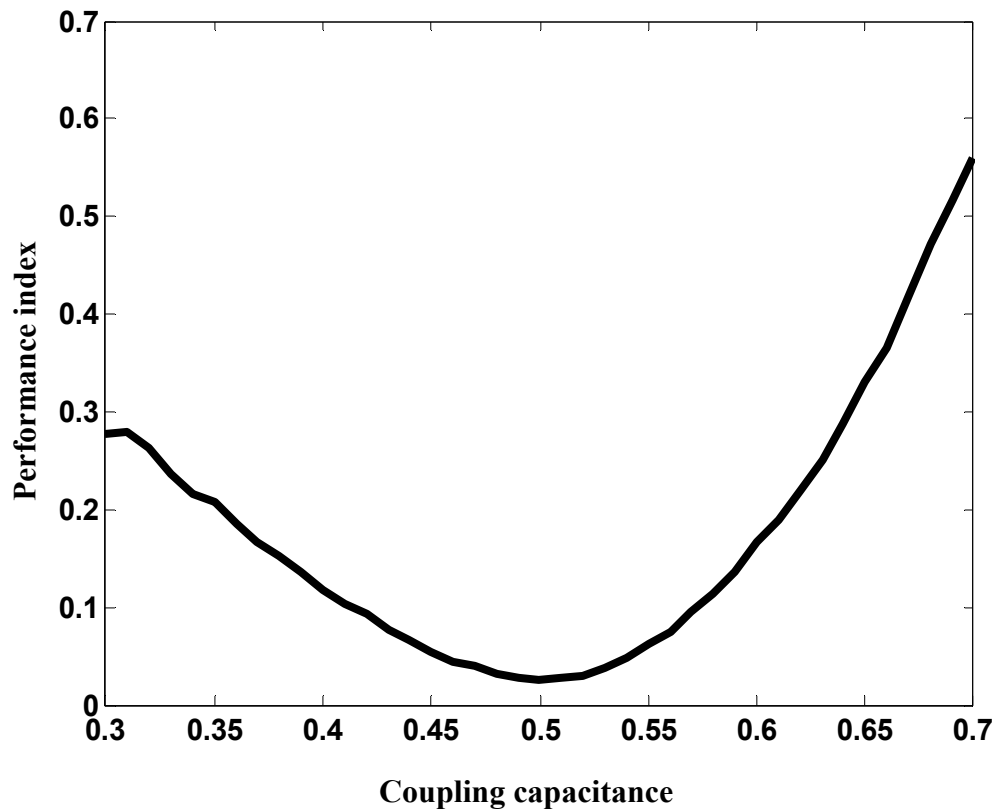
Figure **4-7**: Effect of detuning in $R_a$ on network performance for $\xi=0.1$ (optimal $R_a=0.5$).

## 4.4.5 System enhancement via negative capacitance

Previous sections show that the system's performance is quite robust under moderate level of random mistuning and electrical element detuning. In this section, we will present an approach, by incorporating negative capacitances into the network, to further improve the system's robustness if needed (i.e., if the mistuning or detuning level is higher, or better vibration suppression performance is required).

As discussed in section 2.4 of Chapter 2, negative capacitance can increase the generalized electro-mechanical coupling coefficient and greatly improve the delocalization effect. Here, by increasing the electro-mechanical coupling, more mechanical vibration energy can be transformed into the electrical form and be dissipated by the resistance. Further reduction in the maximum blade amplitude can be achieved by this means with negative capacitance, thus improving the performance of the network. More discussions on negative capacitance can be found in Chapter 2 and (Tang and Wang, 2001). Here in our simulation, we consider two cases of increased electro-mechanical coupling coefficient after negative capacitance is used: $\xi=0.2$ and $\xi=0.3$. Monte Carlo simulation is performed with these two higher coupling coefficients for the cases shown in Figure 4-3 and Figures 4-5 to 4-7. The results are shown in Figures 4-8 to 4-11.

It can be seen from Figure 4-8 (corresponding to Figure 4-3) that with negative capacitance (thus higher $\xi$), the performance index is lowered throughout the entire range of stiffness mistuning level. For example, with $\xi=0.2$, for mistuning level as large as $\sigma=0.08$, the performance index is below 0.02, meaning 98% reduction in the maximum forced response. Higher $\xi$ ($\xi=0.3$) yields even better vibration suppression results.

When circuitry parameter detuning is considered, results with negative capacitance are shown in Figures 4-9 to 4-11. In these figures, with negative capacitance (thus higher electro-mechanical coupling $\xi$), the performance index can be further reduced, not only making the network more robust against detuning around optimal

tuning, but also making the network capable of tolerating a wider range of detuning. For example, if the performance satisfaction threshold is set at performance index equal to 0.05 in Figure 4-9 with detuning in $\delta$, then without negative capacitance the detuning tolerance range in $\delta$ is roughly [0.8, 1.3]. On the other hand, with negative capacitance, for $\xi$=0.2, $\delta$ can be detuned within the range of [0.6, 1.5], and for $\xi$=0.3, the entire range [0.5, 1.5] can be used. Similar results can be seen in Figures 4-10 to 4-11.
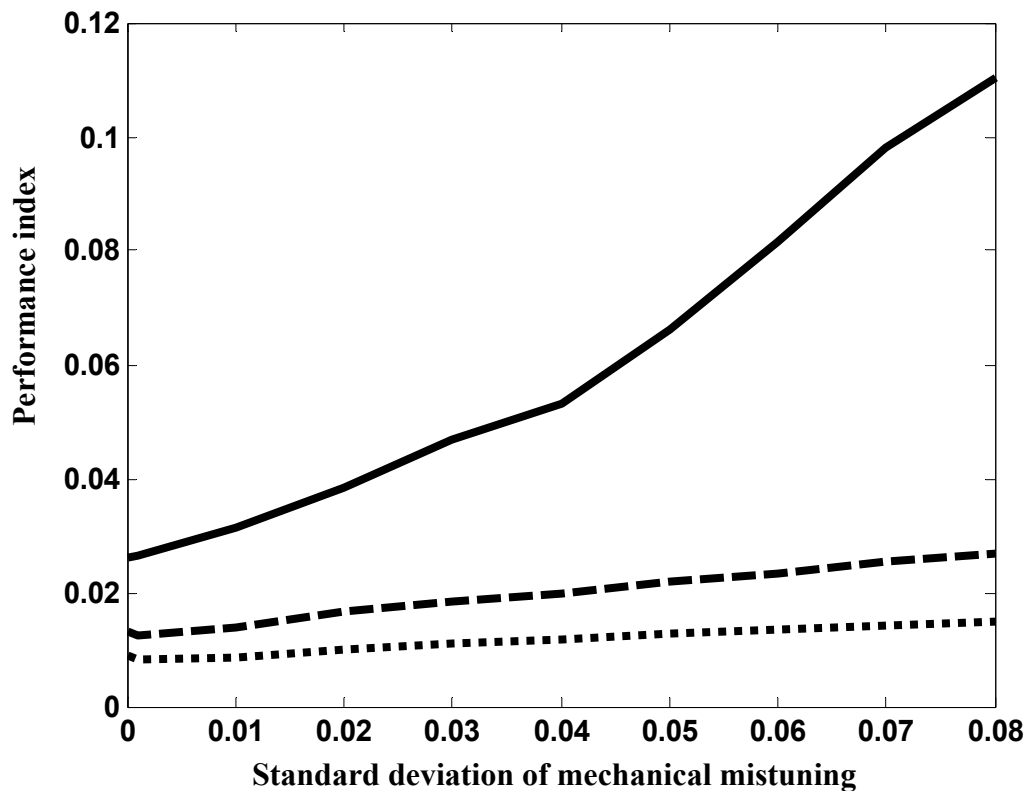


Figure **4-8**: Performance index versus standard deviation comparison between without negative capacitance case (solid line for $\xi$=0.1) and with negative capacitance case (dashed line for $\xi$=0.2 and dotted line for $\xi$=0.3).
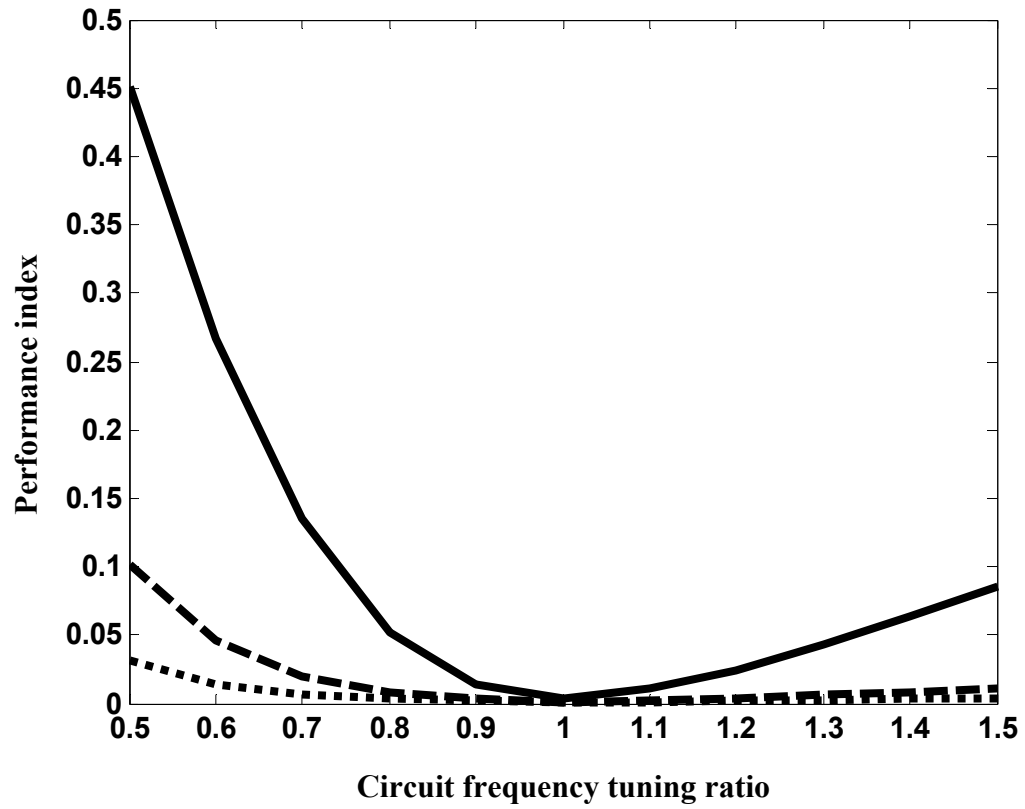
Figure **4-9**:  Detuning effect of circuit frequency tuning ratio $\delta$ on the performance, without negative capacitance (solid line for $\xi = 0.1$) and with negative capacitance (dashed line for $\xi = 0.2$ and dotted line for $\xi = 0.3$).
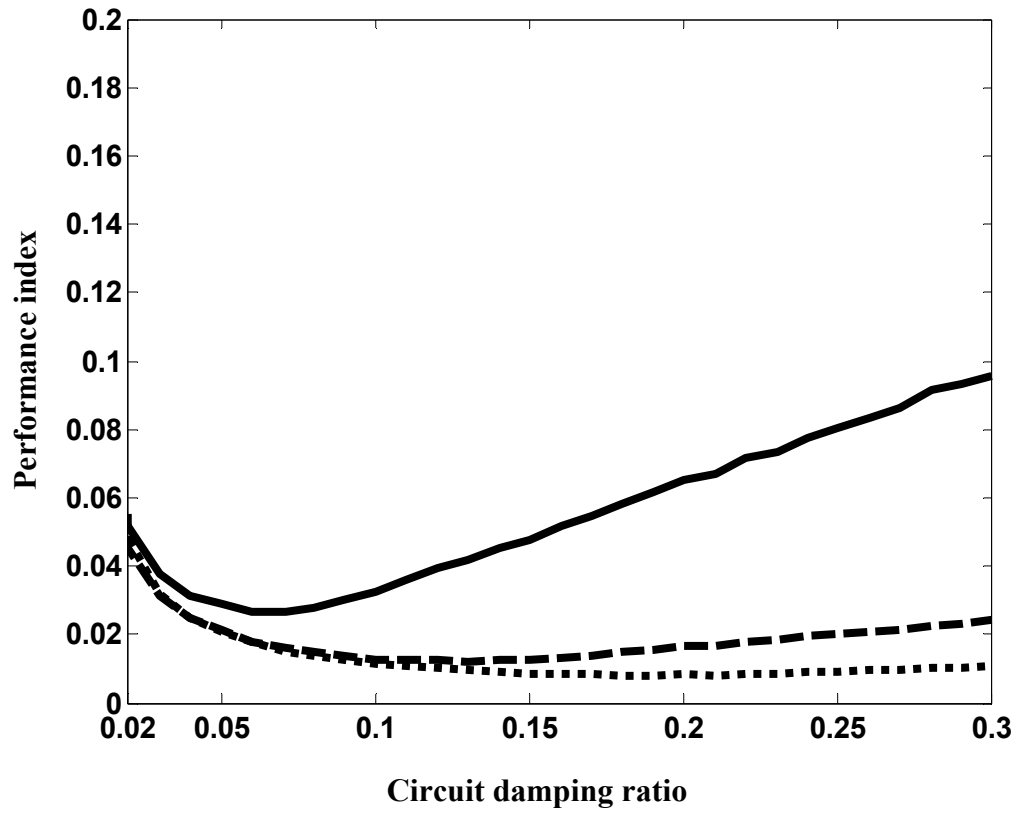
Figure **4-10**: Detuning effect of circuit damping ratio $\zeta_r$ on the performance, without negative capacitance (solid line for $\xi = 0.1$, optimal $\zeta_r = 0.0707$) and with negative capacitance (dashed line for $\xi = 0.2$, optimal $\zeta_r = 0.1414$, and dotted line for $\xi = 0.3$, optimal $\zeta_r = 0.2121$).
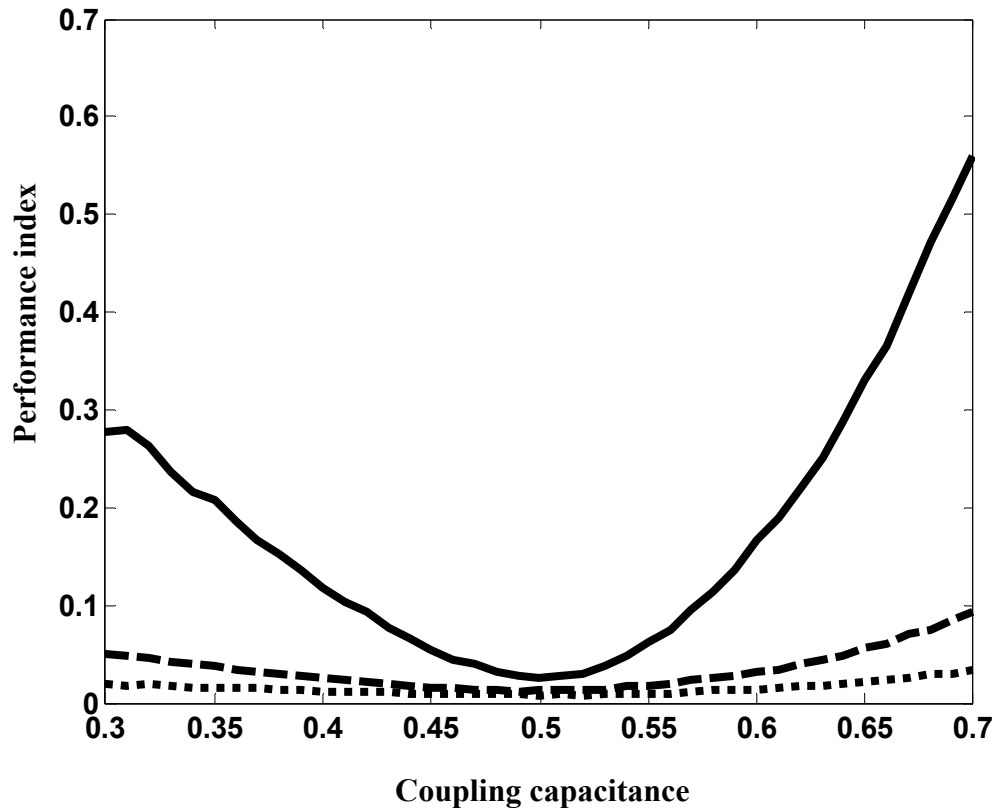
Figure **4-11**: Detuning effect of coupling capacitance $R_a$ on performance, without negative capacitance (solid line for $\xi$=0.1) and with negative capacitance (dashed line for $\xi$=0.2 and dotted line for $\xi$=0.3).

## 4.5 Summary

Piezoelectric networking for vibration suppression of mistuned bladed disk is investigated in this research. An optimal network design that is independent of spatial harmonics is derived using proper design of coupling capacitance. The optimal network's performance is examined through Monte Carlo simulation. Simulation results show that the optimal network, although designed based on the perfectly tuned periodic

structure assumption, is very effective on reducing the maximum forced response of mistuned bladed disk with a range of mistuning level. The network performance is also shown to be robust against small to moderate detuning in the circuitry parameters. Negative capacitance is introduced to further improve the performance and robustness of the network.

**Chapter 5**

**Vibration Suppression Analysis: Coupled Blade-Disk Model and Network**


**5.1 Problem Statement and Research Objective**

In Chapter 4, networked piezoelectric circuits have been investigated for vibration

suppression in mistuned bladed disks.  A simple model for bladed disk was used in that

study, where disk dynamics were neglected for simplicity.  Blades were modeled as

cantilever beams, and the coupling between blades were modeled by springs that directly

connect adjacent two springs.  Though simple, this model and its lumped mass-spring

equivalent model have been extensively used in studying the basic mode localization

phenomenon and the mistuning effects on the forced response in bladed disks in literature

(e.g., Castanier and Pierre, 2002; Cha and Sinha, 2002; Tang and Wang, 2003).  It has

been shown that this model can describe the basic dynamics of bladed disk systems

qualitatively and is a good candidate for the analysis of mode localization and forced

vibration of such systems.  However, it is also recognized that this simple model can not

capture some very important features of the bladed disk systems, such as *frequency

veering*, due to the lack of disk dynamics consideration.   Frequency veering (or more

generally known as curve veering) refers to a phenomenon where two curves coming

together and then veer apart at some point without crossing each other (Leissa, 1974;

Balmes, 1993).  Studies in the forced vibration of bladed disks have shown that frequency

veering can increase the sensitivity of the tuned system to mistuning (Bladh et al., 2002;

Kenyon et al., 2004; Kenyon et al., 2005).  Consequently, frequency veering can lead to a much higher amplitude magnification factor compared to the situations where frequency veering does not occur (e.g., in the case where only blade degrees-of-freedom are considered).

With the above argument, to better represent the bladed disk system, we propose a more complex model with disk dynamics considered, as shown in Figure 5-1.  The objective of this research is to analyze the bladed disk system with coupled blade and disk degrees-of-freedom, and explore a new piezoelectric network scheme such that effective vibration suppression can be achieved.  The effectiveness of the network for vibration suppression of mistuned bladed disk systems is investigated.  Variations in circuit parameters are also taken into account, and their effects on the network performance are evaluated.  Finally, a method to further enhance network performance and robustness is discussed.

## 5.2 System Modeling, Analysis and Network Design

### 5.2.1 Bladed disk system modeling and analysis

As discussed in the previous section, to better represent the dynamic characteristics of bladed disk systems, it is necessary to include the disk degrees-of-freedom in the model.   In literature, lumped mass-spring models that include disk degrees-of-freedom have been used in forced vibration studies (Kenyon et al., 2004; Baik et al., 2004).  With the disk degrees-of-freedom, these models can capture the frequency

veering characteristic that relates to blade-disk interaction, and have been shown to provide more insight to the bladed disk dynamics such as mistuning effects on forced vibration of bladed disks. Here, a similar model is proposed in Figure 5-1.
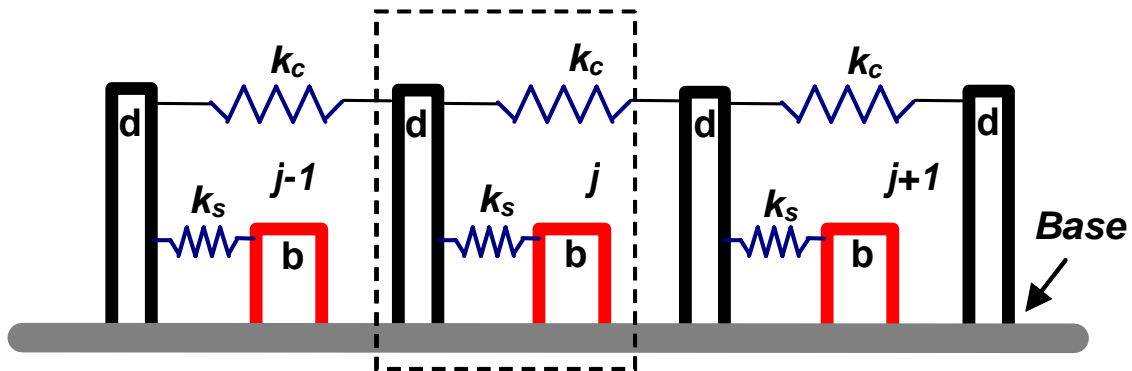


Figure **5-1**: Complex bladed disk model with consideration of disk dynamics.

In this new bladed disk model, assuming that the system has $N$ blades, the system is first virtually partitioned into $N$ repetitive identical *bays*, with each bay consisting of a sector of the disk (therefore, the whole disk is partitioned into $N$ identical disk sectors), and a blade (as shown in Figure 5-1, the $j^{th}$ bay is enclosed in the dotted frame). At each bay, the blade is modeled as a cantilever beam (marked with 'b', and referred to as the 'blade-model beam' hereafter), and for simplicity, the disk sector is also modeled as a cantilever beam (marked with 'd', and referred to as the 'disk-model beam' hereafter). The coupling mechanism of the system is modeled by two parts: spring $k_s$ that emulates the coupling between the blade and disk (blade-disk coupling), and spring $k_c$ that emulates the coupling between adjacent disk sectors (disk-disk coupling). Therefore, the inter-blade coupling is now implicitly modeled through the combination of the blade-disk

coupling and disk-disk coupling. The model is cyclically symmetric with a ring type

rigid base to provide clamping condition for those cantilever beams. It should be noted

that Figure 5-1 only shows a portion of the system for illustration purpose. Assuming

there are $N$ bays, the 1$^{st}$ bay is connected with the last bay (the $N^{th}$) to form a closed loop.

Following the same principle and procedure as used in (Tang and Wang, 1999)

and Chapter 4, one can derive the system equations. Here we only briefly describe the

procedure. For each cantilever beam, only the transverse motion, $w(x,t)$, is considered.

$w(x,t)$ is expanded using only the first mode of the cantilever beams, $\phi(x)$, i.e.,

$w(x,t) = q(t)\phi(x)$. Then using Hamilton's principle, equations of motion for the tuned

system can be derived as shown in Equations (5.1a,b),

$$m_b \ddot{x}_{bj} + k_b x_{bj} + c_1 \dot{x}_{bj} + k_s (x_{bj} - x_{dj}) = f_{bj} \tag{5.1a}$$

$$m_d \ddot{x}_{dj} + k_d x_{dj} + c_2 \dot{x}_{dj} + k_s (x_{dj} - x_{bj}) + k_c (2x_{dj} - x_{dj+1} - x_{dj-1}) = f_{dj} \tag{5.1b}$$

Here, $m_b$, $k_b$, $c_1$ (or $m_d$, $k_d$, $c_2$) are the mass, stiffness, and damping of the blade-

model beams (or disk-model beams); $k_s$ (or $k_c$) is the 'blade-disk' (or 'disk-disk')

coupling spring stiffness; $x_{bj}$ (or $x_{dj}$) is the generalized displacement of the $j^{th}$ blade-

model beam (or disk-model beam); $f_{bj}$ (or $f_{dj}$) is the force on the $j^{th}$ blade-model beam (or

disk-model beam). The force used in the study is the engine order excitation. Engine

order excitation applies the same forcing magnitude to each bay with a fixed phase

difference between adjacent bays. For example, the force on the $j^{th}$ blade-model beam

can be expressed in the form of: $f_{bj} = f_{b0} e^{i\theta(j-1)(E-1)}$, where $f_{b0}$ is the forcing amplitude,

$i = \sqrt{-1}$, $\theta = 2\pi/N$, $N$ is the total blade number, $E$ is the engine order number. The

phase difference between adjacent bays is $\theta(E-1)$, which is determined by the engine order number $E$. In this study, the same engine order excitation formula is applied to the disk-model beams.

To design the network, first the dynamics of the system is studied. The non-dimensional version is used (see Equations (5.2a,b)). Detailed non-dimensional parameters are shown in Equation (11).

$$-\Omega^2 \overline{x}_{bj} + i2\zeta_{c1}\Omega\overline{x}_{bj} + \overline{x}_{bj} + \overline{k}_s\overline{x}_{bj} - \frac{\overline{k}_s}{\sqrt{\overline{m}}}\overline{x}_{dj} = \overline{f}_{bj} \tag{5.2a}$$

$$\begin{aligned} -\Omega^2 \overline{x}_{dj} + i2\zeta_{c2}\delta_d\Omega\overline{x}_{dj} + \delta_d^2\overline{x}_{dj} + (\overline{k}_s/\overline{m})\overline{x}_{dj} \\ + \delta_d^2\overline{k}_c(2\overline{x}_{dj} - \overline{x}_{dj-1} - \overline{x}_{dj+1}) - (\overline{k}_s/\sqrt{\overline{m}})\overline{x}_{bj} = \overline{f}_{dj} \end{aligned} \tag{5.2b}$$

The parameters used for generating Figures 5-2 and 5-3 are: $N$=20, $\delta_d$=0.5, $\overline{m}$=10, $\overline{k}_s = 0.1364$, $\overline{k}_c = 2.1172$. Figure 5-2 depicts an example frequency veering plot based on the new bladed disk model (tuned system). Frequency veering (more generally known as curve veering) refers to a phenomenon where two natural frequency loci converge and then veer apart without crossing each other at certain point as some parameter varies. In this example, frequency veering occurs as the natural frequencies are plotted versus the nodal diameter number of the tuned modes, and occurs at a region around nodal diameter number 4 and 5. Curve veering has been widely studied in physics and engineering, with much attention on localization (Leissa, 1974; Perkins and Mote, 1986; Pierre, 1988; Kenyon et al., 2004; Baik et al., 2004). It has been shown that frequency veering is related to the coupling between mode shapes, which could lead to localization when the structure is disordered (Pierre, 1988). In bladed disk systems,

frequency veering is associated with the interaction between the blade dominant modes and the disk dominant modes. Studies (Bladh et al., 2002; Kenyon et al., 2004) on the forced vibration of bladed disks have shown that frequency veering increases the sensitivity of the tuned system to mistuning. Consequently, frequency veering can lead to a much higher amplitude magnification factor compared to the situations where frequency veering does not occur (e.g., in the case where only the blade degrees-of-freedom are considered).
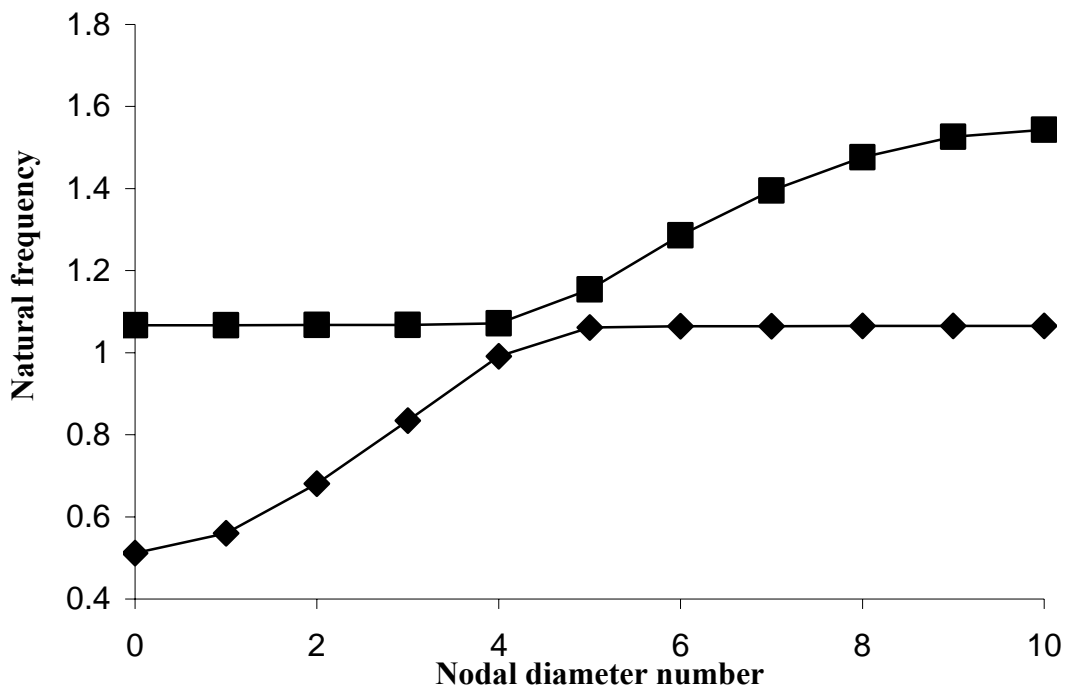


Figure **5-2**: Curve veering characteristics of bladed-disk system.
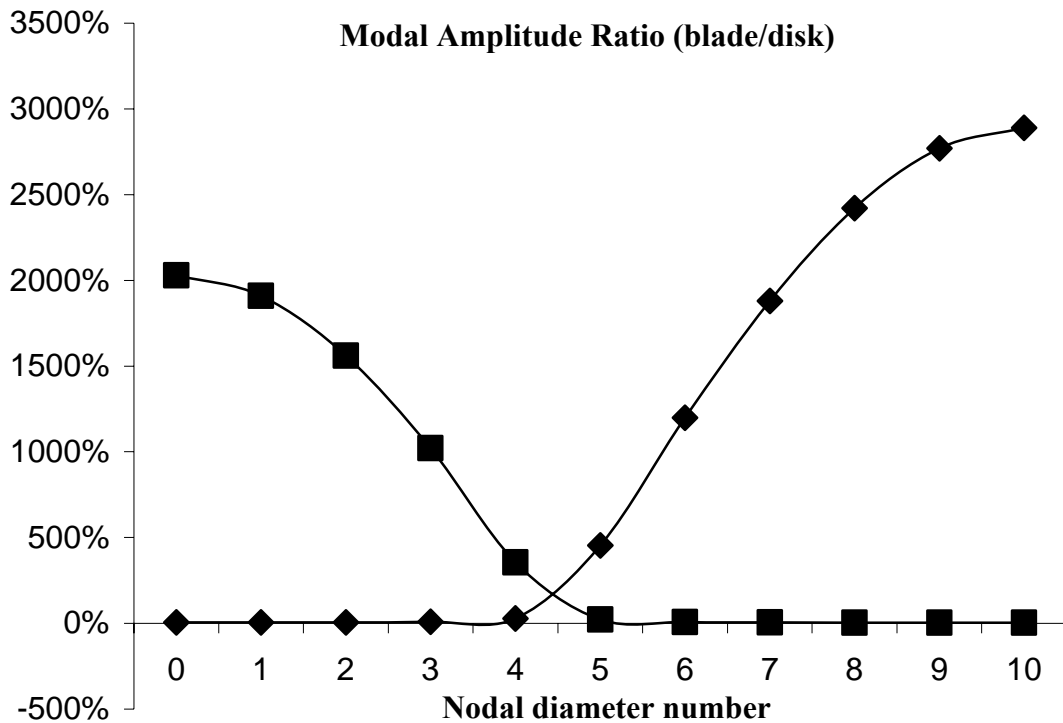
Figure **5-3**: Blade and disk modal amplitude ratio (blade/disk).

Figure 5-3 depicts the ratio between the modal amplitudes of the blade-model beams and the disk-model beams at each mode corresponding to Figure 5-2. Observing Figure 5-3, one can see that before veering, modes in the upper curve (squares) are blade dominant, while in the lower curve (diamonds) are disk dominant. After veering, the modes in the upper curve (diamonds) become disk dominant, while in the lower curve (squares), modes become blade dominant. Although for the modes in the veering region (with nodal diameter 4 and 5), the modal amplitude difference between the blade and disk are not as large as those in the off-veering region, still, one component (either blade or disk) is dominant. From Figures 5-2 and 5-3, it is also observed that the blade dominant

modes are clustered in natural frequencies around frequency 1.1, while disk dominant modes have a wider frequency span (from about 0.5 to 1.6). This characteristic captures one of the modal features of the bladed disk systems, where the blade dominant modes tend to be less affected by the nodal diameter (thus frequency curve is flatter versus nodal diameter), whereas the disk dominant modes tend to be more affected by the nodal diameter (thus frequency curve is steeper versus nodal diameter).

### 5.2.2 Multi-circuit network design and analysis

In this research, a new multi-circuit network architecture is proposed to achieve effective vibration suppression for this bladed disk model. The bladed disk model with integrated new piezoelectric circuitry configuration is shown in Figure 5-4. This new network is constructed in the following fashion. First, piezoelectric patches are embedded to the root of each cantilever beam, as shown in Figure 5-4. The corresponding treatment on the corresponding actual bladed-disk system would be: on each blade, a piezoelectric patch is applied to the position close to the root of the blade (note that the blade is fixed to the disk); and on the disk, each piezoelectric patch is applied to each disk sector, at the root position of the sector (note that the disk is fixed to the rotating shaft, and is first virtually partitioned into $N$ identical sectors as discussed in the previous section). On each blade-model beam, local damped absorber shunt circuit is formed by connecting the piezoelectric patch with an inductor ($L_1$) and a resistor ($R_1$). On each disk-model beam, a coupled circuit network is configured as shown in Figure 5-4 using $L_2$, $R_2$, $C_2$, and $C_a$. Here $L_2$, $R_2$ and the piezoelectric patch form a local shunt.

Capacitor $C_a$ is used to couple these local shunt circuits. The additional capacitor $C_2$ is added to cancel out some effects caused by the mechanical coupling $k_s$ between the blade-model beam and the disk-model beam. The importance of these two capacitive elements will be clearer in the derivation of the optimal network for suppressing multiple harmonics.
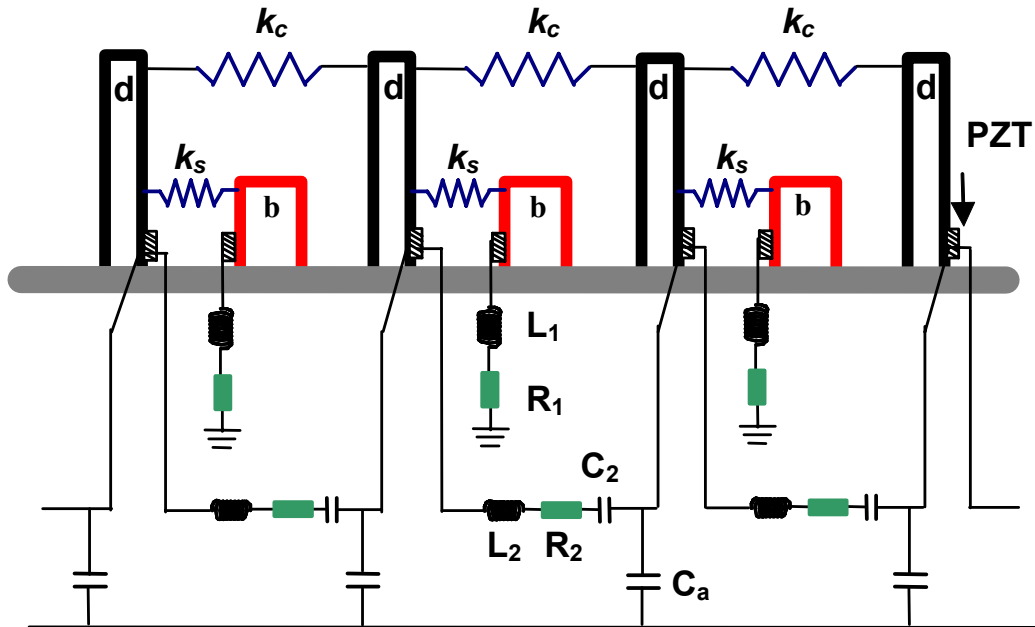


Figure **5-4**: Bladed disk model with piezoelectric network.

The equations of motion for the electro-mechanically integrated system in Figure 5-4 can be derived using Hamilton's principle and circuit analysis procedure similar to that in (Tang and Wang, 2003):

$$m_b \ddot{x}_{bj} + k_b x_{bj} + c_1 \dot{x}_{bj} + k_s (x_{bj} - x_{dj}) + k_{bp1} Q_{1j} = f_{bj} \tag{5.3a}$$

$$L_1 \ddot{Q}_{1j} + k_{pzt1} Q_{1j} + R_1 \dot{Q}_{1j} + k_{bp1} x_{bj} = 0 \qquad (5.3b)$$

$$m_d \ddot{x}_{dj} + k_d x_{dj} + c_2 \dot{x}_{dj} + k_c (2x_{dj} - x_{dj-1} - x_{dj+1}) + k_s (x_{dj} - x_{bj}) + k_{bp2} Q_{2j} = f_{dj} \qquad (5.3c)$$

$$L_2 \ddot{Q}_{2j} + k_{pzt2} Q_{2j} + R_2 \dot{Q}_{2j} + k_2 Q_{2j} + k_a (2Q_{2j} - Q_{2j-1} - Q_{2j+1}) + k_{bp2} x_{dj} = 0 \qquad (5.3d)$$

Here, Equation (5.3b) is derived from the circuit branch on the $j^{th}$ blade-model beam, and Equation (5.3d) is derived from the circuit branch on the $j^{th}$ disk-model beam. In Equation (5.3), $k_{bp1}$ (or $k_{bp2}$) are parameters related to the electro-mechanical coupling factors of the piezoelectric patches on the blade-model beams (or disk-model beams); $L_1$, $R_1$ (or $L_2$, $R_2$) are inductance and resistance in the circuit connected to piezoelectric patch on the blade-model beams (or disk-model beams). $k_{pzt1}=1/C_{pzt1}$ (or $k_{pzt2}=1/C_{pzt2}$) is the inverse of piezoelectric capacitance on the blade-model beams (or disk-model beams). $k_2=1/C_2$, is the inverse of the additional capacitance $C_2$; and $k_a=1/C_a$, is the inverse of coupling capacitance $C_a$; $Q_{1j}$ (or $Q_{2j}$) is the charge flow across the piezoelectric patch on the $j^{th}$ blade-model beam (or disk-model beam).

Due to the complexity of the system, it is very difficult to analytically derive the closed form optimal circuit parameter tuning from the original equations of motion in Equations (5.3a,b,c,d). However, based on the observation from the analyses in Figure 5-2 and Figure 5-3, it is reasonable to separate the design problem into two parts: (a) the blade-dominant case and (b) the disk-dominant case. In part (a), where the system dynamics are blade dominant, Equations (5.3a) and (5.3b) can be approximated by neglecting the disk degree of freedom $x_{dj}$, and simplified as Equations (5.4a,b). In part (b), where the dynamics are disk dominant, Equations (5.3c) and (5.3d) can be

approximated by neglecting blade degree of freedom $x_{bj}$, and simplified as shown in Equations (5.4c,d).

$$m_b \ddot{x}_{bj} + k_b x_{bj} + c_1 \dot{x}_{bj} + k_s x_{bj} + k_{bp1} Q_{1j} = f_{bj} \tag{5.4a}$$

$$L_1 \ddot{Q}_{1j} + k_{pzt1} Q_{1j} + R_1 \dot{Q}_{1j} + k_{bp1} x_{bj} = 0 \tag{5.4b}$$

$$m_d \ddot{x}_{dj} + k_d x_{dj} + c_2 \dot{x}_{dj} + k_c (2x_{dj} - x_{dj-1} - x_{dj+1}) + k_s x_{dj} + k_{bp2} Q_{2j} = f_{dj} \tag{5.4c}$$

$$L_2 \ddot{Q}_{2j} + k_{pzt2} Q_{2j} + R_2 \dot{Q}_{2j} + k_2 Q_{2j} + k_a (2Q_{2j} - Q_{2j-1} - Q_{2j+1}) + k_{bp2} x_{dj} = 0 \tag{5.4d}$$

Following the same U-transformation technique and design procedures that are used in (Tang and Wang, 1999) and Chapter 4, an optimal solution can be derived from Equations (5.4a,b) for $L_1$ and $R_1$ tuning, which are given in Equations (5.5a,b). The detailed process is omitted here.

$$L_{1opt} = k_{pzt1} m_b / (k_b + k_s) \tag{5.5a}$$

$$R_{1opt} = k_{bp1} \sqrt{2m_b k_{pzt1}} / (k_b + k_s) \tag{5.5b}$$

From Equations (5.4c,d), following the same design procedure, one can derive inductance tuning for $L_2$,

$$L_2 = \frac{[k_{pzt2} + k_2 + 2k_a(1 - \cos((j-1)\theta))]m_d}{k_d + k_s + 2k_c(1 - \cos((j-1)\theta))} \tag{5.6}$$

where $j$ now denotes the $j^{th}$ spatial harmonic. From Equation (5.6), it is clear that this inductance tuning is dependent on the spatial harmonic $j$. However, if one tune the additional capacitor ($C_2$) and coupling capacitor ($C_a$) such that Equations (5.7a,b) are satisfied, one can simplify the expression Equation (5.6) and obtain a solution that is independent of spatial harmonic $j$, as shown in Equation (5.8). Here, one can see that in order to get this solution, $k_a$ and $k_2$ play an very important role.

$$k_2 / k_{pzt2} = k_s / k_d \tag{5.7a}$$

$$k_a / k_{pzt2} = k_c / k_d \tag{5.7b}$$

$$L_{2opt} = k_{pzt2} m_d / k_d \tag{5.8}$$

Following the same procedure as used in Chapter 4 and (Zhang and Wang, 2002), circuit resistance tuning can be derived. Since our previous studies have shown that network performance is not sensitive to resistance tuning, which will also be seen in the study that follows, the resistance tuning in the circuits on the disk-model beams is tuned to spatial harmonic $j=1$, as shown below:

$$R_{2opt} = k_{bp2} \sqrt{2m_d k_{pzt2}} / k_d \sqrt{1 + k_s / k_d} \tag{5.9}$$

The system equations in Equations (5.3a,b,c,d) can also be non-dimensionalized, as shown in Equations (5.10a,b,c,d). Future simulation is conducted using these non-dimensionalized equations of motion. These equations are for a tuned system. For a mistuned system, the equations can be modified by adding additional random mistuning to the appropriate terms, the details of which are not discussed here.

$$-\Omega^2 \overline{x}_{bj} + i2\zeta_{c1}\Omega \overline{x}_{bj} + \overline{x}_{bj} + \overline{k}_s \overline{x}_{bj} - \frac{\overline{k}_s}{\sqrt{\overline{m}}} \overline{x}_{dj} + \delta_{e1}\xi_1 \overline{Q}_{1j} = \overline{f}_{bj} \tag{5.10a}$$

$$-\Omega^2 \overline{Q}_{1j} + \delta_{e1}^2 \overline{Q}_{1j} + i2\zeta_{R1}\Omega\delta_{e1}\overline{Q}_{1j} + \delta_{e1}\xi_1 \overline{x}_{bj} = 0 \tag{5.10b}$$

$$-\Omega^2 \overline{x}_{dj} + i2\zeta_{c2}\delta_d\Omega \overline{x}_{dj} + \delta_d^2 \overline{x}_{dj} + (\overline{k}_s / \overline{m}) \overline{x}_{dj}$$
$$+\delta_d^2 \overline{k}_c (2\overline{x}_{dj} - \overline{x}_{dj-1} - \overline{x}_{dj+1}) - (\overline{k}_s / \sqrt{\overline{m}}) \overline{x}_{bj} + \delta_{e2}\delta_d\xi_2 \overline{Q}_{2j} = \overline{f}_{dj} \tag{5.10c}$$

$$-\Omega^2 \overline{Q}_{2j} + \delta_{e2}^2 \overline{Q}_{2j} + i2\zeta_{R2}\Omega\delta_{e2}\overline{Q}_{2j} + \delta_{e2}^2 \overline{k}_2 \overline{Q}_{2j}$$
$$+\delta_{e2}^2 \overline{k}_a (2\overline{Q}_{2j} - \overline{Q}_{2j-1} - \overline{Q}_{2j+1}) + \delta_{e2}\delta_d\xi_2 \overline{x}_{dj} = 0 \tag{5.10d}$$

Here, the non-dimensionalization parameters are:

$$\Omega = \omega / \omega_b, \ \delta_d = \omega_d / \omega_b, \ \omega_b = \sqrt{k_b / m_b}, \ \omega_d = \sqrt{k_d / m_d}, \ \overline{x}_{bj} = x_{bj}\sqrt{m_b}, \ \overline{x}_{dj} = x_{dj}\sqrt{m_d},$$

$$\overline{k}_s = k_s / k_b, \ \overline{k}_c = k_c / k_d, \ \overline{m} = m_d / m_b, \ \overline{f}_{bj} = f_{bj}\sqrt{m_b} / k_b, \ \overline{f}_{dj} = f_{dj}\delta_d^2\sqrt{m_d} / k_d,$$

$$\zeta_{c1} = c_1 / (2m_b\omega_b), \ \zeta_{c2} = c_2 / (2m_d\omega_d), \ \delta_{e1} = \omega_{e1} / \omega_b, \ \delta_{e2} = \omega_{e2} / \omega_b, \ \overline{Q}_{1j} = Q_{1j}\sqrt{L_1}, \quad (11)$$

$$\overline{Q}_{2j} = Q_{2j}\sqrt{L_2}, \ \overline{k}_2 = k_2 / k_{pzt2}, \ \overline{k}_a = k_a / k_{pzt2}, \ \xi_1 = k_{bp1} / \sqrt{k_b k_{pzt1}}, \ \xi_2 = k_{bp2} / \sqrt{k_b k_{pzt2}},$$

$$\zeta_{R1} = R_1 / (2L_1\omega_{e1}), \ \zeta_{R2} = R_2 / (2L_2\omega_{e2})$$

The key tuning factors in the circuits are: (1) for the non-coupled circuit branch on the blade-model beams: the electric circuit frequency tuning ratio $\delta_{e1}$ (related to inductance $L_1$), and circuit damping ratio $\zeta_{R1}$ (related to resistance $R_1$); (2) for the coupled circuit branch on the disk-model beams: the circuit frequency tuning ratio $\delta_{e2}$ (related to inductance $L_1$), the circuit damping ratio $\zeta_{R2}$ (related to resistance $R_2$), capacitance ratio $\overline{k}_2$ (related to the additional capacitance $C_2$), and coupling capacitance ratio $\overline{k}_a$ (related to the coupling capacitance $C_a$).

The non-dimensionalized counterparts for the circuit tunings in Equations (5.5a,b) and Equations (5.7) – (5.9) are shown in Equations (5.12a,b) and Equations (5.13)-(5.16).

For circuits on the blade-model beams:

$$\delta_{e1} = \sqrt{1 + \overline{k}_s} \tag{5.12a}$$

$$\zeta_{R1} = \xi_1 / \sqrt{2(1 + \overline{k}_s)} \tag{5.12b}$$

For circuits on the disk-model beams:

$$\overline{k}_2 = \overline{k}_s / m / \delta_d^2 \tag{5.13}$$

$$\bar{k}_a = \bar{k}_c \tag{5.14}$$

$$\delta_{e2} = \delta_d \tag{5.15}$$

$$\zeta_{R2} = \xi_2 / \sqrt{2(1+\bar{k}_2)} \tag{5.16}$$

### 5.2.3 Multiple-harmonic vibration suppression

Next, the effectiveness of this network for multiple harmonic vibration suppression of bladed disks is examined by analysis. In all the simulations thereafter, parameters for the baseline bladed disk system are: $N$=20, $\zeta_{c1}$=0.05%, $\zeta_{c2}$=0.05%, $\delta_d$=0.5, $\bar{m}$=10, $\bar{k}_s = 0.1364$, $\bar{k}_c = 2.1172$, $|\bar{f}_{bj}|$=1, $|\bar{f}_{dj}|$=5.

Figures 5-5 shows the comparison of the vibration suppression performances between the newly developed network (black solid line) and the 'traditional' absorber (grey solid line). The black dotted line is the forced response of the baseline bladed disk system without any circuit. The 'traditional' absorber design is referred to as simple uncoupled individual *LCR* circuits applied to each cantilever beam (regardless of representing blade or disk sector) in Figure 5-1, without $C_2$ and $C_a$ elements. More specifically, for the blade-model beams, the circuits remain the same; for the disk-model beams, circuits with the same architecture as those used on the blade-model beams are applied here. Following the same derivation procedure in Chapter 4, it can be shown that the optimal inductance tuning for traditional absorber is dependent on spatial harmonic $j$, the mathematical expression of which is $L_{opt\_trad} = \dfrac{k_{pzt2} m_d}{k_d + k_s + 2k_c(1 - \cos((j-1)\theta))}$. This

means traditional absorber can only be tuned to suppress a specific spatial harmonic ($j$) in engine order excitations.  In Figure 5-5, the spatial harmonic $j$ for the traditional absorber is arbitrarily chosen to be $j=1$.  The force is a summation of all engine order excitations, thus contains multiple harmonics.

Figure 5-5 shows the maximum response of the blade-model beams.  It can be seen that compared to the traditional absorber, the optimal network is much more effective in suppressing multiple harmonics simultaneously, and as a result, the maximum responses are much lower.
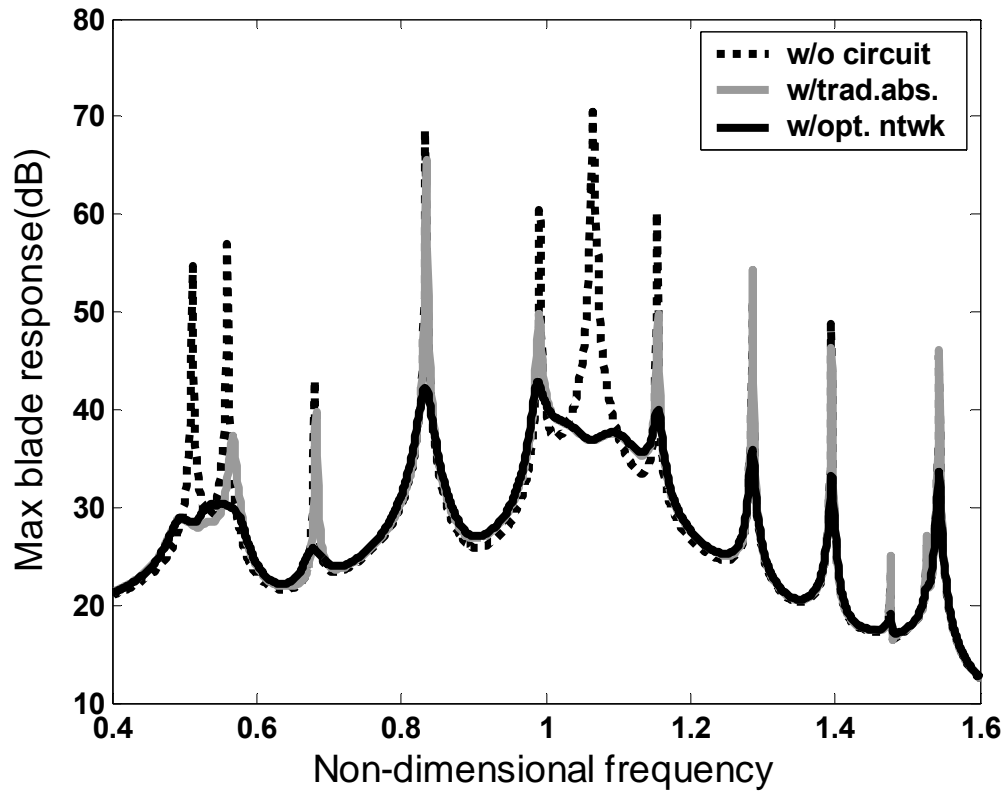
Figure **5-5**: Maximum response of the blade-model beams versus frequency for: without circuit case, with traditional absorber case, and with the new optimal network case.

## 5.3 Analysis of Network Performance

In this section, the performance of the newly designed network for vibration suppression of mistuned bladed disks is systematically analyzed. The evaluation is conducted through Monte Carlo simulation. The performance is first examined for bladed disk with different random mistuning levels, where circuits are assumed to be tuned as defined in Equations (5.12) to (5.16). Then, the performance and robustness of

the network are examined by considering mistuning and detuning in the circuit parameters. When considering mistuning in the circuit parameters, the mechanical system (bladed disk) is assumed to be tuned. When considering detuning in circuit parameters, the mechanical system is assumed to be mistuned with standard deviation $\sigma$ =0.01.

### 5.3.1 Monte Carlo simulation

Monte Carlo simulation is used in the following analyses. In our study, random mistuning is quantified by its standard deviation $\sigma$. For a given standard deviation, there are virtually infinite sets of random realizations; therefore, one has to generate a large number of mistuned systems in order to obtain a relatively solid conclusion. Here, for the trade-off of accuracy and computational time, the number of realizations is chosen to be 100. That is, for each standard deviation of mistuning, 100 mistuned systems are generated. Then forced response is solved for each mistuned system with frequency sweep. The force is engine order excitation, with all engine orders considered, one at a time. Then the maximum blade responses of 'with circuit' case and 'without circuit' case are extracted and a *maximum blade response ratio r* is defined:

$$r = \frac{\text{max blade response with circuit}}{\text{max blade response without circuit}}$$

Monte Carlo simulation produces 100 ratios. A statistical data, the 95$^{\text{th}}$ percentile value is extracted from the distribution of these results. The 95$^{\text{th}}$ percentile value is the one that only five percent of the data exceeds, and is used as the *performance index*.

From the definition of *r*, it is clear that smaller *r* indicates better performance, so, smaller index means better performance.

### 5.3.2 Performance with mechanical mistuning

First, the network performance for vibration suppression of mistuned bladed disk is considered.  The network is tuned according to Equations (5.12) to (5.16).  Random mistuning in both blades and disk sectors are taken into account.  For simplicity, in this model, we assume the mistuning only exists in the stiffness of the blade-model beams and the disk-model beams.  Mistuning patterns follow normal distribution with the same standard deviation.  Hereafter, only the blade vibration amplitudes are analyzed.  The result from Monte Carlo simulation is shown in Figure 5-6.  Figure 5-6 plots the performance index versus mechanical mistuning level (the standard deviation $\sigma$), within a reasonable range from $\sigma = 0$ to $\sigma = 0.08$.  It can be seen from Figure 5-6 that the performance of the network degrades as mistuning level increases.  For the tuned case ($\sigma = 0$, no mistuning), the performance index is about 0.06, which means, compared to the baseline mechanical system without circuits, the network can reduce the maximum blade response by 94%.  At the highest mistuning level considered, $\sigma = 0.08$, the ratio is below 0.11, which only increases from the tuned case by 0.05.  The curve shows that an 89% reduction in blade vibration can be achieved over the whole mistuning range by using the network.  Therefore, from the simulation results, one can conclude that although the network is designed based on the tuned system through an approximation approach, it performs very well for vibration suppression of mistuned system as well.
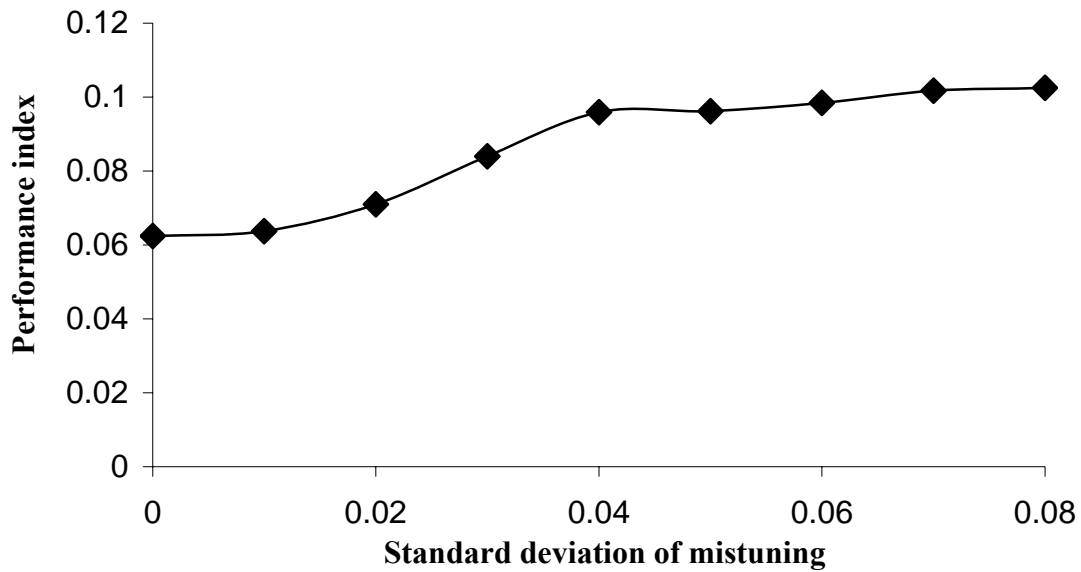
Figure **5-6**: Performance index versus standard deviation of mechanical mistuning.

### 5.3.3 Performance with circuit parameter variations

In this complicated circuit network, there are many components. It is possible that variations between the same components in different local branches may exist. In the following study, variations such as mistuning and detuning are taken into account for the evaluation of the circuit performance and robustness. The baseline circuit network is the optimal network with parameters tuned according to Equations (5.12)-(5.16). In this study, the variations in the non-dimensionalized circuit tuning parameters listed in the left hand side of Equations (5.12)-(5.16) will be examined. Here, the effects of both mistuning and detuning in those key parameters on network performance will be evaluated. Similar to the mistuning consideration of mechanical parameters, mistuning in electrical parameters is also assumed to be random numbers quantified by the standard

deviation σ. Mistuning range is also taken to be σ =0 to σ =0.08. Detuning refers to the case where the same parameters in each local branch are uniformly off-tuned by the same amount. Detuning can be caused by errors such as modeling error, and can be larger than mistuning, therefore, a range of [-20%, +20%] detuning is considered in our study.

First, let us discuss the effects of circuit parameter mistuning on the performance of the network. In this case, the bladed disk is assumed to be tuned. The results are shown in Figures 5-7 to 5-10.

Figure 5-7 and Figure 5-8 show the effect of mistuning in $\delta_{e1}$, the frequency tuning ratio for the piezoelectric circuits on the blade-model beams, and the effect of mistuning in $\delta_{e2}$, the frequency tuning ratio for the piezoelectric circuits on the disk-model beams. It can be seen from both figures, that increasing mistuning level in these two parameters will generally increase the performance index, which means mistuning in these two parameters will degrade the network performance. For both mistuning cases, the largest performance index is less than 0.3 at the largest mistuning level (σ =0.08). This means more than 70% vibration can be reduced within the whole range of mistuning in $\delta_{e1}$ or $\delta_{e2}$. For the smaller range of mistuning ($\sigma \leq 0.04$), the vibration amplitude reduction is more than 90% for the mistuned $\delta_{e1}$ case and more than 80% for the mistuned $\delta_{e2}$ case. Another interesting observation from Figure 5-7 is that, smaller mistuning in $\delta_{e1}$ ($\sigma \leq 0.04$) has little effect on the performance compared to the tuned case (σ =0), while with larger mistuning level in $\delta_{e1}$ (σ > 0.04), the network performance is more sensitive.
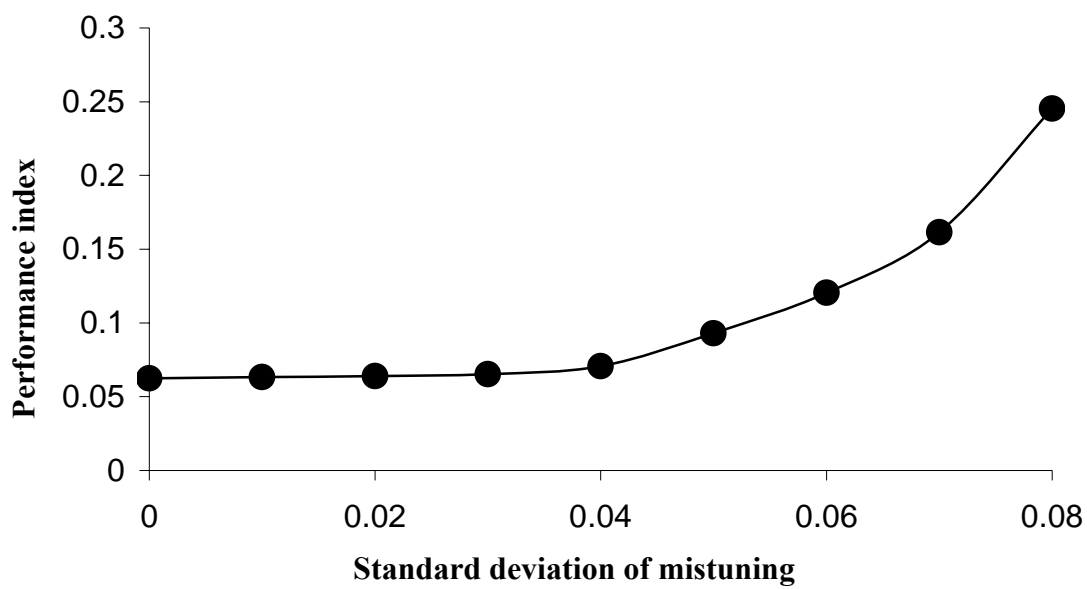
Figure **5-7**:   Performance index versus standard deviation of mistuning in circuit frequency tuning ratio $\delta_{e1}$.
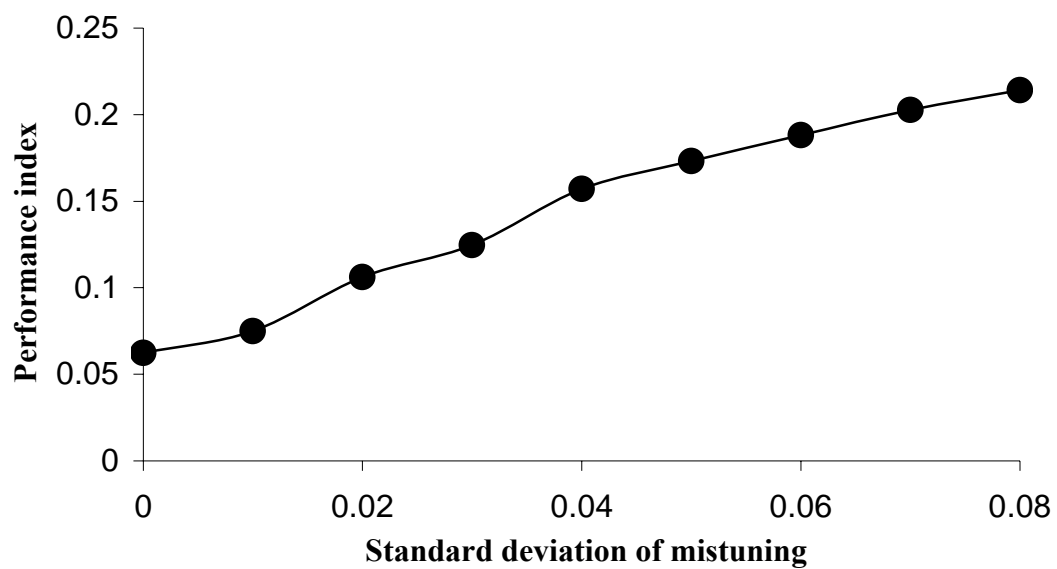
Figure **5-8**: Performance index versus standard deviation of mistuning in circuit frequency tuning ratio $\delta_{e2}$.
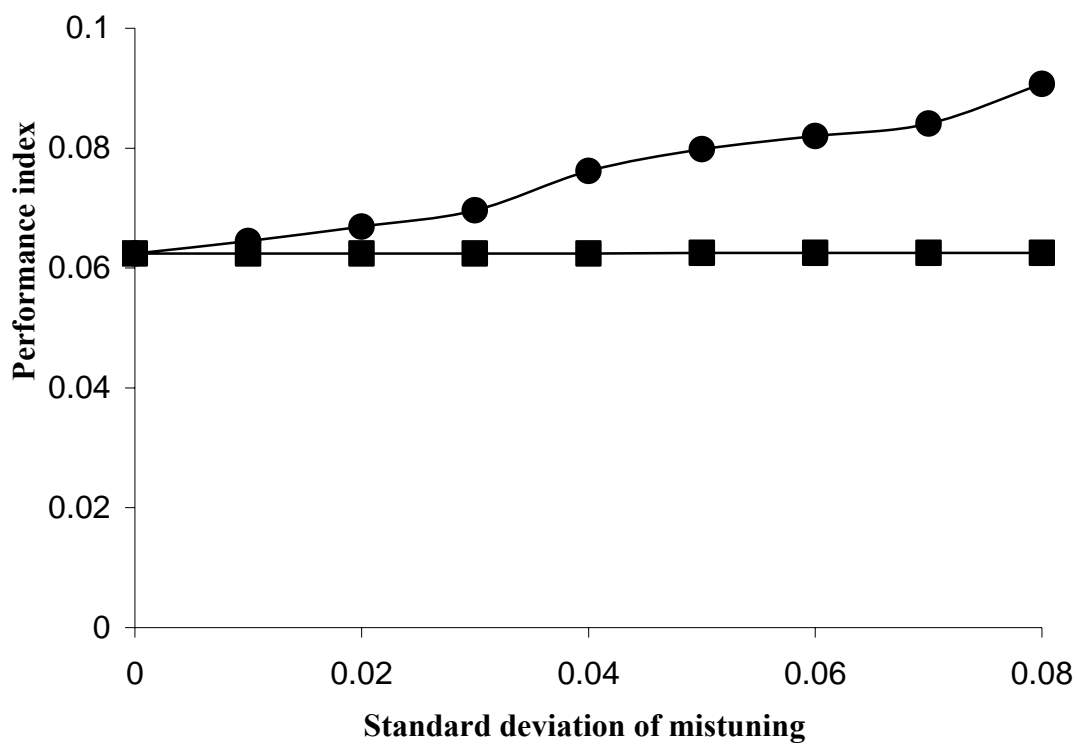
Figure **5-9**:  Performance index versus standard deviation of mistuning in additional capacitance tuning ratio $\bar{k}_2$ (■) and coupling capacitance tuning ratio $\bar{k}_a$ (●).
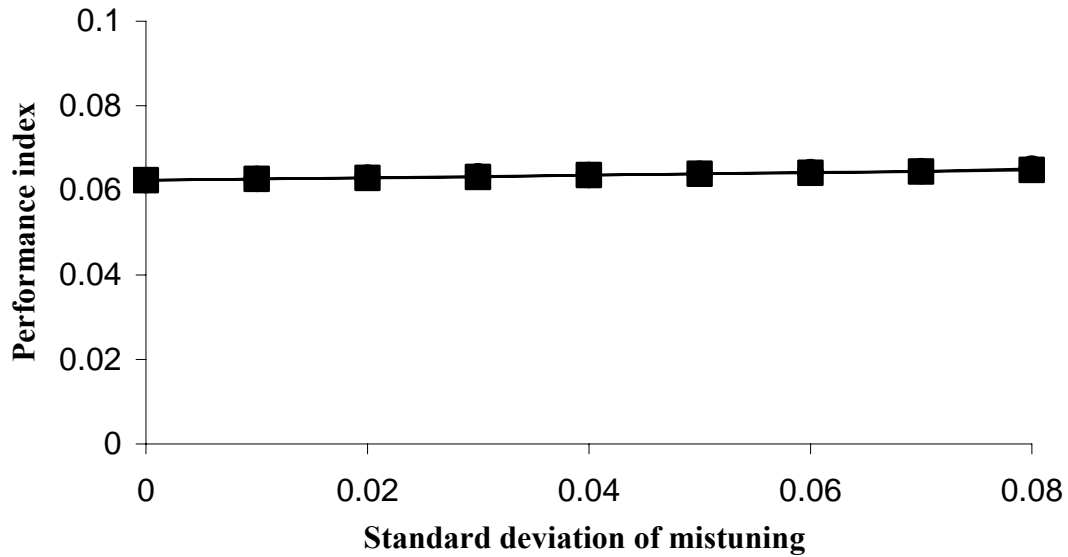
Figure **5-10**:  Performance index versus standard deviation of mistuning in resistance damping ratio $\zeta_{R1}(\blacksquare)$ and $\zeta_{R2}(\bullet)$.

Figure 5-9 shows the results with mistuning consideration in two parameters associated with the circuits on the disk-model beams: $\overline{k}_a$, which is related to the coupling capacitance, and $\overline{k}_2$, which is related to the additional capacitance.  As the figure shows, the performance index remains almost unchanged when the mistuning level is increased from $\sigma = 0$ to $\sigma = 0.08$ for $\overline{k}_2$.  This means the network is not sensitive to mistuning in the additional capacitance.  For $\overline{k}_a$, the index is slightly increased as mistuning level is increased, as shown in Figure 5-9.  With the largest mistuning level in $\overline{k}_a(\sigma = 0.08)$, the index is still less than 0.1, indicating over 90% reduction in the maximum blade response.

Figure 5-10 shows the results with mistuning in electrical damping ratios: $\zeta_{R1}$, which is related to the resistance in the circuits on the blade-model beams, and $\zeta_{R2}$,

which is related to the resistance in the circuits on the disk-model beams. As both curves show, the mistuning effects in these two parameters on the network performance are negligible.

In summary, from the above analyses, it is clear that among these key parameters, the network is relatively more sensitive to the circuit frequency tuning ratios $\delta_{e1}$ and $\delta_{e2}$, and less sensitive to the coupling capacitance (reflected in $\bar{k}_a$), additional capacitance (reflected in $\bar{k}_2$), and resistance damping ratio $\zeta_{R1}$ and $\zeta_{R2}$ for the case studied. At the largest mistuning level in all cases, all the performance indices are less than 0.3, which means over 70% reduction in the maximum blade response. Therefore, the overall performance of the network can be regarded as quite robust against the mistuning in circuit parameters. For those parameters with higher sensitivity to mistuning, a method with negative capacitance can be used to improve the performance and robustness, which will be discussed later.

Next, the circuit network performance is studied by considering detuning in the circuit parameters. As mentioned earlier, detuning is different from mistuning. Detuning is a uniform off-tune for the same parameters in all circuit branches from their nominal values, while mistuning is random. In this study, the detuning range is taken to be [-20%, +20%] for each parameter. The results are shown in Figures 5-11 to 5-14. The nominal values for the parameters before detuning are according to Equations (5.12) to (5.16).

Figure 5-11 shows the effect of detuning in $\delta_{e1}$. On the horizontal axis, 0% corresponds to 'no detuning' case (the nominal case). The best performance seems to occur not at the nominal case, but at -5% detuning. This could be due to the reason that

the set of approximated equations (Equations (5.4a,b,c,d)) are used to derive the optimal tuning. However, the performance index only changes slightly when the parameter is detuned to the -5% detuning point from the nominal case (0% detuning case). The worst situation in the whole detuning range has an index of 0.25 (at -20% detuning), which means a 75% vibration reduction. Within a more modest range of detuning, [-10%, +10%], the effects of detuning on network performance tend to be very small. For instance, the performance index only changes from 0.054 (or 94.6% vibration reduction) at the lowest point (with -5% detuning) to 0.08 (or 92% vibration reduction) at the highest point (with 10% detuning). For detuning greater than 10% in magnitude, the effect on the network performance becomes larger, as indicated by the relatively deeper slope.

Figure 5-12 shows the effect of detuning in $\delta_{e2}$. In this figure, the 'no detuning' case (0%) shows the best performance. Detuning towards either positive or negative direction will increase the index monotonically. Compared to Figure 5-11, detuning in $\delta_{e2}$ has larger effect on system performance than that in $\delta_{e1}$, in other words, system performance is more sensitive to detuning in $\delta_{e2}$ than in $\delta_{e1}$. In the worst situation, a -20% detuning in $\delta_{e2}$ will increase performance index to about 0.7, which means only 30% reduction can be achieved. Further treatment to improve the robustness of the network against $\delta_{e2}$ will be discussed later.

Figure 5-13 plots the result concerning detuning in $\bar{k}_a$. It also shows that the nominal case (0% detuning) has best performance. Both positive and negative detuning will degrade the network performance. In the worst situation, at -20% detuning, the performance index is 0.25, which corresponds to a 75% reduction in vibration.

Figure 5-14 depicts detuning in three parameters: the additional capacitance tuning ratio $\overline{k}_2$, circuit resistance damping ratios $\zeta_{R1}$ and $\zeta_{R2}$. As seen from the figure, the detuning in these three parameters will not change the network performance much, in other words, the network is quite robust against these parameters.
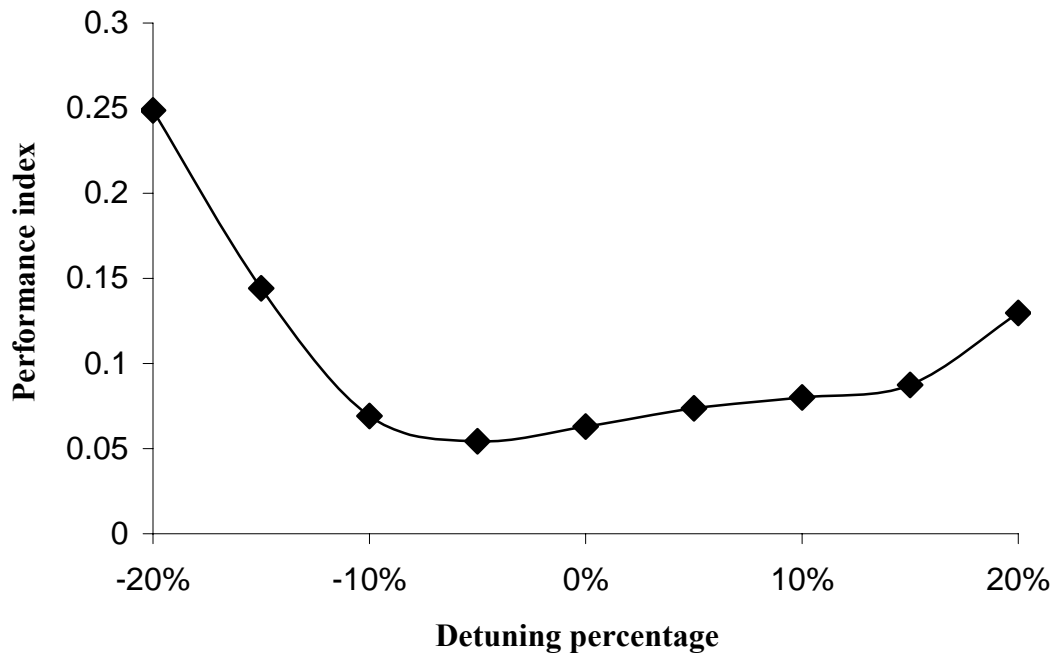


Figure **5-11**:  Performance index versus detuning in circuit frequency tuning ratio $\delta_{e1}$.
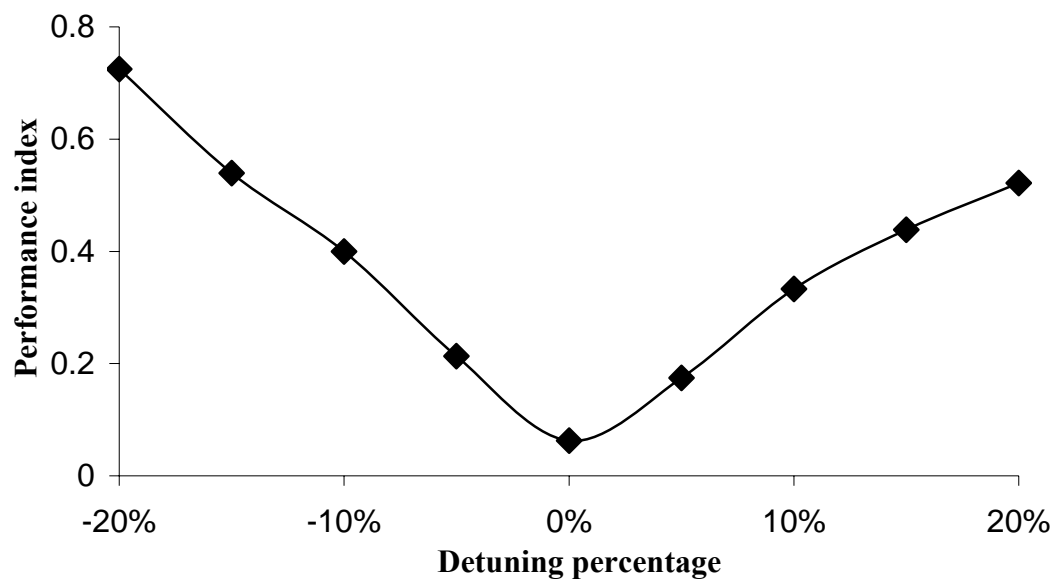
Figure **5-12**:  Performance index versus detuning in circuit frequency tuning ratio $\delta_{e2}$.
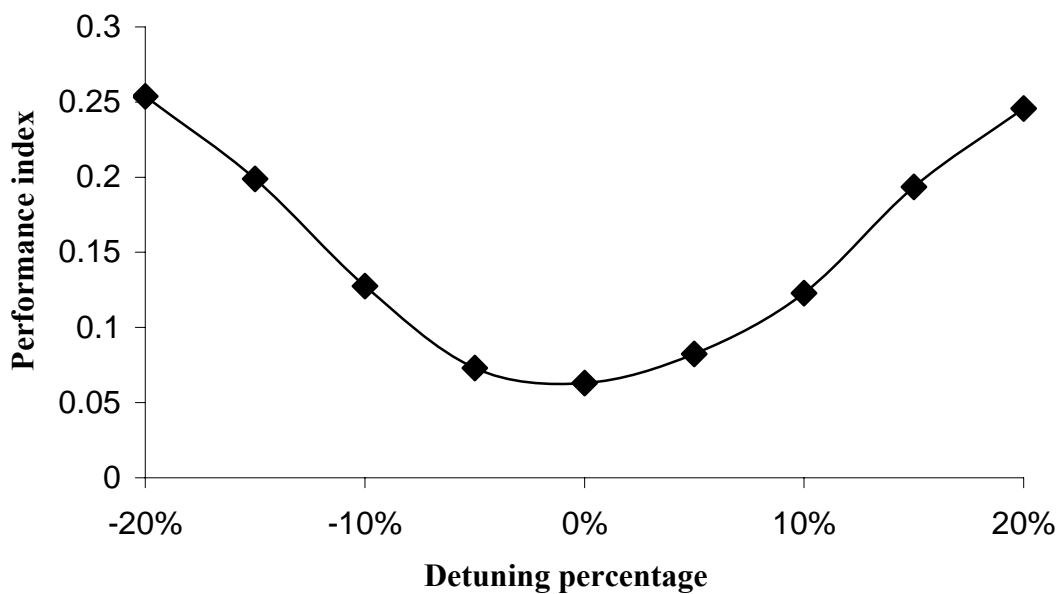


Figure **5-13**:  Performance index versus detuning in coupling capacitance tuning ratio $\bar{k}_a$.
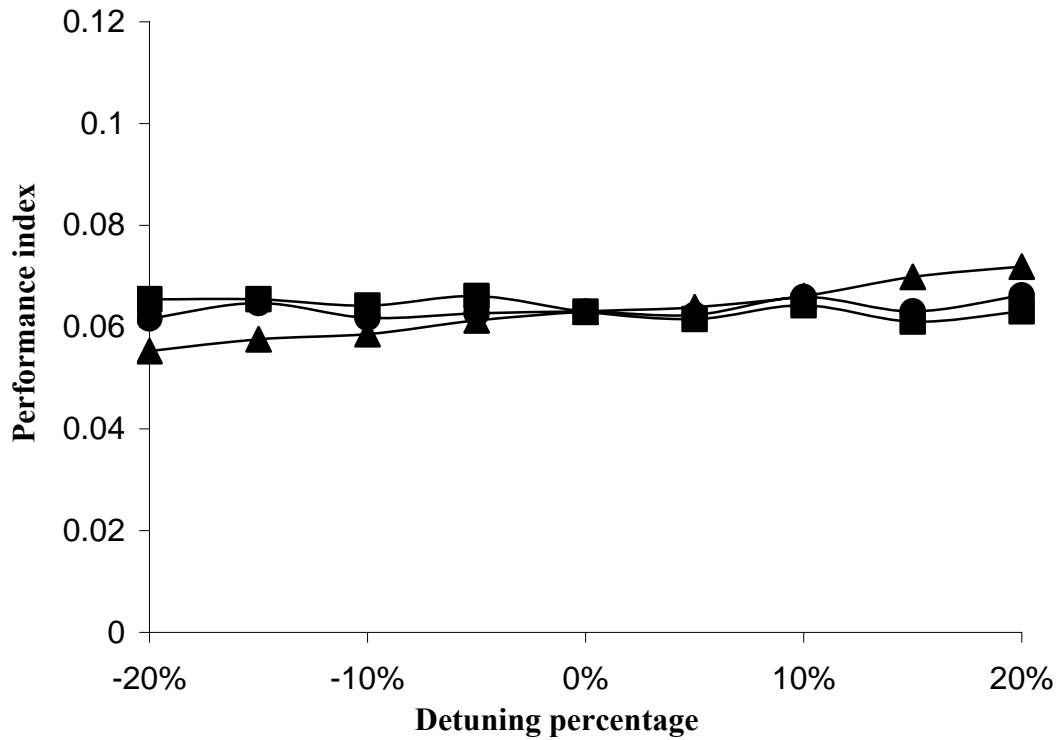
Figure **5-14**: Performance index versus detuning in additional capacitance tuning ratio $\bar{k}_2$ ($\bullet$), resistance damping ratio $\zeta_{R1}$ ($\blacksquare$) and resistance damping ratio $\zeta_{R2}$ ($\blacktriangle$).

In summary, the study shows that the network performance is relatively more sensitive to the detuning in $\delta_{e2}$ and less sensitive to the detuning in $\bar{k}_2$, $\zeta_{R1}$ and $\zeta_{R2}$. For most parameters (except $\delta_{e2}$), the network can achieve at least 75% reduction in vibration amplitude within the whole detuning range investigated. Network performance can be severely degraded if detuning in $\delta_{e2}$ is large (e.g., -20%), as shown in Figure 5-12. In this situation, a more advanced treatment with negative capacitance can help improve the robustness and performance of the network, which will be discussed next.

**5.3.4 Performance enhancement with negative capacitance**

It is shown in above analyses that in most cases with modest range of mistuning and detuning ($\sigma \leq 0.04$ for mistuning, and within ±10% for detuning), the network can provide good vibration suppression results. However, in some cases (e.g., $\delta_{e2}$), large detuning can severely degrade the suppression performance. Therefore, one may need to use further treatments to improve the performance and robustness of the network. Negative capacitance has been shown to be able to fulfill this purpose, as discussed in Chapters 2, 3, 4. Negative capacitance can be realized by a negative impedance circuit (Tang and Wang, 2001). It has been shown that negative capacitance can be used to increase the electro-mechanical coupling of piezoelectric transducers. The effect of the negative capacitance on improving network performance and robustness has been shown in Chapter 4. Here similar study is conducted for all cases with mechanical mistuning, and circuit parameter mistuning and detuning, where similar conclusions are found. That is, by increasing the electro-mechanical coupling of the piezoelectric transducers using negative capacitance, the network performance and robustness can be improved. Here, only some examples are shown for illustration purpose in Figures 5-15 to 5-17. In the analyses in previous sections, the electro-mechanical coupling of piezoelectric transducers on the blade-model beams and the disk-model beams are assumed to be $\xi_1$=0.1, $\xi_2$=0.1. With negative capacitance, one can choose to add it to the circuits on the blade-model beams to increase $\xi_1$, or to the circuits on the disk-model beams to increase $\xi_2$. In this study, for demonstration purpose, we assume that with negative capacitance, $\xi_1$ or $\xi_2$ can be increased to 0.2. Figure 5-15 shows the effect of negative

capacitance on the network performance and robustness with detuning in $\delta_{e1}$. The result in Figure 5-11 is also shown here for comparison purpose ($\xi_1$=0.1). Here, negative capacitance is only added to the circuits on the blade-model beams, therefore, $\xi_2$ remains unchanged (0.1), $\xi_1$ is increased to 0.2. As we can see from the figure, with negative capacitance, the curve becomes quite flat, meaning the network becomes insensitive to the detuning in $\delta_{e1}$. Also, for the large detuning case, the performance is significantly improved. For example, for -20% detuning, without negative capacitance, the original performance index is 0.25 (75% vibration reduction); with negative capacitance, the index is reduced to 0.05 (95% vibration reduction).
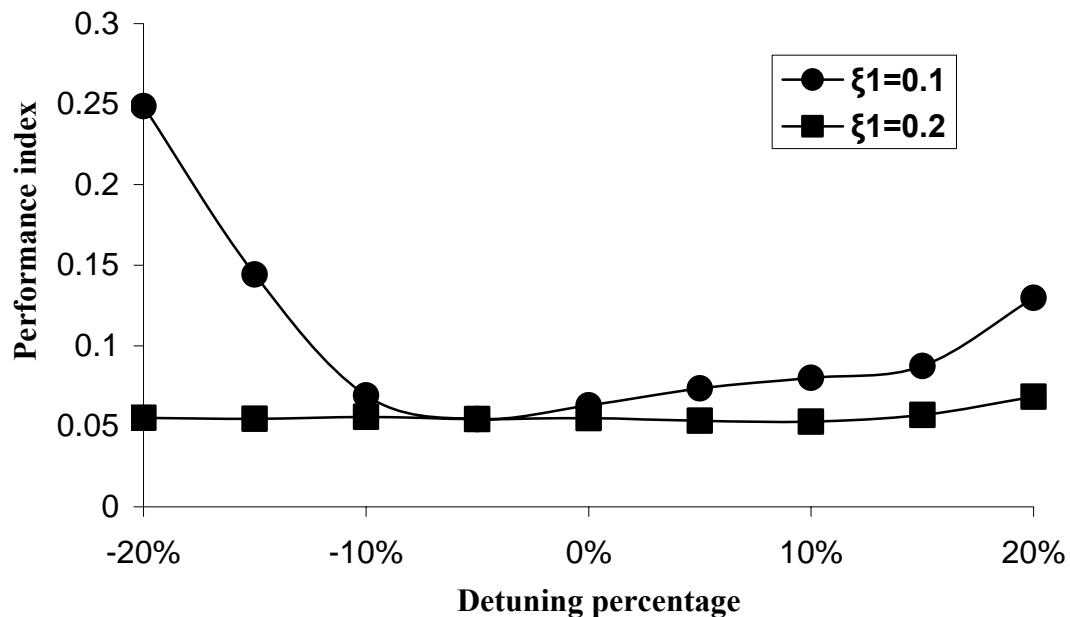


Figure **5-15**: Performance comparison with detuning in $\delta_{e1}$ for the cases of without negative capacitance ($\xi_1$=0.1, ●) and with negative capacitance ($\xi_1$=0.2, ■).

Figure 5-16 shows the effect of negative capacitance with detuning in $\delta_{e2}$. Here, negative capacitance is added to the circuits on the disk-model beams, therefore, $\xi_1$ remains at the nominal value (0.1), and $\xi_2$ is increased to 0.2. It is shown in the figure that the performance index is generally reduced throughout the detuning range. Significant reduction in the index is achieved at the larger detuning levels. For example, for -20% detuning, the original index is about 0.7 without negative capacitance, and is reduced to only 0.35 with negative capacitance. With negative capacitance, the slopes of the curve become smaller for either positive detuning or negative detuning. Also, larger detuning range can be tolerated if one has a pre-set performance index threshold. For example, if the performance threshold is set at index=0.25, the tolerable detuning range for the case without negative capacitance is about [-5%, +8%], while with negative capacitance, for $\xi_2$=0.2, the tolerance range can be increased to about [-15%, +20%].

Similar improvement is shown in Figure 5-17, where 'with' and 'without' negative capacitance for detuning of $\bar{k}_a$ is compared. In this case, only $\xi_2$ is increased to 0.2 by adding negative capacitance to the circuits on the disk-model beams. It also shows improvement in both network performance and robustness.
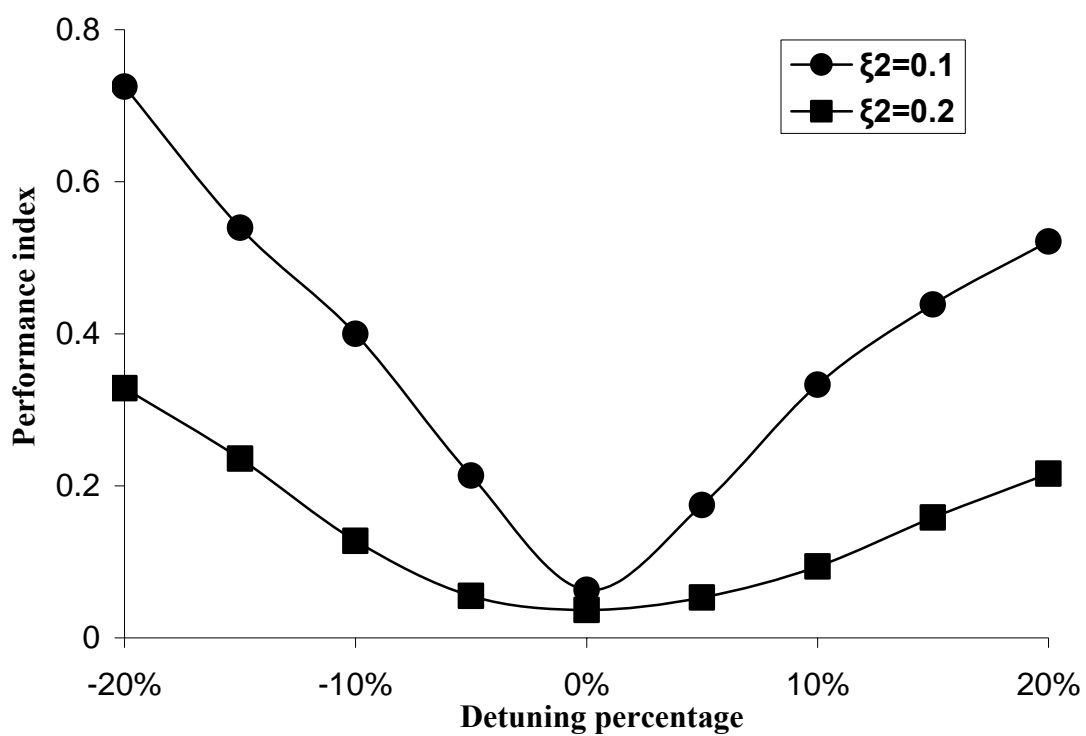
Figure **5-16**: Performance comparison with detuning in $\delta_{e2}$ for the cases of without negative capacitance ($\xi_2$=0.1, ●) and with negative capacitance ($\xi_2$=0.2, ■).
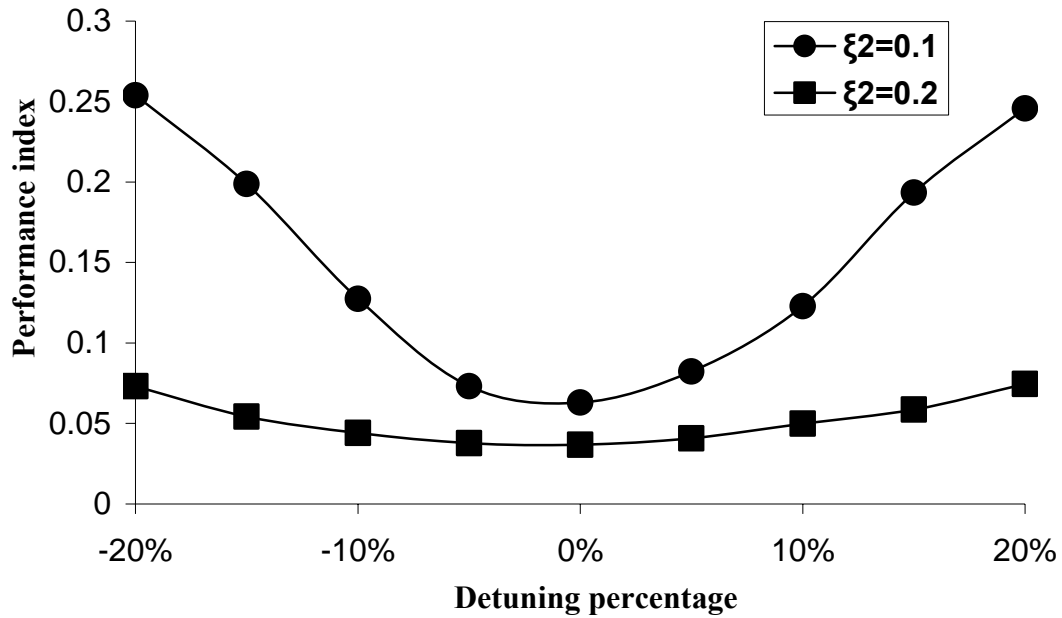
Figure **5-17**: Performance comparison with detuning in $\bar{k}_a$ for the cases of without negative capacitance ($\xi_2$=0.1, ●) and with negative capacitance ($\xi_2$=0.2, ■).

## 5.4 Summary

In this research, piezoelectric circuitry is explored for effective vibration suppression of a mistuned coupled bladed-disk system. A bladed disk model including both blade and disk dynamics is proposed to represent the systems. With this system model, a new multiple-circuit piezoelectric network design is proposed to achieve multi-harmonic vibration suppression. Based on the model, an optimal network is analytically designed using the U-transformation technique. Multiple-harmonic vibration suppression

is demonstrated. The network performance and robustness issues are addressed using Monte Carlo simulation. It is found that the network, although designed based on tuned bladed disk systems, is quite effective for suppressing vibration in mistuned bladed disk systems. The effects of mistuning and detuning in key circuit parameters on the network performance are also examined. The results show that the network is quite robust against mistuning and detuning in most parameters, and can provide good vibration suppression within the variation range studied. The network is relatively more sensitive to the detuning in circuit frequency tuning ratio $\delta_{e2}$, which is related to the circuits on the disk-model beams. It is demonstrated that the treatment with negative capacitance can be used to enhance the performance and robustness of the network.

## Chapter 6

## Vibration Suppression Experimental Investigation

### 6.1 Objective

The purpose of this experiment is to verify the multiple harmonic vibration suppression effect of the piezoelectric network for mistuned bladed disk system under engine order excitation.

### 6.2 Experimental Setup

The baseline bladed disk model system with piezoelectric patches is shown in Figure 6-1. This system is designed according to the new bladed disk model presented in Chapter 5.

In this periodic system, there are twelve aluminum beams forming six bays, with each bay consisting of a shorter beam, a longer beam and two connecting springs. As presented in the new model in Chapter 5, the shorter beams are the blade-model beams that simulate the blade dynamics; and the longer beams are disk-model beams which simulate the disk dynamics. The steel base with twelve slots provides cantilever conditions to the equally spaced beams. The effect of the base vibration on the beams is negligible due to the heavy mass of the base. The major avenues for coupling of beam dynamics are through the coupling springs, with longer ones corresponding to $k_c$ in Figure 5-1 and shorter ones corresponding to $k_s$ in Figure 5-1. The longer spring emulates

the coupling between adjacent disk-model beams, and the shorter spring emulates the coupling between blade-model beams and disk-model beams. The springs are fixed to the beams through specially designed fixtures that are glued to the beams. Identical piezoelectric transducers (patch type) are bonded to the root of each beam on both sides, with one functioning as an exciter to provide engine order excitation for the structure (transforming electric energy to mechanical energy); and the other functioning as a part of the piezoelectric circuitry network (transforming mechanical vibration energy into electrical form). These piezoelectric transducers use the negative electrode wrap up design, which makes the transducers electrically insulated from the beams. The dimension and material properties of the beams and piezoelectric patches are shown in Table 6-1 and Table 6-2. The properties of the springs are shown in Table 6-3. This periodic bladed disk system is intrinsically mistuned due to many sources that can cause differences among bays, including the variations in the lengths of beams, the clamping conditions, the piezoelectric patches' bonding conditions, the spring fixing conditions, etc.
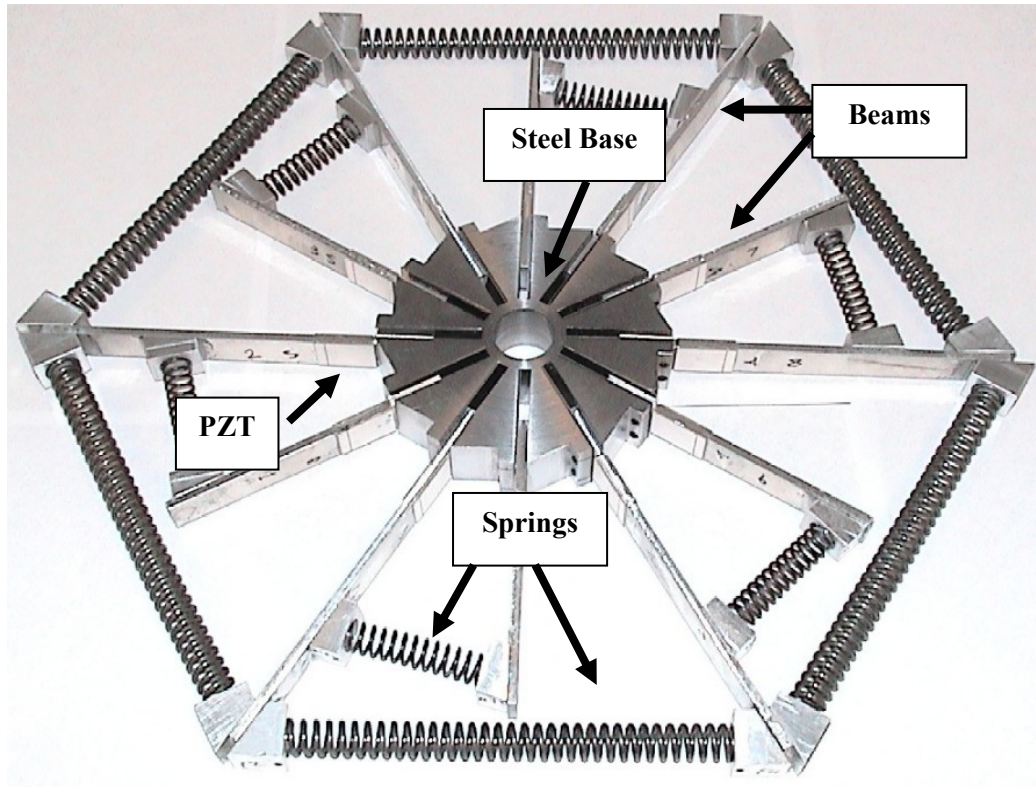
Figure **6-1**:  Baseline bladed disk model system with piezoelectric patches.

Table **6-1**:  Dimension and Material Property of Beams

| Dimension ($10^{-2}$ m) | Material Property |
|---|---|
| Effective Length: 8 (shorter), 11.5 (longer) <br> Width (same for all beams): 1.5 <br> Thickness (same for all beams): 0.3 | Material Type: Aluminum <br> Young's Modulus: $69*10^9$ ($N/m^2$) <br> Density: 2700 ($kg/m^3$) |

Table **6-2**:  Dimension and Material Properties of Piezoelectric Patches

| Dimension ($10^{-2}$ m) | Material Property |
|---|---|
| Effective Length: 2.0 <br> Width: 1.5 <br> Thickness: 0.0508 | Young's Modulus ($Y^E_{11}$): $6.3*10^{10}$ ($N/m^2$) <br> Density: 7700 ($kg/m^3$) <br> Relative Dielectric Constant ($K^T$): 1900 <br> Measured PZT capacitance: 7nF |

Table **6-3**:  Dimension and Properties of Springs

| Shorter Springs | Longer Springs |
|---|---|
| Length: 0.05 (m) <br> Stiffness: 1722.2 (N/m) | Length: 0.14 (m) <br> Stiffness: 4730.2 (N/m) |

The overall experiment setup is shown in Figure 6-2. This testing system includes the bladed disk structure, a traveling wave excitation system, a measurement system, and a piezoelectric circuitry.

The traveling wave excitation system is designed to simulate the engine order excitation force. This system includes a MATLAB/Simulink model that generates sine/cosine wave signals with different phases, a dSpace ControlDesk graphic user interface for controlling the experiment, such as selecting engine orders and calibrating fiber optical sensors, and two six-channel PCB power amplifiers to provide excitation. The Simulink model for the excitation system is shown in Appendix A. The excitation force on the $j^{th}$ blade-model beam (or disk-model beam) can be expressed as: $F_j = F_0 \cos(\omega t + (j-1)\phi)$, where $\phi = 2\pi E / N$, N=6, and E is the engine order number, E=0, …, N/2. Using simple trigonometry, the force formula above can be equivalently expressed as $F_j = F_0 \cos((j-1)\phi)\cos(\omega t) - F_0 \sin((j-1)\phi)\sin(\omega t)$ (Judge et al., 2001), which is easier for Simulink implementation. The Simulink model uses this formula to generate harmonic signals with different phases, determined by the engine order E, then feeds these signals to the PCB power amplifiers that are connected to the piezoelectric exciters bonded on the bladed disk system. This system provides one engine order excitation at a time. Since the periodic system consists of six bays, the effective engine order numbers are E=0, 1, 2, 3, which are the same as the numbers of spatial harmonics. In the experiment, we used frequency sweep for each engine order within a specified

frequency range at a resolution of 1Hz, the process of which is automated by a Matlab code.

Displacement measurements are taken using six fiber optic sensors (Philtec D20) positioned in the close proximity of the tips of blade-model beams (shorter beams). The sensitivities of these sensors are listed in Appendix B. The displacement data is acquired by the Simulink model and dSpace, and processed by a Matlab code.
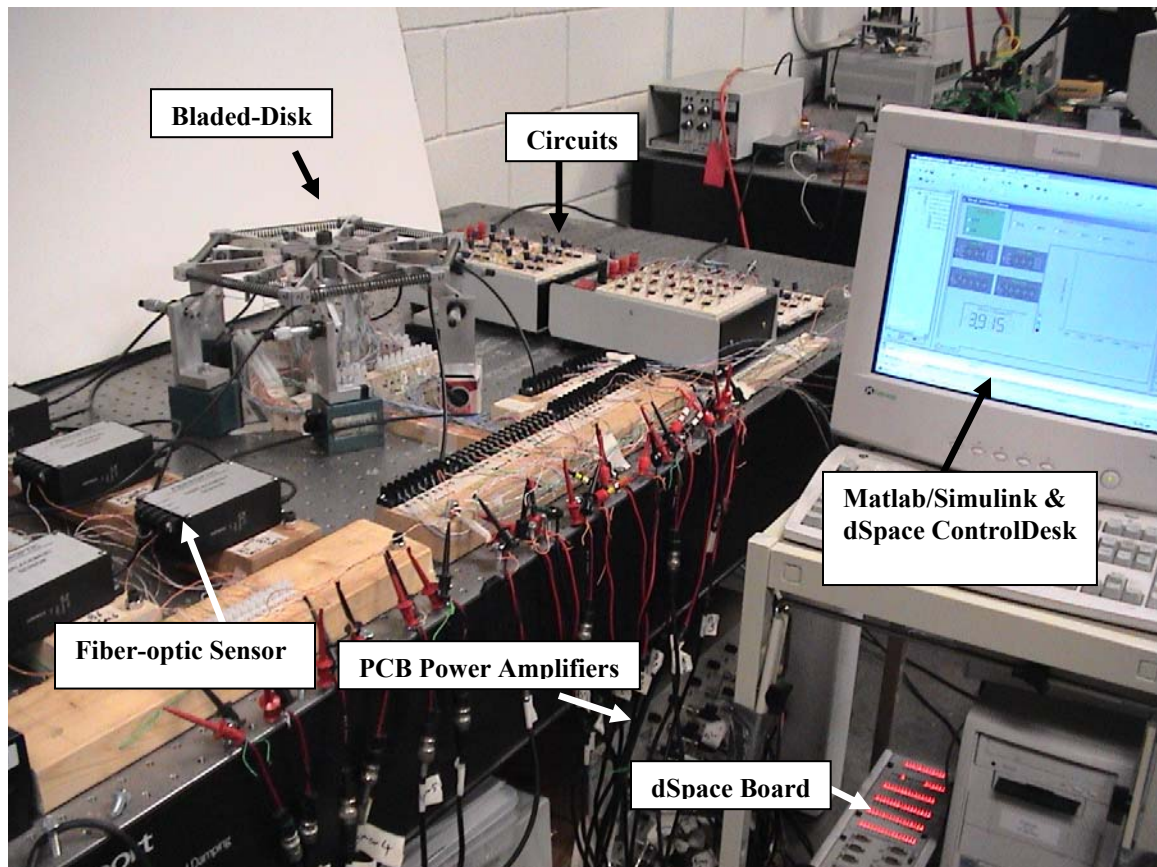


Figure **6-2**: Overall experiment setup for vibration suppression study.

Due to the complexity and the mistuned nature of the bladed-disk system, it was found very difficult to accurately identify the system parameters since a rigorous system identification method for mistuned periodic structures is generally not available. In this experiment, an analytical model is first developed for the theoretically tuned system. The system parameters are then estimated based on the analytical model calculation and adjustment via trial and error. The guideline is to make the natural frequencies of the analytically tuned system to be around those resonant frequencies obtained from the experimental frequency responses of the mistuned system. The analytically estimated system parameters are shown in Table 6-4. Table 6-5 shows the natural frequencies of the tuned system calculated based on the estimated parameters in Table 6-4, and the resonant frequencies of the mistuned system obtained from experiment. It is shown that the tuned system's natural frequency range is pretty close to the range of the experimentally obtained resonant frequencies of mistuned system.

On the other hand, it is also noted that the analysis in Chapter 5 suggests that the network is quite robust in terms of circuitry parameter detuning which could be caused by the error in the parameter identification of the mechanical system. Therefore, the purpose of this experiment, that is, the demonstration of the multiple harmonic vibration suppression effect of the network, may still be fulfilled even if the mechanical system's parameters were not identified accurately, and the network were not tuned at the optimal point. So, in the following test, the estimated system parameters listed in Table 6-4 are used in the circuitry design.

Table **6-4**:  System Parameters for Bladed Disk Model Structure

| $m_b$ | 0.0388 (*kg*) |
|---|---|
| $k_b$ | 104772 (*N/m*) |
| $k_s$ | 6500 (N/m) |
| $m_d$ | 0.0425 (kg) |
| $k_d$ | 103710 (N/m) |
| $k_c$ | 434450 (N/m) |
| $k_{bp1}$ | 494042 (N/m) |
| $k_{bp2}$ | 259330(N/m) |

Table **6-5**:  Frequencies From Analytical Estimate and Experimental Data

| Analytical Estimate: Tuned System's Natural Frequency (Hz) | 252.6, 268.0, 269.1, 269.2, 273.0, 304.0, 379.0, 411.6 |
|---|---|
| Experimental Data: Mistuned System's Resonant Frequency (Hz) | 257.0, 265.0, 267.0, 272.0, 273.0, 276.0, 277.0, 279.0, 280.0, 282.0, 283.0, 284.0, 288.0, 398.0, 405.0, 407.0 |

For the circuitry, a network is designed and tuned according to the optimal solutions presented in Chapter 5, as shown in Equation (5.5) and Equations (5.7) to (5.9). Table 6-6 lists the values of these circuit design parameters. In this experiment, synthetic inductors are used. The synthetic inductor has been used in our previous mode delocalization experiment in Chapter 3, which is based on operational-amplifiers (Chen, 1986). Similar to the traditional passive inductors, these synthetic inductors have internal

resistances. With the inductance value shown in Table 6-6, the inherent resistance values are measured to be 12.45k Ohms for $L_1$, and 14.4k Ohms for $L_2$. The theoretically optimal (total) resistance values ($R_1$ and $R_2$) are shown in Table 6-6, which are also applicable to the traditional absorber case. The external resistance needed for optimal damping is then calculated after taking into account of the internal resistance of the synthetic inductors. In the network case, for the circuits with $L_1$ (connected to the blade-model beams), the external resistance theoretically needed is 2.33k Ohms, and for the circuits with $L_2$ (connected to disk-model beams) it is zero ohms because the inherent resistance of $L_2$ is already higher than the theoretical calculation. For the traditional absorber design, the circuits connected to the disk-model beams are designed as described in Chapter 5. The coupling capacitors ($C_a$) and the additional capacitors ($C_2$) are removed. Individual $LR$ shunt circuits that have the same architecture as those circuits attached to the blade-model beams are used for the disk-model beams. For the traditional absorber, the inductors are designed for harmonic (or engine order) 0, that is, letting $j=1$ in Equation (5.6) (also $k_2=k_a=0$), the inductance of which is 55 (Henry) with an intrinsic resistance of 13.1k Ohms (thus the theoretical external resistance needed is 1.68k Ohms). However, in the experiment, different trials found that with an external 330-Ohm resistor in the circuits with $L_1$, both the network and the traditional absorber perform better than using the calculated external resistance. This might be due to the error in the estimation of the system parameters. Therefore, in the results shown later, 330-Ohm external resistors are used in the circuit with $L_1$.

Table **6-6**: Circuit Network Parameters

| Inductance $L_1$ | 49.8 (Henry) |
|---|---|
| Inductance $L_2$ | 58.5 (Henry) |
| Additional capacitance $C_2$ | 0.11 (uF) |
| Coupling capacitance $C_a$ | 0.016 (uF) |
| Optimal damping resistance $R_1$ | 14.78 k ohms |
| Optimal damping resistance $R_2$ | 8.45 k ohms |

## 6.3 Experimental Results

Figures 6-3 to 6-6 compare the vibration suppression results of the network and the traditional absorber within the frequency range of interest, where without circuit, the blade forced response shows large amplitude under engine order excitation. In each figure, the maximum blade response curve corresponding to the 'without circuit' case (i.e., the baseline mechanical system case) is the black dotted line, the grey solid line represents the 'with traditional absorber' case, and the 'with network' case is denoted by the black solid line. The maximum blade responses are obtained from all blades. Each figure uses one specific engine order excitation, $E$=0, 1, 2, 3. The maximum response ratios are shown in Table 6-7. This ratio is defined by taking the division between the maximum response of with circuit case (with network or with traditional absorber) and that of the baseline mechanical system case. Therefore, the ratio indicates the vibration suppression effectiveness, with smaller value meaning more vibration reduction. For

example, the ratio of 0.445 for engine order 0 ('with network') means that the maximum blade response is suppressed by 55.5% with the use of the network.   Observing Figures 6-3 to 6-6 and Table 6-7, one can see that at engine order 0, the performance of the network and the traditional absorber is similar in terms of maximum response ratio. However, the ratios for traditional absorber are much higher than that for the network when the structure is under other engine orders ($E$=1,2,3).  This is expected since the traditional absorber is tuned to engine order 0.  The experimental results indicate that the piezoelectric network is effective for vibration suppression at all engine order excitations, and outperforms the traditional absorber that is only effective at one specific engine order excitation.

Table **6-7**:  Maximum Blade Response Ratio

| Engine Order | With network | With traditional absorber |
|:---:|:---:|:---:|
| 0 | 0.445 | 0.543 |
| 1 | 0.374 | 0.756 |
| 2 | 0.331 | 0.883 |
| 3 | 0.226 | 0.966 |
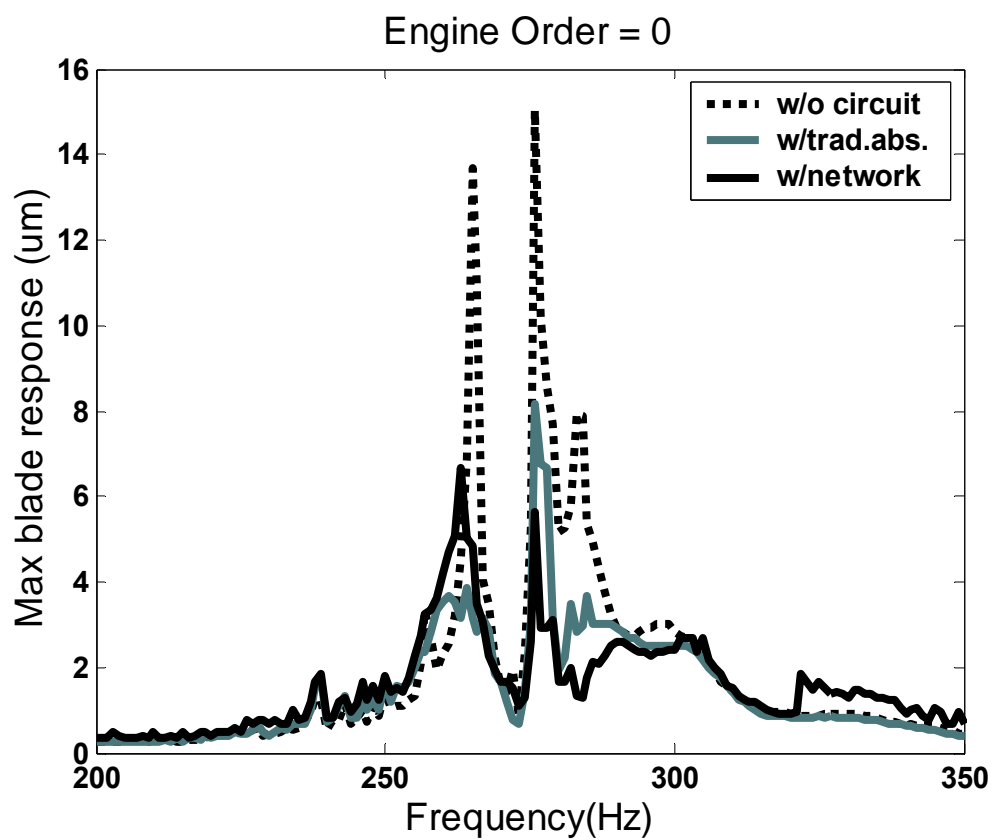
Figure **6-3**: Maximum blade response vs. frequency for without circuit case (dotted line), with traditional absorber case (grey solid line) and with network case (black solid line) under engine order 0 excitation.
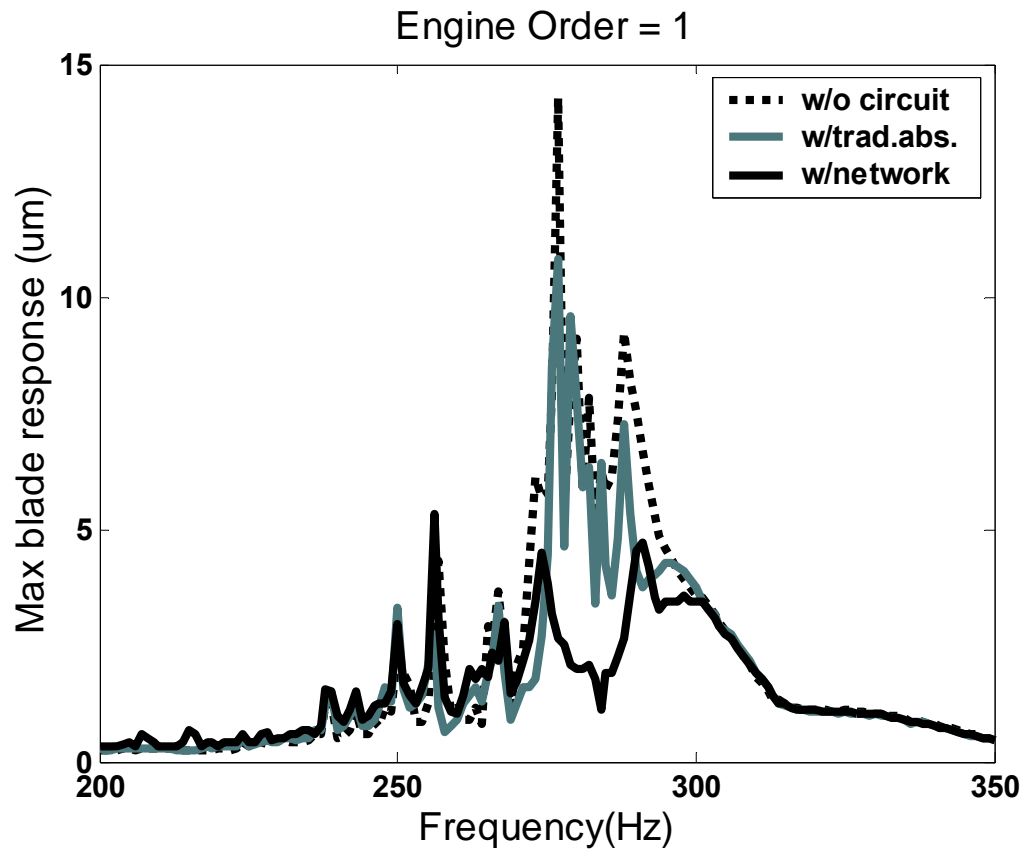
Figure **6-4**: Maximum blade response vs. frequency for without circuit case (dotted line), with traditional absorber case (grey solid line) and with network case (black solid line) under engine order 1 excitation.
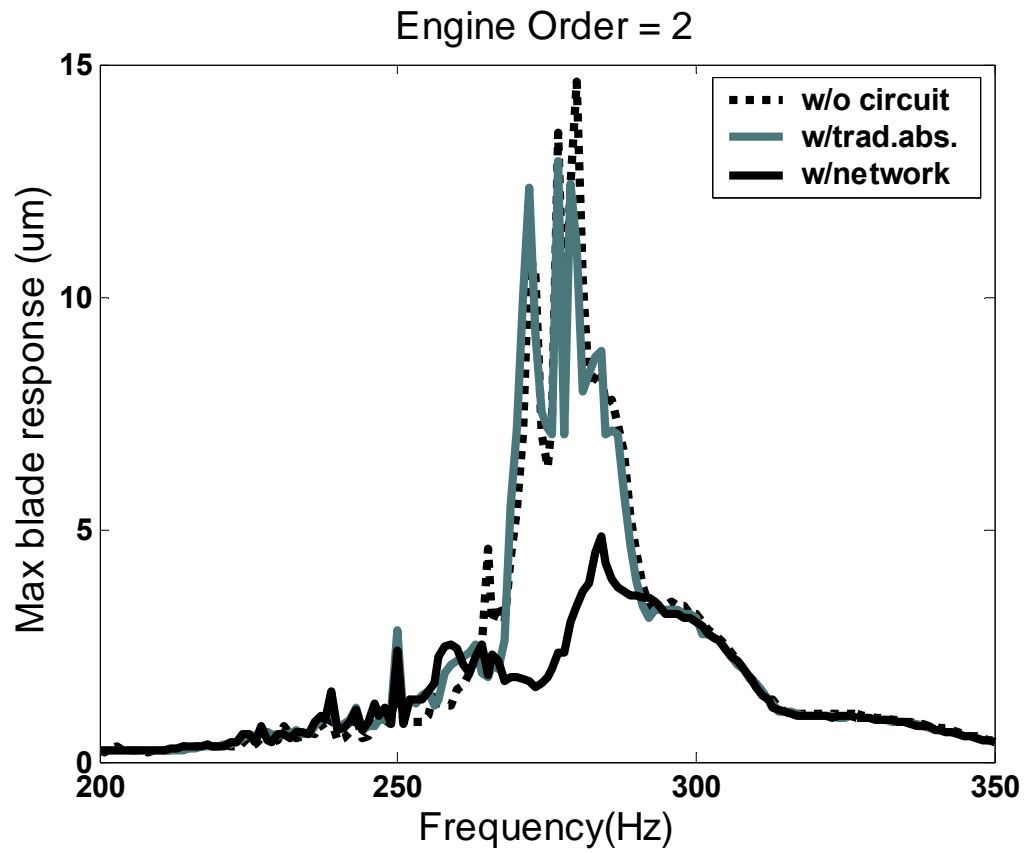
Figure **6-5**: Maximum blade response vs. frequency for without circuit case (dotted line), with traditional absorber case (grey solid line) and with network case (black solid line) under engine order 2 excitation.
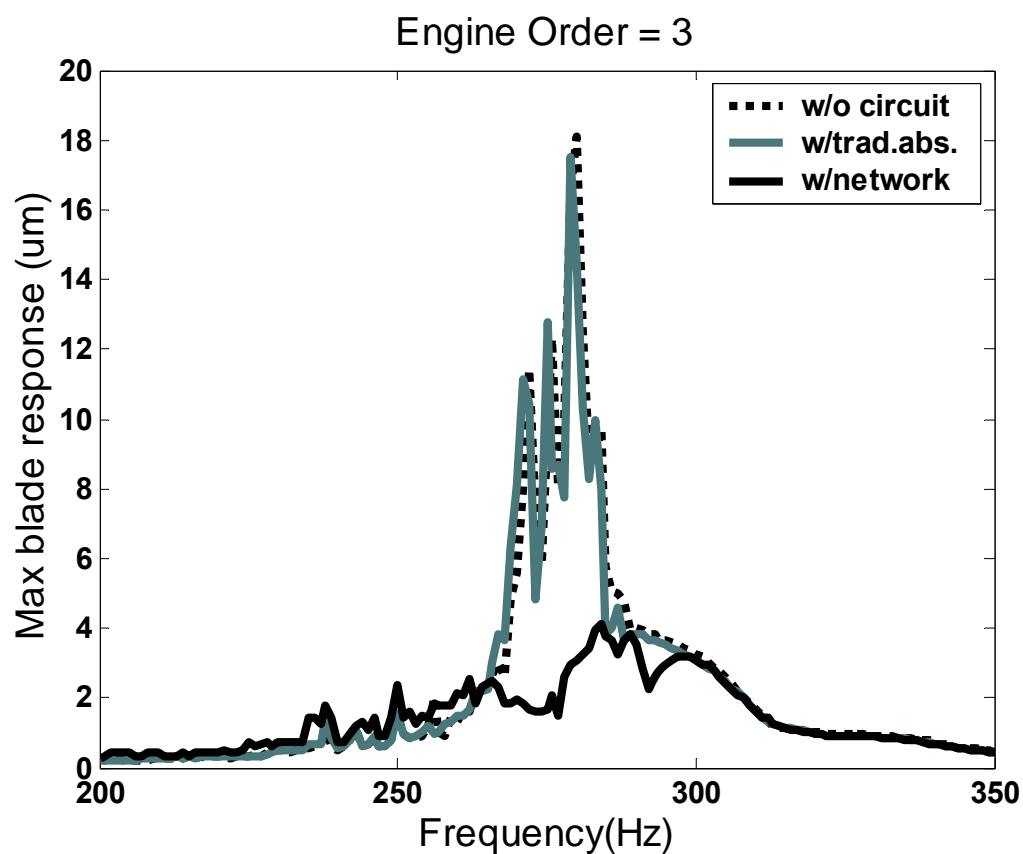
Figure **6-6**: Maximum blade response vs. frequency for without circuit case (dotted line), with traditional absorber case (grey solid line) and with network case (black solid line) under engine order 3 excitation.

**6.4 Summary**

Experiments are performed to study the multiple harmonic vibration suppression effect of piezoelectric network for mistuned bladed disk system. A six bay bladed disk model system is built using cantilever beams and springs according to the bladed disk model presented in Chapter 5. A traveling wave excitation system is realized using piezoelectric patches, power amplifiers, MATLAB/Simulink and dSpace experimental control software. A piezoelectric network is designed and applied to the baseline system. Investigations are conducted to examine the vibration suppression effects of the new network and the traditional absorber. The experimental results verified that network can effectively suppress vibration of a mistuned bladed disk for multiple engine order excitations, whereas, traditional absorber is only effective for certain spatial harmonic excitation, as predicted in the analysis in Chapter 5.

# Chapter 7

## Conclusion and Future Work

In this Chapter, we summarize the major efforts and contributions of this thesis, and provide recommendations for the future work.

### 7.1 Mode Delocalization Analysis and Experiment

A piezoelectric networking configuration with enhanced electro-mechanical coupling is analyzed for vibration mode delocalization. The model of the periodic structure integrated with the piezoelectric network is derived via Hamilton's principle. An effort is made to define the localization index for quantifying the degree of localizaiton. Lyapunov exponents of the periodic system are examined. The correlation of the Lyapunov exponents and the exponential spatial decay rate of localized modes of the electro-mechanically coupled system is studied. Based on the analysis, a localization index is defined using the average of the lower Lyapunov exponents within the original frequency passbands. A comprehensive parameter study, with varying circuitry parameters, is performed using this localization index to evaluate the effectiveness of the proposed scheme and provide guidelines for the circuitry design.

An active coupling enhancement method using negative capacitance is utilized to increase the electro-mechanical coupling of the piezoelectric patches. The analysis

shows that by increasing the electro-mechanical coupling coefficient, the negative capacitance can improve the delocalization effect of the piezoelectric network.

Experiments are performed to validate the concept of piezoelectric networking for delocalization. The experiments use an 18-blade inherently mistuned periodic system as the baseline mechanical structure. A piezoelectric network is designed, synthesized and integrated with the structure. The experimental results show that with the piezoelectric network, vibration localization level of the mistuned mechanical system can be reduced. Furthermore, the experiments also confirmed that adding negative capacitance can effectively improve the delocalization effectiveness of the network.

## 7.2 Vibration Suppression Analysis and Experiment

The piezoelectric networking concept is extended for vibration suppression of mistuned bladed disks. The analysis involves two parts. The study is first conducted based on a simple bladed disk model, which only considers blade dynamics and neglects the disk motion. The second part considers a more complex bladed disk model, where coupled blade-and-disk dynamics are taken into account. Finally, experiments are also conducted to validate the vibration suppression effect of the piezoelectric network.

To explore the design of piezoelectric network for vibration suppression of mistuned bladed disks, first, the study is conducted based on a simple bladed disk model, which only considers blade motion, and neglects the disk dynamics. The system equations are derived using Hamilton's principle, and then decoupled using the U-transformation technique. An optimal network is analytically derived. The vibration

suppression effectiveness of the optimal network is compared with that of the traditional absorber design. Analysis shows that although traditional absorber can suppress some specific engine order excitations, it loses its effectiveness at others. Whereas, the optimal network can effectively suppress all engine order excitations, therefore, outperforms the traditional absorber design in terms of multiple harmonic vibration suppression. Monte Carlo simulation is performed to evaluate the effectiveness of the piezoelectric network for vibration suppression of mistuned bladed disks with various mistuning levels, and the performance and robustness of the optimal network with circuitry parameter variations. The simulation analysis shows that the optimal piezoelectric network performs well for quite a large mechanical mistuning level. The performance of the optimal network is also quite robust against the circuitry parameter variations. The analysis also shows that inclusion of the negative capacitance can further improve the performance and robustness of the network.

The vibration suppression study of the piezoelectric network is further extended in the second part of the study by considering a more complex model for bladed disks with coupled blade-disk interaction. This complex model can better represent the dynamic characteristics of a bladed disk in that it can capture the frequency veering phenomenon that is often present in bladed disk systems. With the analysis of this model, a new piezoelectric network configuration is proposed for multi-harmonic vibration suppression. Based on the analysis of the dynamics of the bladed disk model, closed form solutions are analytically obtained for the optimal network design. Multiple harmonic vibration suppression effect of this new network is demonstrated and compared to that of the traditional absorber design. It is shown that the new optimal network,

although designed based on the tuned system assumption, is quite effective for mistuned mechanical systems. The robustness of the network is also examined via Monte Carlo simulation by considering the mistuning and detuning in the key circuitry parameters. Simulation results show that the new optimal network is also quite robust in most parameters, and can provide good vibration suppression results within the variation ranges studied. Among these parameters, it is found that the network is most sensitive to the detuning in the circuit frequency tuning ratio of the circuits on the disk-model beams. The treatment with negative capacitance also enhances the performance and robustness of the new network.

Experiments are also carried out to validate the vibration suppression effect of the piezoelectric network. The baseline structure used in the experiment is designed according to the new complex bladed disk model presented in the analysis in the second part of the analysis. A traveling wave excitation system is built to emulate the engine order excitation force that real bladed disk systems experience due to aerodynamic loading. The network designed based on the analysis is applied to the mistuned periodic mechanical test structure. The maximum blade amplitudes under engine order excitations are obtained and compared for the 'without circuit' case (the pure mechanical system case), 'with traditional absorber' case, and 'with network' case. The results show that the network is effective in vibration suppression for all engine order excitations, and outperforms the traditional absorber design, which is only effective for a specific engine order.

**7.3 Recommendation for Future Work**

Comprehensive studies have been conducted in this research, and good achievements have been obtained and presented in this thesis. Below are some recommendations for the future work to advance the state of the art of this piezoelectric networking technology.

**7.3.1 Improvement of current technology**

1. In this thesis, the Lyapunov exponent is used as the localization index for vibration delocalization study. The computation of this index is very time consuming, and is based on wave propagation. Defining an index that directly works on mode shapes would be very interesting and valuable.

2. Often times, the periodic mechanical structures have low natural frequencies. When applying the piezoelectric network experimentally, one has to use tunable synthetic inductors. However, the synthetic inductor design used in this research is not stable enough. A more robust design is desirable for real application.

3. To better utilize the optimal piezoelectric network design for vibration suppression, it is desirable to develop an accurate system identification method for the mechanical system.

4. Circuitry network topology other than those used in this research may also be effective for vibration suppression of bladed disks, including active control schemes and passive-active hybrid schemes. These could be explored in the future.

**7.3.2 Extension of current technology for damage detection**

In addition to vibration control, the networking technology may also be used for damage detection of mistuned bladed disks.

Bladed disks are common structures in jet engines. When a small crack starts to develop in a blade, catastrophic consequences may occur if the crack is not detected in time. However, detection of a small crack in bladed disks is extremely challenging. Currently available techniques for damage detection of bladed disks are mostly based on ultrasound and eddy current technologies (Patkanen et al., 2001). These methods are usually off-line methods, which require the disassembling of the engine, and are usually position sensitive. Vibration based damage detection methods have also been explored (Salawu, 1997; Zou et al, 2000). These methods use frequency response function or mode shapes of a structure for damage information extraction. However, for mistuned bladed disks, which usually have high modal intensity, these methods may fail. Also, for mistuned system, a small damage might not cause drastic change in the dynamic characteristics. From the studies in the previous chapters, it is clear that in mistuned bladed disks, localization often occurs. One possibility is to utilize this unique characteristic to create a method for damage detection. When the engine speed up and speed down, the bladed disk will be subject to engine order excitation due to aerodynamic loading. With sensing technologies such as BTT (Blade Tip Timing) (Zielinski and Ziller, 2000; Dimitriadis et al., 2002), one is possible to measure the blade forced response and extract useful information from the measurement for damage detection. The idea here is to create innovative piezoelectric circuitry that can temporarily

induce or intensify structural vibration localization to amplify the damage effect (since damage is a form of mistuning) on the system vibratory signature during the inspection stage. In this manner, one can better capture the damage by comparing the BTT measurements before and after damage occurs.

# Bibliography

Afolabi, D., 1985, "Frequency response of mistuned bladed disk assemblies," *Vibrations of Blades and Bladed Disk Assemblies,* pp. 15-21.

Agnes, G.S., 1999, "Piezoelectric coupling of bladed-disk assemblies," *Proceedings of SPIE, Smart Structures and Materials*, v 3672, pp. 94-103.

Anderson, P.W., 1958, "Absence of diffusion in certain random lattices," *Physics Review*, v 109, n 5, pp. 1492-1505.

Baik, S., Castanier, M. P., and Pierre, C., 2004, "Mistuning sensitivity prediction of bladed disks using eigenvalue curve veerings," *Proceedings of the 9th National Turbine Engine High Cycle Fatigue Conference*, Pinehurst, NC.

Balmes, E., 1993, "High modal density, curve veering, localization: a different perspective on the structural response," *Journal of Sound and Vibration*, v 161, n 2, pp. 358-363.

Behrens, S., Moheimani, S.O.R., and Fleming, A.J., 2003, "Multiple mode current flowing passive piezoelectric shunt controller," *Journal of Sound and Vibration*, v 266, n 5, pp. 929-942.

Bendiksen, O.O., 1987, "Mode localization phenomena in large space structures," *AIAA Journal*, v 25, n 9, pp. 1241-1248.

Bladh, R., Pierre, C., Castanier, M.P., and Kruse, M.J., 2002, "Dynamic response prediction for a mistuned industrial turbomachinery rotor using reduced-order modeling," *Journal of Engineering for Gas Turbines and Power*, v 124, n 2, pp. 311-324.

Bouzit, D. and Pierre, C., 1992, "Vibration confinement phenomena in disordered, mono-coupled, multi-span beams," *Journal of Vibration and Acoustics*, v 114, n 4, pp. 521-530.

Cai, G. Q. and Lin, Y. K., 1991, "Localization of wave propagation in disordered periodic structures," *AIAA Journal*, v 29, n 3, pp. 450-456.

Castanier, M. P., Ottarsson, G. and Pierre, C., 1997, "A reduced order modeling technique for mistuned bladed disks," *Journal of Vibration and Acoustics,* v 119, n 3, pp. 439-447.

Castanier, M.P. and Pierre, C., 1995, "Lyapunov exponents and localization phenomena in multi-coupled nearly-periodic systems," *Journal of Sound and Vibration*, v 183, n 3, pp. 493-515.

Castanier, M.P. and Pierre, C., 2002, "Using intentional mistuning in the design of turbomachinery rotors," *AIAA Journal,* v 40, n 10, pp. 2077-2086.

Cha, P.D., and Pierre, C., 1991, "Vibration localization by disorder in assemblies of monocoupled, multimode component systems," *Journal of Applied Mechanics*, v 58, n 4, pp. 1072-1081.

Cha, P.D. and Pierre, C., 1997, "A statistical investigation of the forced response of finite, nearly periodic assemblies," *Journal of Sound and Vibration*, v 203, n 1, pp. 158-168.

Cha, D. and Sinha, A., 2002, "Effects of the nature of excitation on the response of a mistuned bladed disk assembly," *Journal of Turbomachinery*, v 124, n 4, pp. 588-596.

Chen, W., 1986, *Passive and active filters, theory and implementation*, John Wiley & Sons, New York.

Choi, B.-K., Lentz, J., Guerra-Rivas, A.J., and Mignolet, M.P., 2003, "Optimization of intentional mistuning patterns for the reduction of the forced response effects of unintentional mistuning: formulation and assessment," *Journal of Engineering for Gas Turbines and Power,* v 125, n 1, pp. 131-140.

Cornwell, P.J. and Bendiksen, O.O., 1989, "Localization of vibrations in large space reflectors," *AIAA Journal*, v 27, n 2, pp. 219-226.

Cornwell, P.J. and Bendiksen, O.O., 1992, "Numerical study of vibration localization in disordered cyclic structures," *AIAA Journal*, v 30, n 2, pp. 473-481.

Cox, A.M. and Agnes, G.S., 1999, "A statistical analysis of space structure mode localization," *Proceedings of the 1999 AIAA/ASME/ASCE/AHS/ASC Structures, Structural Dynamics, and Materials Conference and Exhibit*, v 4, pp. 3123-3133.

Crawley, E. F., and de Luis, J., 1987, "Use of piezoelectric actuators as elements of intelligent structures," *AIAA Journal*, v 25, n 10, pp. 1373-1385.

Davis, P.J., 1979, *Circulant Matrices,* Wiley, NY.

Den Hartog, J.P., 1934, *Mechanical Vibrations,* McGraw Hill, NY.

Dimitriadis, G., Carrington, I.B., Wright, J.R., and Cooper. J.E., 2002, "Blade-tip timing measurement of synchronous vibrations of rotating bladed assemblies," *Mechanical Systems and Signal Processing*, v 16, pp.599 – 562.

Duffield, C.J., and Agnes, G.S., 2001, "An experimental investigation on periodic forced vibrations of a bladed disk," *Collection of Technical Papers - AIAA/ASME/ASCE/AHS/ASC Structures, Structural Dynamics and Materials Conference*, v 5, pp. 3599-3608.

Forward, R. L., 1979, "Electronic damping of vibrations in optical structures," *Applied Optics*, v 18, n 5, pp. 690-697.

Furstenberg, H., 1963, "Noncommuting random products," *Transactions of the American Mathematical Society*, v 108, n 3, pp. 377-428.

Gordon, R. W. and Hollkamp, J. J., 2000, "An experimental investigation of piezoelectric coupling in jet engine fan blades," *Collection of Technical Papers – AIAA/ASME/ASCE/AHS/ASC Structures, Structural Dynamics and Materials Conference*, v 1, n III, pp. 1975-1983.

Griffin, J. H. and Hoosac, T. M., 1984, "Model development and statistical investigation of turbine blade mistuning," *Journal of Vibration, Acoustics, Stress, and Reliability in Design,* v 106, n 2, pp. 204-210.

Hagood, N.W., and von Flotow, A., 1991, "Damping of structural vibrations with piezoelectric materials and passive electric networks," *Journal of Sound and Vibration,* v 146, n 2, pp. 243-268.

Hodges, C.H., 1982, "Confinement of vibration by structural irregularity*," Journal of Sound and Vibration*, v 82, n 3, pp. 411-424.

Hodges, C.H. and Woodhouse, J., 1983, "Vibration isolation from irregularity in a nearly periodic structure: theory and measurements," *Journal of Acoustical Society of America*, v 74, n 3, pp. 894-905.

Hodges, C.H. and Woodhouse, J., 1989, "Confinement of vibration by one-dimensional disorder, I: theory of ensemble averaging," *Journal of Sound and Vibration*, v 130, n 2, pp. 253-268.

Hollkamp, J.J., 1994, "Multimodal passive vibration suppression with piezoelectric materials and resonant shunts," *Journal of Intelligent Materials Systems and Structures*, v 5, n 1, pp. 49-56.

Horowitz, P. and Hill W., 1989, *The art of electronics*, second edition, Cambridge University Press.

Hou, J., and Cross, C., 2005, "Minimizing blade dynamic response in a bladed disk through design optimization," *AIAA Journal,* v 43, n 2, pp. 406-412.

Institute of Electrical and Electronics Engineers, 1988, *IEEE Standard on Piezoelectricity* (ANSI/IEEE Std. 176-1987), IEEE, New York.

Judge, J., Pierre, C. and Mehmed, O., 2001, "Experimental investigation of mode localization and forced response amplitude magnification for a mistuned bladed disk," *Journal of Engineering for Gas Turbines and Power,* v 123, n 4, pp. 940-950.

Kahn, S. P., and Wang, K. W., 1994, "Structural vibration controls via piezoelectric materials with active-passive hybrid networks," *American Society of Mechanical Engineers, Design Engineering Division (Publication) DE, v 75, Active Control of Vibration and Noise,* pp. 187-194.

Kenyon, J. A., and Griffin, J. H., 2003, "Forced response of turbine engine bladed disks and sensitivity to harmonic mistuning," *Journal of Engineering for Gas Turbines and Power*, v 125, n 1, pp.113-120.

Kenyon, J. A., Griffin, J. H. and Feiner, D. M., 2003, "Maximum bladed disk forced response from distortion of a structural mode," *Journal of Turbomachinery*, v 125, n 2, pp. 352-363.

Kenyon, J.A., Griffin, J.H., and Kim, N.E., 2004, "Frequency veering effects on mistuned bladed disk forced response," *Journal of Propulsion and Power,* v 20, n 5, pp. 863-870.

Kenyon, J.A., Griffin, J.H., and Kim, N.E., 2005, "Sensitivity of tuned bladed disk response to frequency veering," *Journal of Engineering for Gas Turbines and Power,* v 127, n 4, pp. 835-842.

Kissel, G.J., 1987, "Localization in disordered periodic structures," *28th AIAA/ASME/ASCE/AHS Structures, Structural Dynamics and Materials Conference*, April 6-8, Monterey, CA, pp. 1046-1055.

Kissel, G.J., 1991, "Localization factor for multichannel disordered systems," *Physics Review A*, v 44, n 2, pp. 1008-1014.

Kruse, M. J., Pierre, C. 1997, "Experimental investigation of vibration localization in bladed disks, Part II: Forced response," *American Society of Mechanical Engineers (Paper)*, 97-GT-502, 8p.

Leissa, A.W., 1974, "On a curve veering aberration," *Journal of Applied Mathematics and Physics,* v 25, pp. 99-111.

Lesieutre, G. A., and Davis, C. L., 1997, "Can a coupling coefficient of a piezoelectric device be higher than those of its active material?" *Journal of Intelligent Material Systems and Structures,* v 8, n 10, pp. 859-867.

Lesieutre, G.A., 1998, "Vibration damping and control using shunted piezoelectric materials," *Shock and Vibration Digest,* v 30, n 3, pp. 187-195.

Lust, S.D., Friedmann, P.P. and Bendiksen, O.O., 1993, "Mode localization in multispan beams," *AIAA Journal*, v 31, pp. 348-355.

Mead, D. J., 1975a, "Wave propagation and natural modes in periodic systems: I. Mono-coupled systems," *Journal of Sound and Vibration,* v 40, n 1, pp. 1-18.

Mead, D. J., 1975b, "Wave propagation and natural modes in periodic systems: II. Multi-coupled systems, with and without damping," *Journal of Sound and Vibration,* v 40, n 1, pp. 19-39.

Mester, S.S. and Benaroya, H., 1995, "Periodic and near-periodic structures," *Shock and Vibration*, v 2, n 1, pp. 69-95.

Ottarsson, G. and Pierre, C., 1993, "Vibration localization in mono- and bi-coupled bladed disks – a transfer matrix approach," *34th AIAA/ASME/ASCE/ASH Structures, Structural Dynamics and Materials Conference*, Pt 6, pp. 3683-3697.

Ottarsson, G. and Pierre, C., 1996, "A transfer matrix approach to free vibration localization in mistuned blade assemblies," Journal of Sound and Vibration, v 197, n 5, pp. 589-618.

Pitkanen, J., Hakkarainen, T., Jeskanen, H., Kuusinen, P., Lahdenpera, K., Sarkiniemi, P., Kemppainen, M., and Pihkakoski, M., 2001, "NDT methods for revealing anomalies and defects in gas turbine blades," *Insight: Non-Destructive Testing and Condition Monitoring,* v 33, n 9, pp. 601-604.

Perkins, N.C. and Mote, C.D. Jr., 1986, "Comments on curve veering in eigenvalue problems," *Journal of Sound and Vibration,* v 106, n 3, pp. 451-463.

Pierre, C., Tang, D.M. and Dowell, E.H., 1987, "Localized vibrations of disordered multi-span beams: theory and experiment," *AIAA Journal*, v 25, n 9, pp. 1249-1257.

Pierre, C., 1988, "Mode localization and engenvalue loci veering phenomena in disordered structures," *Journal of Sound and Vibration,* v 126, n 3, pp. 485-502.

Pierre, C, 1990, "Weak and strong vibration localization in disordered structures: a statistical investigation." *Journal of Sound and Vibration*, v 139, n 1, pp. 111-132.

Pierre, C., Castanier, M.P., and Chen, W.J., 1996, "Wave localization in multi-coupled periodic structures: application to truss beams," *Applied Mechanics Review*, v 49, n 2, pp. 65-86.

Salawu, O.S., 1997, "Detection of structural damage through changes in frequency: a review," *Engineering Structures,* v 19, n 9, pp. 718-723.

Sinha, A., and Chen, S, 1989, "A higher order technique to compute the statistics of forced response of a mistuned bladed disk assembly," *Journal of Sound and Vibration,* v 130, n 2, pp. 207-221.

Slater, J. C., Minkiewicz, G.R., and Blair, A.J., 1999, "Forced response of bladed disk assemblies – a survey," *The Shock and Vibration Digest*, v 31, n 1, pp. 17-24.

Tang, J., Liu, Y., and Wang, K.W., 2000, "Semi-active and active-passive hybrid structural damping treatments via piezoelectric materials," *Shock and Vibration Digest,* v 32, n 3, pp. 189-200.

Tang, J., and Wang, K.W., 1999, "Vibration control of rotationally periodic structures using passive piezoelectric shunt networks and active compensation," *Journal of Vibration and Acoustics,* v 121, n 3, pp. 379-390.

Tang, J. and Wang, K. W., 2001, "Active-passive hybrid piezoelectric networks for vibration control: comparisons and improvement," *Journal of Smart Materials and Structures*, v 10, n 4, pp. 794-806.

Tang, J. and Wang, K. W., 2003, "Vibration delocalization of nearly periodic structures using coupled piezoelectric networks," *Journal of Vibration and Acoustics*, v 125, n 1, pp. 95-108.

Tsi, M.S., and Wang, K. W., 1996, "Control of a ring structure with multiple active-passive hybrid piezoelectric networks," *Smart Materials and Structures,* v 5, pp. 695-703.

Wei, S.-T. and Pierre, C., 1988, "Localization phenomena in mistuned assemblies with cyclic symmetry part I: free vibrations," *Journal of Vibration, Acoustics, Stress and Reliability in Design*, v 110, n 4, pp. 429-438.

Whitehead, D.S., 1966, "Effect of mistuning on the vibration of turbomachine blades induced by wakes," *Journal of Mechanical Engineering Science*, v 8, n 1, pp. 15-21.

Wolf, A., Swift, J.B., Swinney, H.L., and Vastano, J.A., 1985, "Determining Lyapunov exponents from a time series," *Physica D,* v 16, pp. 285-317.

Wu, S.-Y., 1999, "Method for multiple mode piezoelectric shunting with single PZT transducer for vibration control," *Journal of Intelligent Material Systems and Structures,* v 9, n 12, pp. 991-998.

Xie W.-C. and Ariaratnam, S.T., 1996a, "Vibration mode localization in disordered cyclic structures, I: single substructure mode," *Journal of Sound and Vibration*, v 189, n 5, pp. 625-645.

Xie W.-C. and Ariaratnam, S.T., 1996b, "Vibration mode localization in disordered cyclic structures, II: multiple substructure mode," *Journal of Sound and Vibration*, v 189, n 5, pp. 647-660.

Yu, H., Wang, K.W. and Zhang, J., 2006, "Piezoelectric networking with enhanced electromechanical coupling for vibration delocalization of mistuned periodic structures – theory and experiment," *Journal of Sound and Vibration,* v 295, n1-2, pp. 246-265.

Zhang, J. and Wang, K. W., 2002, "Electromechanical tailoring of piezoelectric networks for vibration delocalization and suppression of nearly-periodic structures," *Proceedings of the 13ᵗʰ International Conference on Adaptive Structures and Technologies*, Potsdam, Berlin, Germany, pp. 199-212.

Zielinski, M., and Ziller, G., 2000, "Noncontact vibration measurements on compressor rotor blades," *Measurement Science and Technoligy*, v 11, pp. 847 – 856.

Zou, Y., Tong, L., and Steven, G.P., 2000, "Vibration-based model-dependent damage (delamination) identification and health monitoring for composite structures – a review," *Journal of Sound and Vibration*, v 230, pp. 357-378.

# Appendix A

## Matlab/Simulink Model for Traveling Wave Excitation

The figure shown below is the Matlab/Simulink model for the traveling wave excitation system (upper group) and the fiber-optical sensor data acquisition system (lower group).
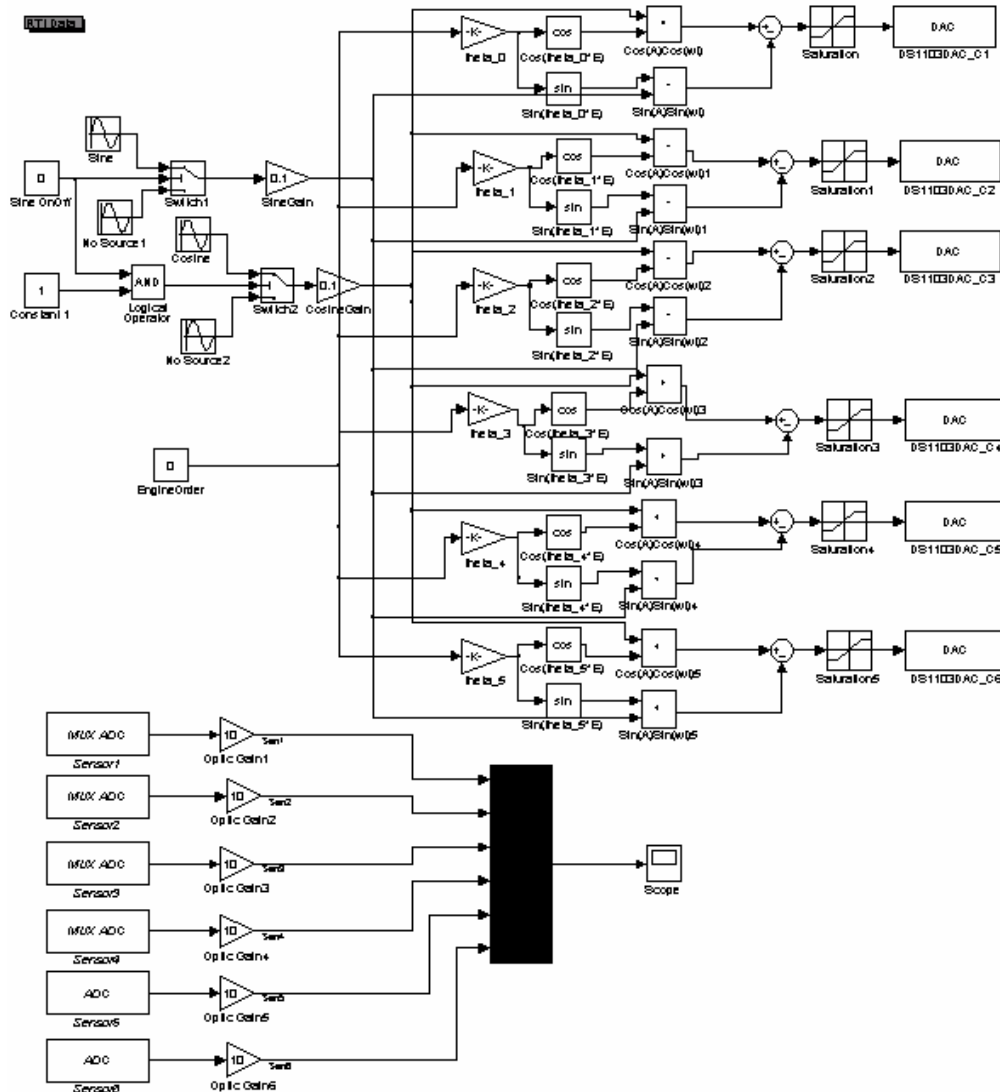
# Appendix B

## Fiber-Optical Sensor Sensitivities

This table shows the sensitivity data for the fiber-optical sensors used in the experiment.

Table **B-1**: Sensitivities of Fiber-Optical Sensors

| Sensor # | Sensitivity (mv/mil) |
|----------|----------------------|
| 1 | -240.6 |
| 2 | -219.2 |
| 3 | -250.9 |
| 4 | -234.4 |
| 5 | -237.8 |
| 6 | -237.5 |

**VITA**

**Hongbiao Yu**

Hongiao Yu was born in a small village in Zhejiang Province of China in 1979. He attended Chun An County High School. After high school, he enrolled in the Mechanics department of Peking University in 1997, where he studied theories in Mechanics and Engineering, and graduated with a Bachelor of Science degree in 2001. In college, he was also awarded several fellowships and scholarships, in recognition of his excellent academic and social work. Upon graduation, he joined Penn State University as a Ph.D. student in mechanical engineering under the supervision of Dr. Kon-Well Wang. He studied and conducted research in the Structural Dynamics and Controls Lab. In addition to his thesis research, he also worked on damage detection of turbine engine, mentored a fresh Ph.D. student, and served as the lab manager. He published several peer-reviewed journal and conference papers. He earned his Ph.D. degree in August, 2007.